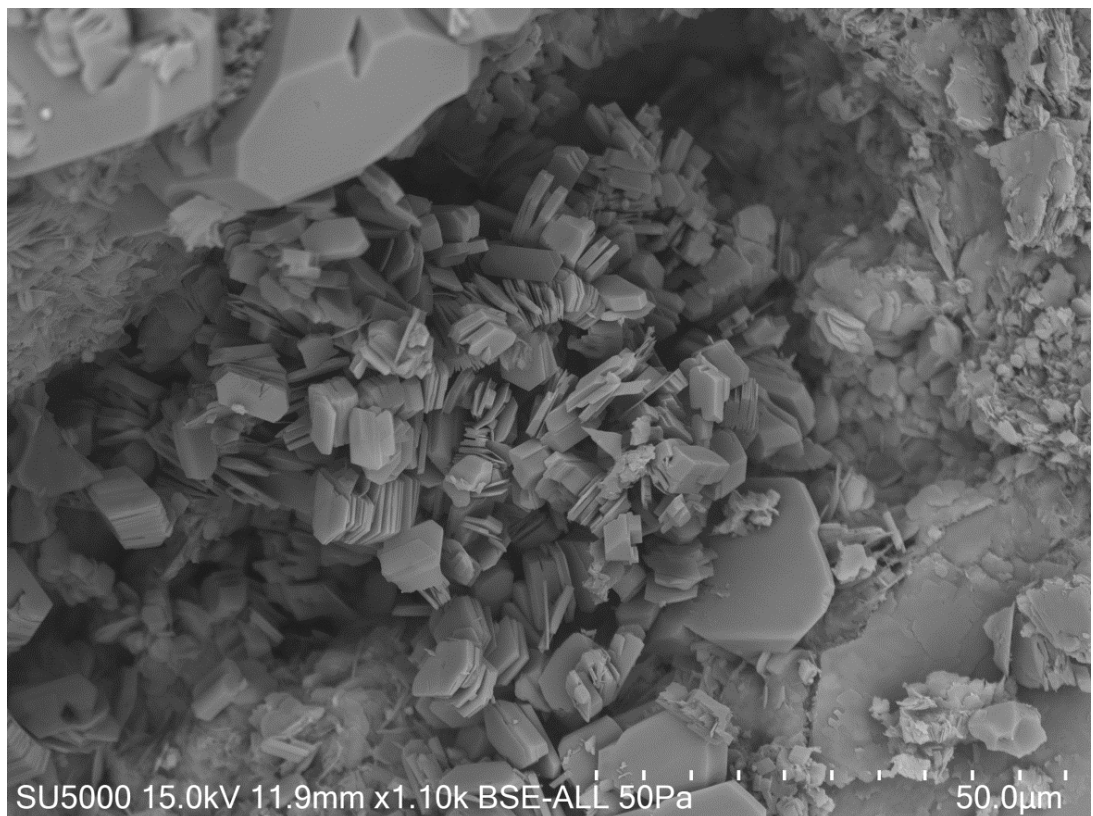


Master Thesis, Department of Geosciences

# Reservoir Quality of the Triassic Snadd and Kobbe Formations in the Barents Sea

Tímea Gyenis



**UNIVERSITY OF OSLO**

**FACULTY OF MATHEMATICS AND NATURAL SCIENCES**



# **Reservoir Quality of the Triassic Snadd and Kobbe Formations in the Barents Sea**

**Tímea Gyenis**



**Master Thesis in Geosciences**

**(60 credits)**

**Discipline: Sedimentology**

**Department of Geosciences**

**Faculty of Mathematics and Natural Sciences**

**University of Oslo**

**01.12.2016**

© Tímea Gyenis, 2016

Tutor(s): **Jens Jahren, Lina Hedvig Line (UiO)**

This work is published digitally through DUO – Digitale Utgivelser ved UiO

<http://www.duo.uio.no>

It is also catalogued in BIBSYS (<http://www.bibsys.no/english>)

All rights reserved. No part of this publication may be reproduced or transmitted, in any form or by any means, without permission.



## **PREFACE**

This thesis is submitted to the Department of Geosciences, University of Oslo (UiO), in candidacy of MSc degree in Geology.

The research has been performed at the Department of Geosciences, University of Oslo, during January 2016 to December 2016 under the supervision of Jens Jahren, Professor at Department of Geosciences, University of Oslo and Lina Hedvig Line, PhD Candidate at Department of Geosciences, University of Oslo, Norway.



## **ACKNOWLEDGEMENT**

I would like to express my sincere gratitude to my supervisor Professor Jens Jahren and co-supervisor PhD candidate Lina Hedvig Line for their patience, guidance and encouragement. Our discussions and their knowledge and motivation helped me during my work and grow both academically and as a person.

I am very grateful to Berit Løken Berg and PhD candidate Beyene Girma Haile for their precious time given for sample preparation and technical support during XRD and SEM analysis.

Special thanks to my fellow student Chloé Marcilly for our helpful discussions and exchange ideas giving me motivation to improve my thesis.

It has been a great pleasure to study at the Department of Geosciences, at the University of Oslo in Norway. I am very thankful to all my teachers for their wisdom, knowledge and love for their work.

At last but not least my warmest and greatest thanks to my lovely family and my beloved boyfriend, Owais, without them this master thesis would not have been possible.



## **ABSTRACT**

Geologically, the Barents Sea with deep sedimentary basins, highs and platforms is a complex mosaic and formed as a result of different geologic and tectonic processes with complex geological history. The history of the Barents Sea started 400 million years ago and continued until continental crustal separation which led to develop the Atlantic and Arctic oceans. The Barents Sea is a challenging area for hydrocarbon exploration. The reservoirs are mainly Jurassic age sandstones. The predominance of gas over oil and leakage of hydrocarbons from the traps are source of the problems in the exploration. These problems are related to Cenozoic erosion and uplift of the Barents Sea area.

The Triassic Snadd and Kobbe Formations located on the southern part of the Bjarmeland Platform in SW Barents Sea are the focus of this study. The Snadd and Kobbe reservoirs are several meters thick and has good (Snadd) and poor (Kobbe) reservoir quality.

Sedimentological, petrographic and petrophysical analysis have been done providing core material, thin sections and well log dataset from well 7222/11-1 (Caurus). The main objective was to characterize reservoir properties within these formations.

The depositional environment for both sandstones has been interpreted as tide-dominated delta system with several subenvironments. The Kobbe Formation deposited during low energy conditions such as muddy shelf, inter- to supratidal flats, while the Snadd sandstones have been interpreted as tidal channel sandstone bodies.

The Snadd Formation is well-sorted very fine- to fine-grained sandstone with moderate clay and carbonate content and the Kobbe Formation is moderately-sorted, very fine-grained sandstone with high clay content. Both formations are lithic arenites. Compositionally there is no significant difference between the two formations and the source area has been interpreted as eastern source area (Uralides) for both Kobbe and Snadd Formations.

The main diagenetic minerals in both Kobbe and Snadd Formations are chlorite coating, pore-filling chlorite, kaolinite, pyrite, carbonate and quartz cement. The chlorite coating is well-developed in the Snadd Formation and preventing quartz cementation, while in the Kobbe Formation the chlorite coating is non-continuous hence there are slightly more quartz overgrowths present. The chlorite may have formed when fresh river water brought iron-rich material into seawater and the clay particles flocculated in the fluvial-marine mixing zone. The source of pore-filling authigenic kaolinite is mainly the dissolved mica and feldspar grains. Kaolinite is generally associated with pore-filling fibrous chlorite and microporosity. Two types of siderite cements are present in the formations, rhombic shape siderite, which sometimes appears within expanded mica grains, and small spherulitic patches of siderite within the samples. The iron-rich material brought by river water could be a source of siderite. The source of calcite cement is mainly the carbonate fossils are present in the samples. The pyrite is present both as framboidal and blocky crystals in the sandstones.

The Snadd Formation sandstones show good porosity (4-28.2%) due less effect of mechanical compaction and chlorite coating preserves porosity. The permeability is mostly good but where the pore-filling authigenic clay minerals are present in the pore space the permeability shows low value. The Snadd Formation has been interpreted to have good reservoir quality. The Kobbe Formation sandstones has very fine grain size, high clay and matrix content, therefore mechanical compaction affects more in the Kobbe sandstones, resulting low porosity and permeability values. The Kobbe Formation has been interpreted to have poor reservoir quality.

The presence of quartz overgrowths indicate that the two formations have been buried at deeper depth than at present. The absence of illite suggests that the temperature did not exceed 130 °C before uplift. The maximum uplift has been estimated 1.3-1.6 km in well 7222/11-1. The Kobbe Formation was more deeply buried (3.5-3.8 km) than the Snadd Formation (2.6-2.9 km).

# **TABLE OF CONTENT**

## **Contents**

PREFACE .....	i
ACKNOWLEDGEMENT .....	iii
ABSTRACT .....	v
TABLE OF CONTENT .....	vii
LIST OF FIGURES .....	xi
LIST OF TABLES .....	xv
LIST OF APPENDIX .....	xvi
1. Introduction .....	1
1.1 Purpose of the study and project description .....	1
1.2 Study area .....	1
2. Geological settings .....	3
2.1 Regional geology of the Barents Sea .....	3
2.2 Triassic evolution of the Barents Sea .....	5
2.3 Structural geology of the Barents Sea .....	9
2.3.1 The Bjarmeland Platform .....	10
2.4 Stratigraphic framework .....	12
2.4.1 Sassendalen Group .....	13
2.4.2 Kapp Toscana Group .....	14
2.5 Source rocks in the Barents Sea .....	15
2.6 Reservoir rocks in the Barents Sea .....	17
3. Theoretical background .....	19
3.1 Sedimentological effect on reservoir quality .....	19
3.2 Diagenetic processes in sandstones .....	21
3.2.1 Early diagenesis .....	21
3.2.2 Mechanical compaction .....	24
3.2.3 Chemical compaction .....	25
3.2.4 Porosity preservation .....	27
4. Methodology .....	29
4.1 Sedimentological logging .....	29

4.2	Mineralogical and Petrographic analysis.....	29
4.2.1	Thin section analysis .....	29
4.2.2	X-ray diffractometry (XRD) .....	32
4.2.3	Scanning electron microscope (SEM).....	34
4.3	Petrophysical analysis.....	34
4.3.1	Shale volume estimation .....	34
4.3.2	Porosity estimation.....	36
4.3.3	Permeability estimation.....	37
4.3.4	Net-to-Gross ratio and pay zone.....	38
4.3.5	Estimation of the uplift in the study area .....	38
4.4	Sources of error .....	39
5.	Sedimentology.....	41
5.1	Description of the core .....	41
5.1.1	Core 7222/11-1.....	41
5.2	Facies description .....	46
5.3	Facies association .....	55
6.	Petrographic analysis.....	56
6.1	Snadd Formation.....	56
6.1.1	Lithology and texture .....	56
6.1.2	Detrital grains.....	57
6.1.3	Authigenic minerals .....	57
6.2	Kobbe Formation.....	62
6.2.1	Lithology and texture .....	62
6.2.2	Detrital grains.....	62
6.2.3	Authigenic minerals .....	63
6.3	Modal analysis.....	67
6.3.1	Porosity and Intergranular volume (IGV) .....	69
7.	Petrophysical analysis .....	70
7.1	Snadd Formation.....	70
7.2	Kobbe Formation.....	71
7.3	Porosity versus permeability .....	72
7.4	Uplift estimation .....	74
8.	Discussion .....	76



8.1	Composition of the sandstones and provenance.....	76
8.2	Depositional environment.....	79
8.3	Diagenetic evolution of the sandstones .....	81
8.3.1	Early diagenesis.....	81
8.3.2	Mechanical compaction.....	84
8.3.3	Diagenesis at intermediate depth (2-3.5 km; 65-120°C).....	85
8.3.4	Deep burial diagenesis (>3.5-4 km; >120°C) .....	86
8.4	Reservoir quality.....	86
8.4.1	Snadd Formation .....	86
8.4.2	Kobbe Formation.....	87
8.4.3	Reservoir quality versus depth .....	89
8.4.4	Reservoir quality versus depositional environment .....	90
8.5	Estimated uplift in the study area .....	91
9.	Conclusion.....	92
9.1	Further work .....	94
	REFERENCES.....	95
	APPENDIX .....	100



## **LIST OF FIGURES**

Figure 1.1: Overview of the main structural elements of the SW Barents Sea. The study area is marked by red dot on the map (modified after NPD Factmaps 2016). .....	2
Figure 2.1: Location of the Barents Sea (USGS, 2003). .....	3
Figure 2.2: Regional geology of the Barents Sea to end-Permian time (Gudlaugsson et al., 1998). .....	4
Figure 2.3: Paleogeographic reconstruction of the depositional environments during the Triassic (Glørstad-Clark et al., 2010). The marginal marine facies presented by yellow colour. The green represents the continental facies and the shelfal facies presented by grey color. ....	8
Figure 2.4: The major structural elements of the Barents Sea, the study area (red circle) and the well database (red dot) (modified from Smelror et al., 2009). .....	10
Figure 2.5: The Triassic lithostratigraphy and the Triassic sequence stratigraphic subdivision (2nd order) in the SW Barents Sea (Glørstad-Clark et al., 2010). .....	12
Figure 2.6: The Triassic lithostratigraphy in the Barents Sea and on Svalbard (red circle the studied formations) (Mørk et al., 1999). .....	14
Figure 2.7: Time of deposition of proven and potential source and reservoir rocks in the Norwegian Barents Sea (Doré, 1995). .....	16
Figure 2.8: Geological cross-section of the Snøhvit Field, represents the fault bounded traps in the Norwegian sector (Doré, 1995). .....	18
Figure 3.1: Key elements in sediment transport from the source to the basin (Martinsen et al., 2010). .....	19
Figure 3.2: Occurrences of allogenic clays in sandstones (Wilson and Pittman, 1977). ....	20
Figure 3.3: Biological precipitation of silica. Alteration of opal A to opal CT and then quartz (Bjørlykke, 2010b). .....	22
Figure 3.4: Meteoric water flushing and other diagenetic processes in shallow marine environment (Bjørlykke and Jahren, 2015). .....	23
Figure 3.5: Mechanical and chemical compaction during burial (Bjørlykke and Jahren, 2015). .....	24
Figure 3.6: Compaction of coarse-grained and fine-grained sand (Chuhan et al., 2002). ....	25
Figure 3.7: Dissolution of quartz along stylolites (Bjørlykke and Jahren, 2015). .....	26
Figure 3.8: Occurrence of authigenic clays in sandstones from Wilson and Pittman, (1977). ..	28
Figure 4.1: Location of the different cuts of a core. Logging on the D-cut. ....	29
Figure 4.2: Classification scheme of grain sorting (Compton, 1962). .....	30
Figure 4.3: The roundness of detrital grains (Powers, 1953). .....	30
Figure 4.4: Classification of sandstones (Dott Jr, 1964). .....	31
Figure 4.5: The figure represents the different grain contacts that have been recognized during textural analysis (Santin et al.). .....	32
Figure 4.6: Neutron-density cross plot from Snadd Formation. The cross plot is used to define clay line and sand line for shale volume estimation. ....	36
Figure 5.1: Legend for the logged sections of the Kobbe and Snadd Formations in well 7222/11-1, representing on Figure 5.2 and Figure 5.3. ....	42
Figure 5.2: The logged section for the Kobbe Formation in well 7222/11-1. ....	43

Figure 5.3: The logged section for the Snadd Formation in well 7222/11-1. ....	45
Figure 5.4: Massive sandstone facies with the 4 different subfacies in the Snadd Formation. A: Structureless massive sandstone at 780 m depth; B: Cross-bedded massive sandstone at 783 m depth; C: Massive sandstone with coal flakes at 798 m depth; D: Massive sandstone with bioturbation at 799 m depth. ....	47
Figure 5.5: Siltstone facies in the Snadd and Kobbe Formation. A: Siltstone with sand lenses at 800-800.5 m depth in the Snadd Fm; B: Bioturbated siltstone at 800-800.5 m depth in the Snadd Fm; C: Highly bioturbated siltstone in the Kobbe Fm at 2214.5 m depth. ....	48
Figure 5.6: Heterolithic deposits in the Kobbe Formation. A: Flaser bedding at 2231 m depth; B: Wavy bedding at 2229 m depth; C: Lenticular bedding at 2225 m depth.....	49
Figure 5.7: Heterolithic deposits in the Snadd Formation. A: Flaser bedding at 801 m depth; B: Wavy bedding at 801.5 m depth; C: Lenticular bedding at 802 m depth.....	50
Figure 5.8: Palaeosol represents in the Snadd Formation. ....	50
Figure 5.9: The sample represents carbonate cemented sandstone with the different subfacies. A: Horizontal lamination in the Snadd Fm at 1296 m depth; B: Bioturbation in the Snadd Fm at 1298 m depth; C1: Cross-bedded sandstone in the Snadd Fm; C2: Cross-bedded sandstone in the Kobbe Fm. ....	52
Figure 5.10: A: Bioturbated mudstone in the Snadd Formation; B: Horizontal laminated mudstone in the Kobbe Formation. ....	52
Figure 5.11: A: Vf-f-grained sandstone with bioturbation in the Snadd Formation at 803 m depth; B: Vf-f-grained sandstone with bioturbation from the Kobbe core at 2223-2224 m depth; C: Vf-f-grained sandstone with current ripples in the Kobbe Formation at 2239 m depth. ....	53
Figure 5.12: Alternating mud and sand layers in the Kobbe Formation. ....	54
Figure 6.1: Well-sorted very fine- to fine-grained quartz-rich sandstone at 784.10 m depth. The white grains are quartz, the white to dusty brown grains are feldspar and the dark brown black grains are rock fragments. ....	56
Figure 6.2: A: The sample represents quartz overgrowths (QO), chlorite coating (chl) and rhombic siderite (S) grains at 797.60 m depth in 3D, picture taken by SEM; B: Authigenic pore-filling kaolinite at 780.50 m depth in 3D, picture taken by SEM; C: Chlorite coating (red arrows) in a 2D-view at 784.10 m depth, picture taken by SEM; D: Pore-filling kaolinite (red circles) as viewed through plane polarized light (ppl) at 782.70 m depth. ....	58
Figure 6.3: A: The sample represents rhombic siderite grains within expanded biotite at 782.70 m depth (ppl); B: Siderite cement (S) together with blocky pyrite crystals (Pyr) in mica rich matrix at 797.60 m depth (SEM 2D); C: Rhombic siderite grains (S) filling the pore space at 797.60 m depth (SEM 2D); D: 3D-view of rhombic siderite grains (indicating with black arrow) and framboidal pyrite grains (Pyr) at 797.60 m depth (SEM). ....	59
Figure 6.4: A: The sample contains mainly ankerite with calcite veins (CC), red arrow indicates dolomite grain at 1297.60 m depth (SEM 2D); B: The sample consists of dolomite, quartz (Qtz) and pore-filling chlorite (green arrow) at 1292.15 m depth (SEM 2D); C: Calcite cement replacing chlorite and albite grains at 788.42 m depth (SEM 2D); D: Calcite cemented sandstone (788.42 m) (ppl).....	60
Figure 6.5: Pyrite cement (Pyr) at 797.60 m depth in the Snadd Formation. ....	61

Figure 6.6: Well-sorted very fine-grained quartz-rich sandstone at 2237.65 m depth in the Kobbe Formation.....	62
Figure 6.7: A: The sample represents biotite (bio) grain being replaced by chlorite (chl), blue arrows showing siderite cement at 2214.75 m depth (SEM 2D); B: Pore-filling authigenic chlorite (chl) and kaolinite (kao) at 2230.60 m depth (SEM 2D); C: The sample represent chlorite coating (green arrows), where the coating is incomplete quartz overgrowths are present (red arrows). Authigenic kaolinite is present in the pore space (orange arrows). Chlorite (chl) is replacing mica grain at 2233.60 m depth (SEM 2D); D: Pore-filling authigenic kaolinite (kao) is replacing muscovite (blue arrows) at 2241.65 m depth (SEM 2D); E-F: Pore-filling authigenic kaolinite with chlorite coating (chl) and where the coating is absent quartz overgrowths appear (red arrows) at 2241.65 m depth (SEM 3D).....	65
Figure 6.8: A-B: Calcite cemented sandstone at 2214.75 m depth. Siderite cement (S) scattered all over the sample. Carbonate fossil is presented by orange arrows; C: Rhombic siderite grains (black arrows) within expanded biotite grain at 2241.65 m depth; D: Siderite cement patches in 3D view at 2214.75 m depth (SEM); E: Detrital chlorite grain (chl) is present at 2241.65 m depth. ....	66
Figure 6.9: The figure shows the sandstone composition for the Kobbe and Snadd Formation in the 7222/11-1 well. All samples represent lithic arenite sandstones. ....	67
Figure 6.10: Total porosity and IGV for Snadd and Kobbe Formation. ....	69
Figure 7.1: The composite log section of the Snadd Formation in well 7222/11-1. The clean reservoir interval marked with light blue shading. GR-gamma ray log; RDEP-deep resistivity log; DEN-density log; NEU-neutron log; SW-water saturation; PHIT-total porosity; PHIE-effective porosity.....	71
Figure 7.2: Total porosity and permeability in the Snadd and Kobbe Formations. Kobbe Formation shows low permeability and porosity values comparing to the Snadd Formation. ....	72
Figure 7.3: The figure represents porosity versus permeability according to depth (m) and shale volume (Vsh%) in both formations in well 7222/11-1. ....	73
Figure 7.4: The approximate estimated uplift by using Storvoll et al. (2005) and Mondol (2009) compaction curves in the study area; MC-Mechanical compaction zone; CC-Chemical compaction zone; TZ-Transition zone. ....	74
Figure 8.1: The map is showing the progradation of the deltaic system from Middle (a-b) to Late Triassic-Carnian (c) in the Barents Sea. The study area is marked by red rectangle. Modified from Riis et al., (2008). ....	77
Figure 8.2: The possible interpreted provenance and transport directions in the Barents Sea. The study area marked with red dot. Modified from (Mørk, 1999).....	78
Figure 8.3: Tidally influenced delta system with subenvironments, modified from (Nichols, 2009). The red circle represents the depositional environment for the Snadd Formation and the green for the Kobbe Formation. ....	79
Figure 8.4: The depositional environment for the studied formations, marked with red circle modified from (Halland et al., 2014).....	80
Figure 8.5: Two generations of grain coating chlorite. The precursor coating (orange arrow) covers the grain's surface and authigenic chlorite coating (green arrow) overlays the precursor coating at 2241.65 m depth in the Kobbe Formation. ....	81

Figure 8.6: Chlorite coatings covering all grains preventing quartz overgrowths, where chlorite coating is incomplete quartz overgrowths presence (red circles), Snadd Fm, 780.50 m depth. ....	82
Figure 8.7: Pore-filling calcite cement and siderite cement occurs as spherulitic patches in the Kobbe Formation at 2214.75 m depth.....	82
Figure 8.8: Framboidal (red arrow) and blocky pyrite crystals (black arrow) in the Kobbe Formation sandstone at 2230.60 m depth.....	84
Figure 8.9: Thick chlorite coating (red circles) represents on the grain surfaces in the Kobbe Formation at 2241.65 m depth. Authigenic kaolinite (kao) booklets are present in the pore space. ....	88
Figure 8.10: Porosity and permeability show decrease with increase of burial depth. ....	89

## **LIST OF TABLES**

Table 4.1: Characteristic d-spacing of the common minerals.....	33
Table 4.2: Commonly used non-linear equations for shale volume estimation (Rider and Kennedy, 2011).....	35
Table 5.1: The interpreted facies association with the depositional environments and subenvironments.....	55
Table 6.1: Modal analysis of the Snadd (left) and Kobbe Formations (right) in well 7222/11-1. ....	68
Table 7.1: The results of the petrophysical analysis of the Snadd Formation. ....	70
Table 7.2: The petrophysical results for the Kobbe Formation.....	72
Table 7.3: Estimated uplift, geothermal gradient (G) and transition zone (TZ) depths in well 7222/11-1. The bottom hole temperature has been interpolated from the neighbouring well 7222/11-2 (87.8°C).....	75
Table 7.4: The maximum burial depths and the maximum temperature according to the estimated uplift and the geothermal gradient in well 7222/11-1. The bottom hole temperature has been interpolated from the neighbouring well 7222/11-2 (87.8°C).....	75

## **LIST OF APPENDIX**

A.1: Sedimentary log of Core 1 of the Snadd Formation in well 7222/11-1. ....	100
A.2: Sedimentary log of Core 2 and lower Core 1 of the Snadd Formation in well 7222/11-1. ....	101
A.3: Sedimentary log pf Core 3 of the Snadd Formation in well 7222/11-1. ....	102
A.4: Sedimentary log of the Kobbe Formation in well 7222/11-1. ....	103
B.1: Samples selected for petrographic analysis from Kobbe and Snadd Formations. ....	104
B.2: Point counting results for Snadd (left) and Kobbe (right) Formations in well 7222/11-1 (amounts are presented in %). ....	105
B.3: XRD Bulk results for Snadd and Kobbe Formations in well 7222/11-1. ....	106
C.1: A: Partially dissolved albite at 780.50 m depth in the Snadd Formation; B: Microcline (Kfs) is present in the Snadd Formation at 778.80 m depth. Qtz – quartz; kao – kaolinite; red arrows show chlorite coating. ....	107
C.2: A: The sample represents authigenic kaolinite (kao), chlorite coating (chl) and quartz overgrowths (red arrows) at 780.50 m depth in the Snadd Formation; B: Well- developed chlorite coating (chl) with K-feldspar (Kfs) at 780.50 m depth in the Snadd Formation. ...	108
C.3: A: Folded muscovite (M) grain due to mechanical compaction, being replaced by kaolinite (orange arrows). Black arrows show framboidal pyrite aggregates at 806.60 m depth in the Snadd Formation; B: Zircon mineral shows zonation at 2230.60 m depth in the Kobbe Formation. ....	109
C.4: A: Authigenic pore-filling kaolinite at 2233.60 m depth in the Kobbe Formation; B: The light blue arrows show quartz overgrowths at 2230.60 m depth in the Kobbe Formation. ..	110
C.5: A: The sample shows thick chlorite coating (green arrows) around the detrital grains. The pore space filled with kaolinite (orange arrows), calcite and chlorite at 2241.65 m depth in the Kobbe Formation; B: Non-continuous chlorite coating and quartz overgrowths at 2233.60 m depth in the Kobbe Formation. ....	111



# **1. Introduction**

## **1.1 Purpose of the study and project description**

This master thesis has been accomplished for Department of Geosciences at the University of Oslo as a part of my master degree in geology. The thesis is a one year thesis work and based on sedimentological and petrographic analysis and geophysical logs. The aims of the project to increase the understanding of the distribution, quality and differences within and between the Middle to Late Triassic Snadd Formation and the underlying Middle Triassic Kobbe Formation located in the Barents Sea. The work will contribute to a better understanding of the reservoir quality found in the Kobbe and Snadd Formations. The thesis will also contribute to mapping out the potential for reservoir enhancing processes in the Triassic successions in the Barents Sea.

Reservoir properties of sandstones from the Barents Sea area are a function of initial composition and texture, mechanical and chemical compaction processes. Important factors include grain size, sorting, and mineralogical composition, amount of matrix, amount of quartz cement and amount of early cement (carbonate and kaolinite). These factors are also function of provenance, transport processes, climate, and depositional environment. A good understanding of the factors controlling reservoir properties of different sandstones units is essential for prediction of reservoir properties prior to drilling.

## **1.2 Study area**

The data for this master thesis is taken from well 7222/11-1 (Figure 1.1) that is operated by Statoil Petroleum AS. The well named Caurus was drilled on the Bjarmeland Platform in the Barents Sea to determine hydrocarbons in Snadd Formation of Carnian age and in Kobbe Formation of Anisian age. The well was drilled in 2008 and both oil and gas were discovered. In Snadd Formation two gas bearing levels were found; at the top of the formation of Early Norian age sandstones and at 771 meter depth of Late Carnian age sandstones with a gas/water contact at 785 meter depth. In Kobbe Formation both gas and oil were discovered; at 2112 to 2115 meter depth, oil was found in channelized sandstones of Anisian age. Oil and

gas were found in Anisian marine sandstones at 2210 to 2238 meter depth. The gas/oil contact is at 2233.2 meter depth.

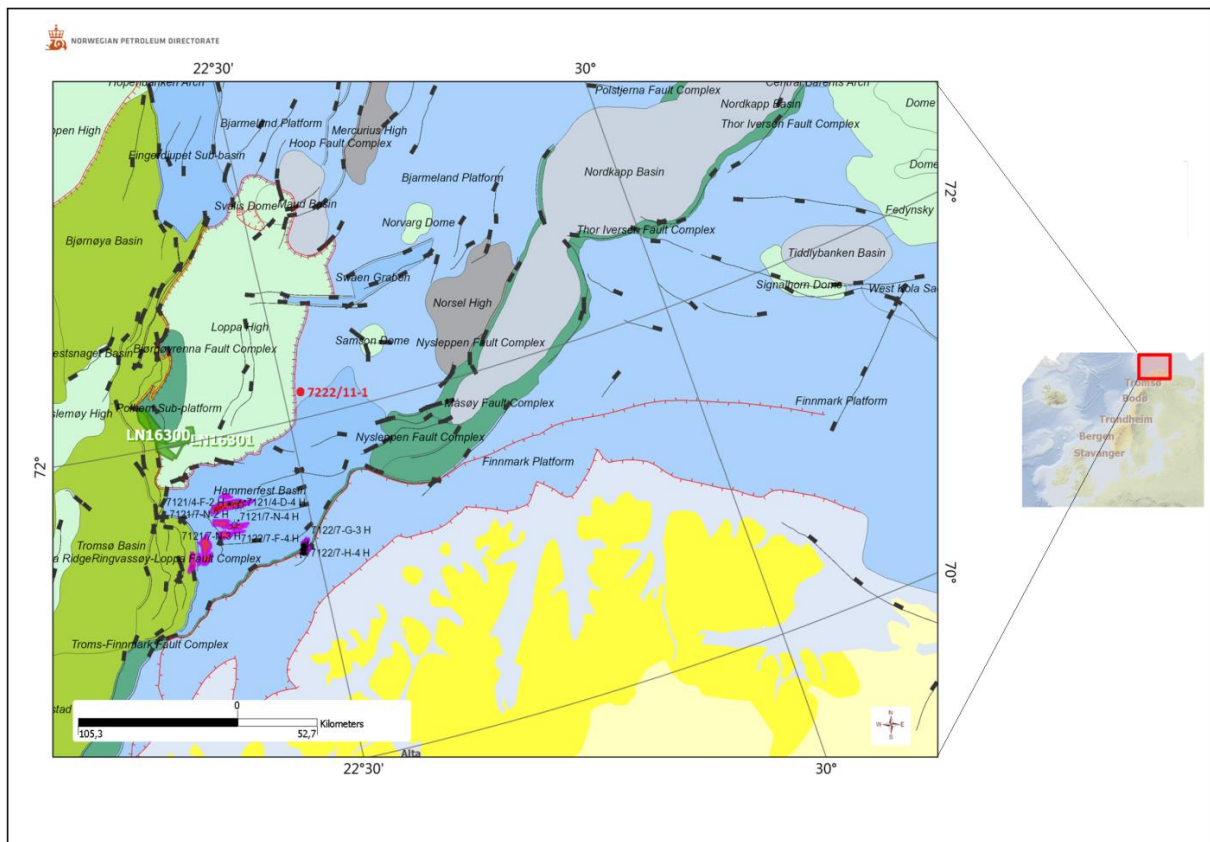


Figure 1.1: Overview of the main structural elements of the SW Barents Sea. The study area is marked by red dot on the map (modified after NPD Factmaps 2016).

## 2. Geological settings

### 2.1 Regional geology of the Barents Sea

The Barents Sea is an epicontinental shelf bounded by young passive margin to the west and north and developed as a result of Cenozoic opening of the Norwegian-Greenland Sea and the

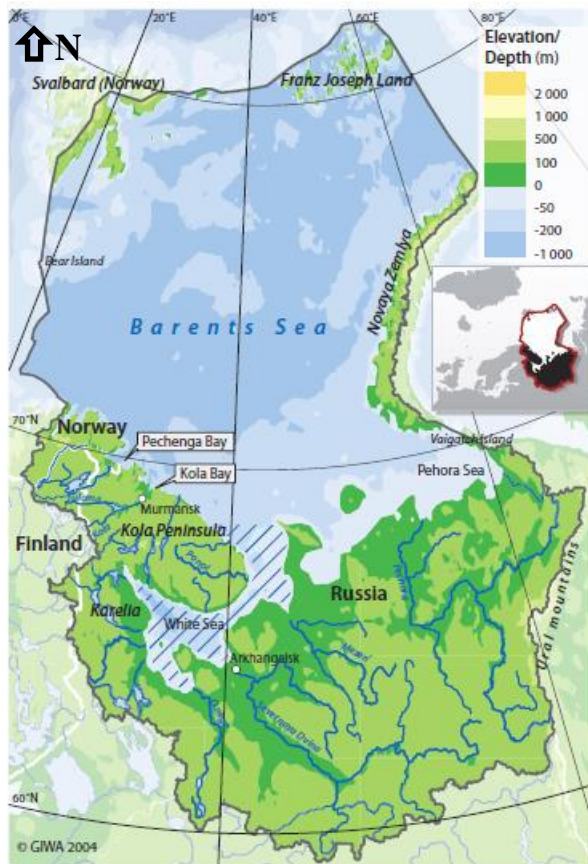


Figure 2.1: Location of the Barents Sea (USGS, 2003).

Eurasia Basin (Faleide et al., 1984, Breivik et al., 1995). The Barents Sea located between the Norwegian-Greenland Sea, Novaya Zemlya and the Arctic Ocean, bordered by Svalbard to the northwest and Franz Josef Land to the northeast (Figure 2.1) (Johansen et al., 1992). The area covers about 1.3 million km<sup>2</sup> with 300 m average water depth (Faleide et al., 1984, Breivik et al., 1995). The continental shelf of the Barents Sea spreads out about 1000 km to north-south and east-west direction and displays a continuous sedimentary succession from late Palaeozoic to Quaternary age. In some places the sedimentary succession exceeds about 15 km in thickness (Faleide et al., 1993a, Faleide et al., 1993b, Gudlaugsson et al., 1998).

The Barents shelf with deep sedimentary basins, highs and platforms are formed as a result of different geological and tectonic processes with complex geological history. The complex geological and tectonic history of the Barents Sea started from the Caledonian mountain building 400 million years ago and continued until continental crustal separation, which led to opening of Northern North Atlantic Ocean (Doré, 1995). The thick sedimentary sequence of the Barents Sea including siliciclastic rocks, carbonates and evaporates range from the Devonian to the Quaternary age (Larsen et al., 1993). The metamorphic basement of the western Barents Sea consolidated during the Caledonian orogeny in the Early Devonian. The

Caledonian orogeny resulted from the collision of Laurentia and Baltica continents with closure of Iapetus Ocean (Figure 2.2). Since the Late Devonian, three major tectonic phases took place and formed the main structural elements of the Barents Sea (Gading, 1993). The three major rift phases took effect from Late Devonian-Carboniferous, Middle Jurassic-Early Cretaceous and Early Tertiary (Faleide et al., 1993a, Faleide et al., 1993b, Faleide et al., 2008).

The Eastern part of the Barents Sea was stable since the Late Carboniferous, while the Western part of the Barents Sea was tectonically active from the Late

Palaeozoic (Gabrielsen et al., 1990). During the Late Palaeozoic crustal extension effected in the Barents Sea area with rift movements to the west, formation of well-defined rift and pull-apart basin to the south resulted strike-slip faults in the north (Faleide et al., 1984). In the Late Devonian-Early Carboniferous Svalbardian transpression and transtension developed faulting and graben formation. In the Middle Carboniferous carbonate shelf was settled and appeared from the Sverdrup Basin to the Pechora Basin. The carbonate sedimentation with evaporates and clastic sedimentation was dominating until the Early Permian. The Early Permian reefs are located on the southern edge of the Nordkapp Basin, while the Late Permian reefs are situated parallel to the present Finnmark Platform to the north. More clastic sedimentation

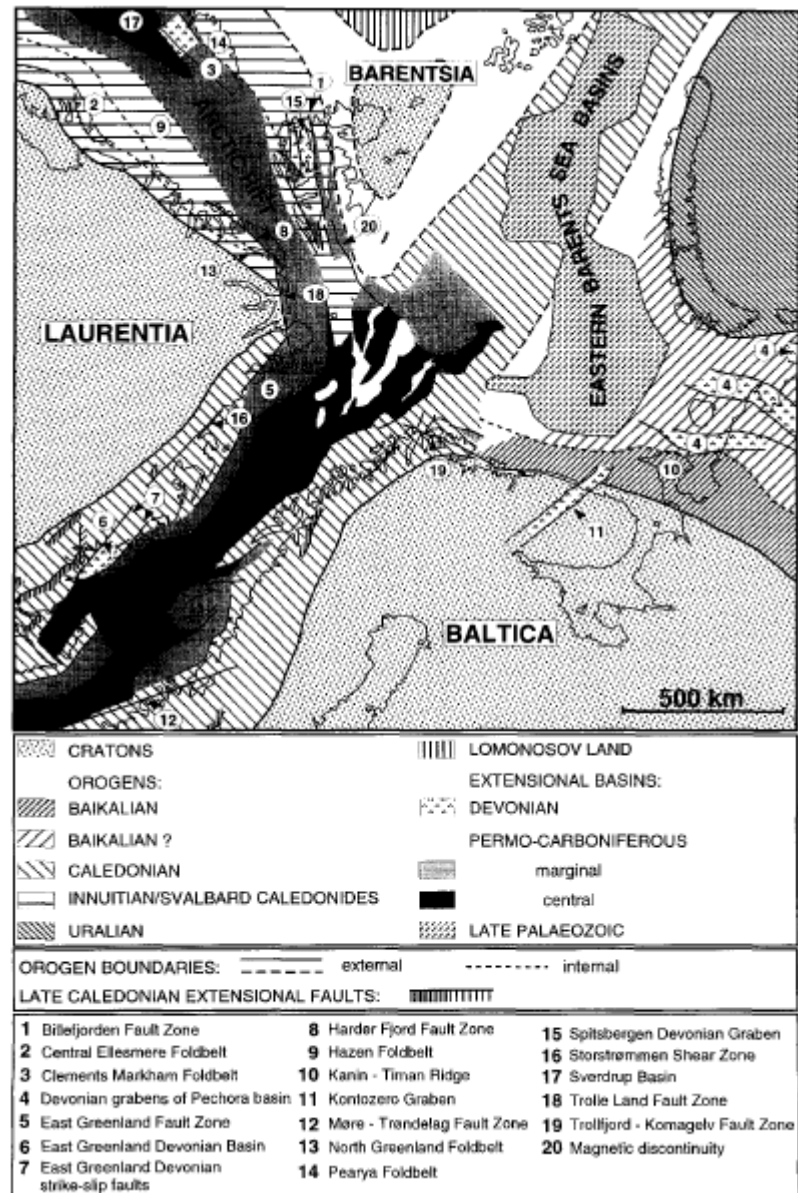


Figure 2.2: Regional geology of the Barents Sea to end-Permian time (Gudlaugsson et al., 1998).

showed up on the shelf area from the Late Permian. Lower impedance sediments deposited between the Permian and the Triassic and it is marked the boundary between the two geologic periods. During this period thick Triassic sediments deposited in the basin as a result of regional subsidence with high sedimentation rates. In the Eastern Barents Sea the Early and Middle Triassic subsidence was more dominated than at the western part and it represented thick sedimentation towards the east. In the Lower Triassic marine conditions was prevailed with shale deposition while in the Late Triassic more sand was deposited with development of coals and the shale content increases to the direction of north. The Triassic was a tectonically stable period.

During the Middle and Late Kimmerian the next major tectonic phase showed up and it has affected the rift systems with restricted basin circulation and reducing regimes developing. This tectonic event resulted large, deep-seated normal faults. During this tectonic and rifting phase, subsidence has been increased with igneous movements and started in the Sverdrup Basin and ended up with dolerite intrusions and basaltic lava flows on Svalbard and on Franz Josef Land. During Cretaceous, subsidence developed in the complete basin. Fault events in the Late Early Cretaceous resulted awakening of the Kimmerian fault systems. In the Late Cretaceous subsidence of the basin was continued but at slower rate.

The Kimmerian fault systems were reactivated again in the Palaeocene during the Laramide phase due to uplift of the Hammerfest and Nordkapp Basin and erosion of the Upper Cretaceous sediments. In the Norwegian-Greenland Sea the Laramide phase prevented the beginning of the sea floor spreading. In the Western Barents Sea uplift and erosion took place in the Cenozoic and Pleistocene. Due to uplift and erosion thick parts of the sedimentary column has been removed and transported in the basin (Gading, 1993).

## **2.2 Triassic evolution of the Barents Sea**

The Triassic was a tectonically quiet period in the western Barents Sea region, except some local tectonic events and faulting or tectonic unconformities, while strong subsidence has been affected in the northern and southern Barents Sea and formed important depocenters (Johansen et al., 1992, Riis et al., 2008). Tectonic movements, climatic changes and northward drift have been affected on the Triassic sedimentary succession in the Barents Sea with controlling the types of the sediments (Jacobsen and van Veen, 1984, Mørk et al., 1992,



Glørstad-Clark et al., 2011). The Svalbard Archipelago shifted from about 40° to 60° N at the same time and the depositional environment developed in arid to humid climate (Steel and Worsley, 1984, Glørstad-Clark et al., 2011) The total thickness of the Triassic sedimentary succession in Svalbard is 250-1200 m and increases to 2000-3000 m in the western Barents Sea (Riis et al., 2008).

The tectonic events of the Barents Sea was dominated by extensional tectonic movements in the Late Palaeozoic and Mesozoic with represented the collapse of the Caledonian and Uralian orogenic belts and progressive break-up of the Pangea supercontinent. These events created the major rift basins and the series of platforms and highs in the Barents Sea area (Doré, 1995).

During the Triassic the Barents Sea area acted as intracratonic basin and the sediments sourced from the eastern part of the area (Ziegler, 1988a, Skjold, 1998). Most of the Barents Sea area was affected by crustal extension and rifting during the Late Palaeozoic, developed uplift and tilting of the Loppa High (Ziegler, 1988b, Skjold, 1998, Glørstad-Clark et al., 2010, Glørstad-Clark et al., 2011). This extensional event marks the Late Permian-Early Triassic transition (Gudlaugsson et al., 1998, Johansen et al., 1994). In the Middle Carboniferous the rift zone was the continuation of the northeast Atlantic rift between Greenland and Norway. Late Palaeozoic structures show a fan-shaped array of NE-SW trending and horst and graben structures due to rifting phase (Gudlaugsson et al., 1998). Continental clastic sediments were deposited during this extensional event in the rift grabens and from the Late Carboniferous it was followed by post-rift carbonate platform and evaporates deposition through the Permian (Faleide et al., 1984, Larssen et al., 2002). Due to uplift of the Uralian Mountains in the southeast and landmasses in the south, evolution of the clastic sediments developed in the Late Permian as well as the Norwegian-Greenland rift system and a continuous seaway opened between the Arctic and the northwest European basins. During the Triassic the seaway was closed (Faleide et al., 1984, Johansen et al., 1992, Larssen et al., 2002).

The Triassic depositional system was developed due to erosion of landmasses from the Uralian Mountains and resulted thick siliciclastic deposits in the Russian and the Norwegian Barents Sea defined by stacked clastic wedges prograding toward the west and northwest. The landmasses are presenting multiple sediment source areas (Jacobsen and van Veen, 1984, Johansen et al., 1992, Skjold, 1998, Riis et al., 2008, Smelror et al., 2009, Glørstad-Clark et al., 2010, Glørstad-Clark et al., 2011). According to Glørstad-Clark et al., (2011) the northern

Barents Sea represents the development of seismic prograding clinoforms from the east and southeast through the Triassic, indicating a continuous shallow shelf area with shelfal to paralic deposition from the southern Barents Sea to the main Svalbard Archipelago (Riis et al., 2008).

From the Early Triassic through the Ladinian the Triassic sedimentary succession represents a gradual infill of the basin. Due to late Palaeozoic rifting the paleotopography has been affected on Early Mesozoic sedimentation. The Loppa and the Stappen Highs mark boundaries at the west part for the sediments prograding from the south and southeast areas (Faleide et al., 1984, Skjold, 1998, Glørstad-Clark et al., 2010, Glørstad-Clark et al., 2011). In the Early and Middle Triassic uplift has been affected on the Loppa High, developing a local source area for smaller-scale depositional environment (Glørstad-Clark et al., 2010, Glørstad-Clark et al., 2011). The accommodation space at the eastern part of the Loppa High was filled with sediments and the further deposition took place at the western part of the Loppa High in the Middle Ladinian. The Loppa High was a main depocenters in the Middle Triassic (Larssen et al., 2002, Glørstad-Clark et al., 2010, Glørstad-Clark et al., 2011). The Svalis Dome and the Maud Basin represent the north-eastern barrier of the Loppa High, developing salt structures and its rim syncline (Gabrielsen et al., 1990).

In the Late Triassic and Early Jurassic the climate changed from arid to humid and resulted transportation of clastic sediments from the continent into the Barents Sea. In the late Middle Jurassic-Early Cretaceous widespread rifting phase took place with strike-slip settings along old features in the SW Barents Sea, resulted Bjørnøya, Tromsø and Harstad rift basins (Faleide et al., 1993a, Faleide et al., 1993b). The continuous rifting phase throughout the Cretaceous observed in very deep basins in the SW Barents Sea. In the Late Jurassic organic-rich shales were deposited across the Barents Sea, indicating a very important source rock for this area. The Triassic succession was uplifted and eroded in the Barents Sea area as well as the north-western and northern areas in Spitsbergen with development of a large igneous area in the Franz Josef Land (Doré, 1991, Faleide et al., 2008, Worsley, 2008).

In the Early Cenozoic the western part of the Barents Sea developed into sheared margin, associated with rifting and continental break-up, pursued by seafloor spreading in the Norwegian-Greenland Sea and Eurasia Basin. During the Cenozoic regional uplift and erosion were the defining processes in the Barents Sea area, resulting a north-south tilting of the crustal block (Faleide et al., 1993a, Faleide et al., 1993b). In the Oligocene the region became

tectonically quiet and stable period but during the Neogene, basin-wide uplift took place, observed the deposition of a large sedimentary wedge consisting glacial deposits from the Late Pliocene-Pleistocene (Faleide et al., 1996). The Figure 2.3 is representing the possible paleogeographic reconstruction of the depositional environments during the Triassic according to Glørstad-Clark et al., (2010).

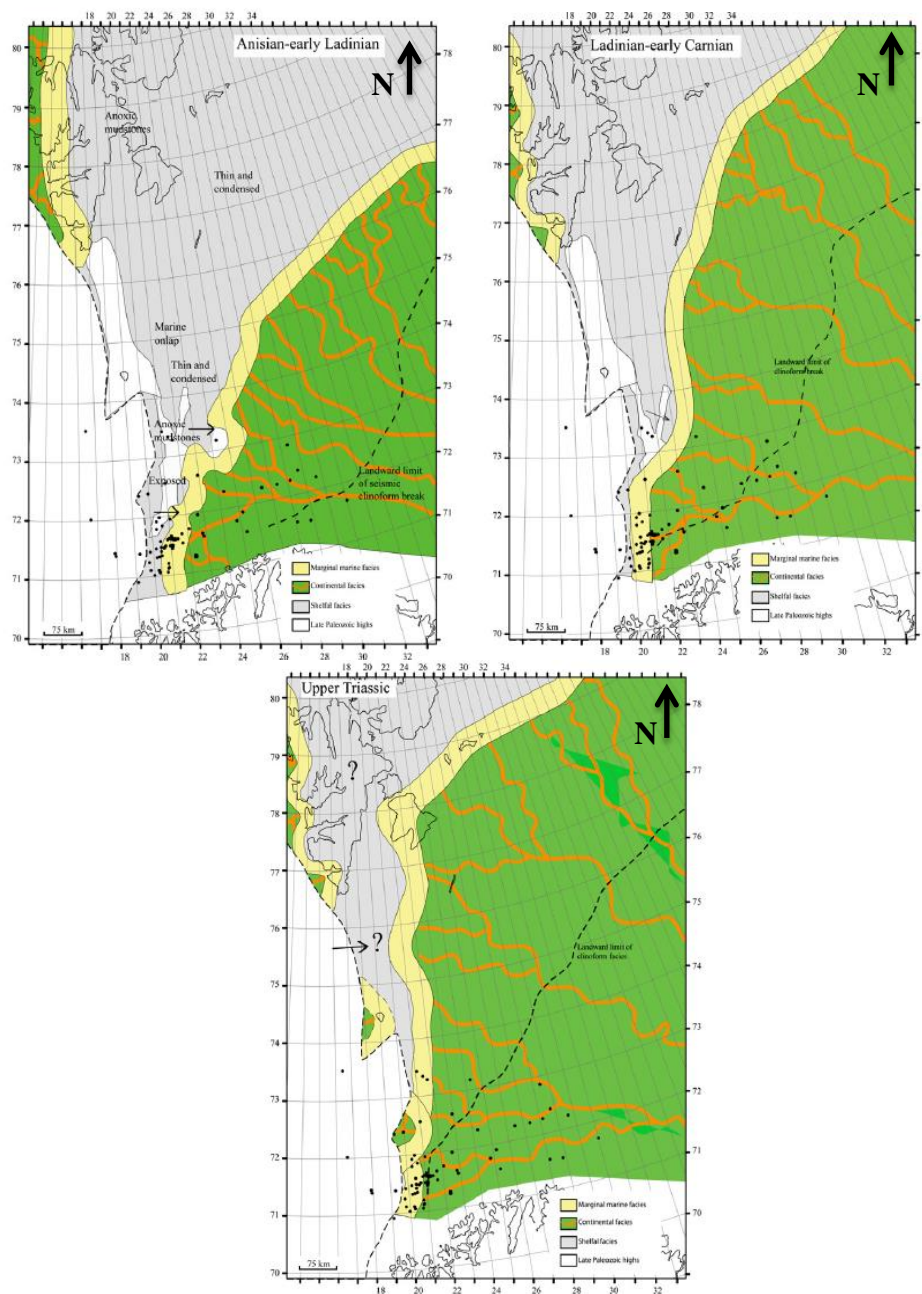


Figure 2.3: Paleogeographic reconstruction of the depositional environments during the Triassic (Glørstad-Clark et al., 2010). The marginal marine facies presented by yellow colour. The green represents the continental facies and the shelfal facies presented by grey color.



## 2.3 Structural geology of the Barents Sea

Southern part of the Barents Sea is dominated by ENE-WSW trends and it is characterized by the major fault complexes which are surrounding the Hammerfest and Nordkapp Basins. It is almost parallel to another major zone to the north characterized by the Veslemøy High and the fault complexes splitting the Loppa High from the Bjørnøya Basin (Gabrielsen et al., 1990, Faleide et al., 1993a, Faleide et al., 1993b). During the Mesozoic and Cenozoic the western part of the Barents Sea was a tectonically active region, while the eastern and northern part of the Barents Sea was relatively stable region since the Late Carboniferous, with few tectonic activities. The SW Barents Sea has three major geological provinces separated by major fault complexes (Faleide et al., 1993a, Faleide et al., 1993b):

1. The Oceanic Lofoten Basin and Vestbakken volcanic province
2. The SW Barents Sea basin province of deep Cretaceous and Early Tertiary basin (Harstad, Tromsø, Bjørnøya, Sørvestsnaget Basins)
3. Mesozoic basins and highs (Finnmark, Bjarmeland Platform, Hammerfest Basin, Loppa High, Fingerdjupet Subbasin)

The Triassic and Early Jurassic were a tectonically quiet period. Tilting events were acting in the Stappen and Loppa High and subsidence took place in the Early Triassic in the eastern areas with sediment influx from the east. In the Nordkapp and Maud Basin salt tectonism was dominant. In the Middle Jurassic the block faulting developed again, continued and increased during the period from the Late Jurassic to Early Cretaceous, formed the present major basins and highs. In the Late Jurassic three complicated structures of the central SW Barents Sea were developed. The Hammerfest Basin was formed in the Late Jurassic and linked to the Loppa High by the Asterias Fault Complex and along these faults syn-tectonic sediments were deposited from the pre-Permian age (Faleide et al., 1996). The Loppa High was created due to the Late Jurassic to Early Cretaceous and the Late Cretaceous-Tertiary tectonic events. The major fault complex was developed during the Late Jurassic tectonism but it was established at shallow part of the Bjørnøya Basin in the Early Cretaceous (Gabrielsen et al., 1990). The Tromsø Basin had developed due to extension in the Late Jurassic-Early Cretaceous and contains salt diapirs in the Late Palaeozoic times. North of the Tromsø Basin situated the Bjørnøya Basin, the two basins were joined together in the Late Palaeozoic and in the Late Cretaceous they separated from each other by the Bjørnøyrenna Fault Complex. The

sediments in the Bjørnøya Basin have an age of Early Cretaceous (Faleide et al., 1993a, Faleide et al., 1993b). The Sørvestsnaget Basin is located in the west and contains very thick Cretaceous succession and sediments from the Tertiary, restricted by the Vestbakken Volcanic region in the north (Gabrielsen et al., 1990).

In the Barents Sea region the major regional fault zones were formed in the Carboniferous or in earlier ages. The area was divided into separate fault blocks analogues to the major fault complexes and defined by deep-seated fault complexes (Gabrielsen, 1984).

The major structural elements of the Barents Sea, the study area and the well database are shown on Figure 2.4. The study area is described in section 2.3.1.

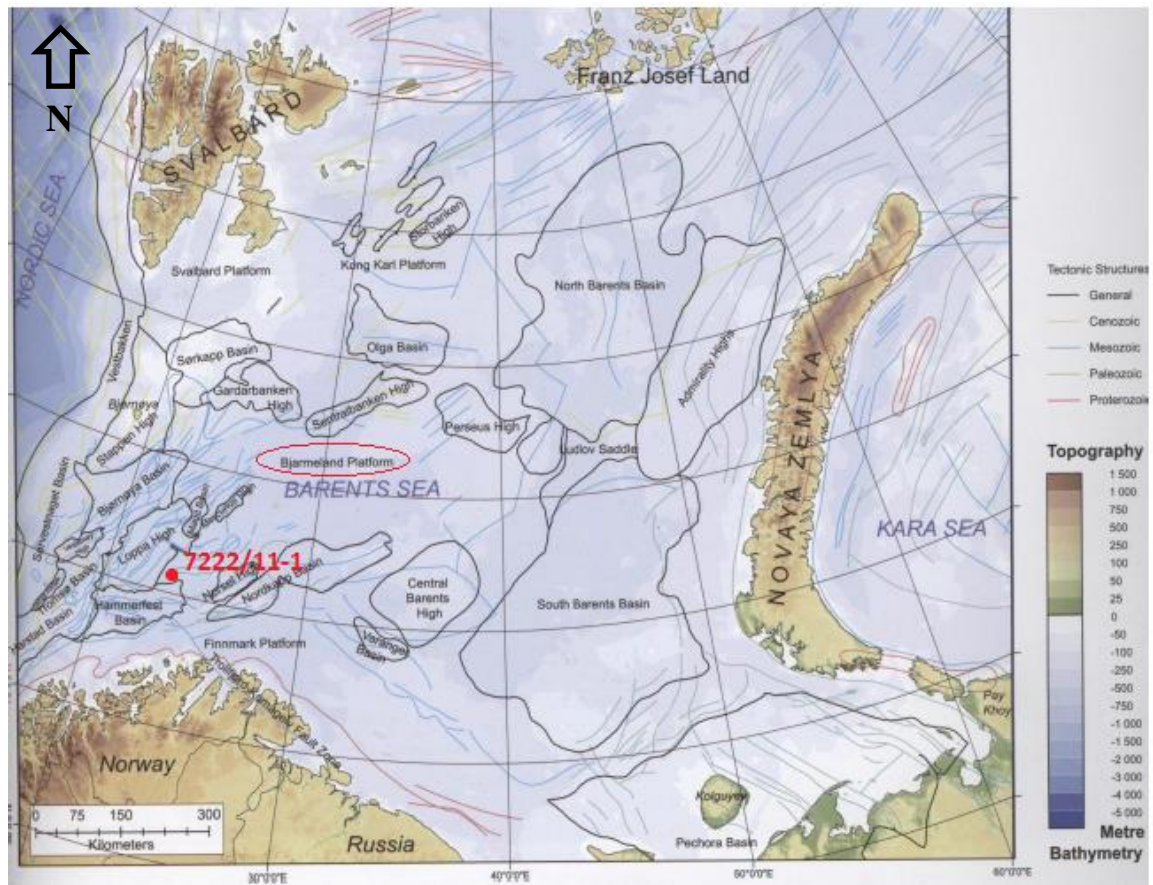


Figure 2.4: The major structural elements of the Barents Sea, the study area (red circle) and the well database (red dot) (modified from Smelror et al., 2009).

### 2.3.1 The Bjarmeland Platform

The well 7222/11-1 was drilled on the Bjarmeland Platform which is located between the Hammerfest and Nordkapp Basins to the south and southeast and the Sentralbanken and the

Garderbanken Highs to the norths (Figure 2.4). The platform is bordered by the Fingerdjupet Subbasin and the Loppa High to the west. The area includes several smaller structures such as the Norsel and Mercurius Highs, the Svalis, Samson and Norvang Domes, the Swaen Graben, the Maud Basin and the parts of the Hoop Fault Complex (Gabrielsen et al., 1990, Gading, 1993). The Svalis Dome characterized by evaporates and salt diapirism. The platform has Permian age but has been tilted due to Tertiary uplift. Due to the uplift the sediments dip to the south and the older sediments subcrop the north at the unconformity at the base of the Quaternary. The Bjarmeland Platform represents a relatively stable structural element since the Late Palaeozoic. The boundary from the Early Carboniferous siliciclastics to the Late Carboniferous to Permian carbonates has been characterized as a transition from a pre-platform development. The Triassic siliciclastics sediments show more than 2 km thickness in the well 7222/11-1 and sourced from the west and east areas and covered the platform. The post-Triassic succession is thin as a result of the erosion in the Tertiary and often contains Jurassic to Cretaceous sediments with less than few hundred meter thicknesses overlain by the Pleistocene to recent sediments (Gabrielsen et al., 1990, Larssen et al., 2002). The Bjarmeland Platform is underlined by Palaeozoic and Precambrian rocks and started to develop as a stable platform in the Late Carboniferous. In the Late Permian to Early Triassic the platform has been affected by fault events, developed structural highs which are parallel with east of the fault zone. This structurally-elevated area consists of Lower and Middle Triassic sequences and maximum thickness of Upper Triassic sediments and it has been transported into the basin. During the Late Mesozoic and Tertiary, tectonic events were active in the basin and developed to the present Loppa High and Fingerdjupet Subbasin, which displays the end of the Bjarmeland Platform to the west now. The structural elements are mainly connected to salt tectonics and weak extension within the platform (Gabrielsen et al., 1990, Gading, 1993, Larssen et al., 2002).

## 2.4 Stratigraphic framework

The Triassic succession consists of several lithostratigraphic formations presented in the Figure 2.5.

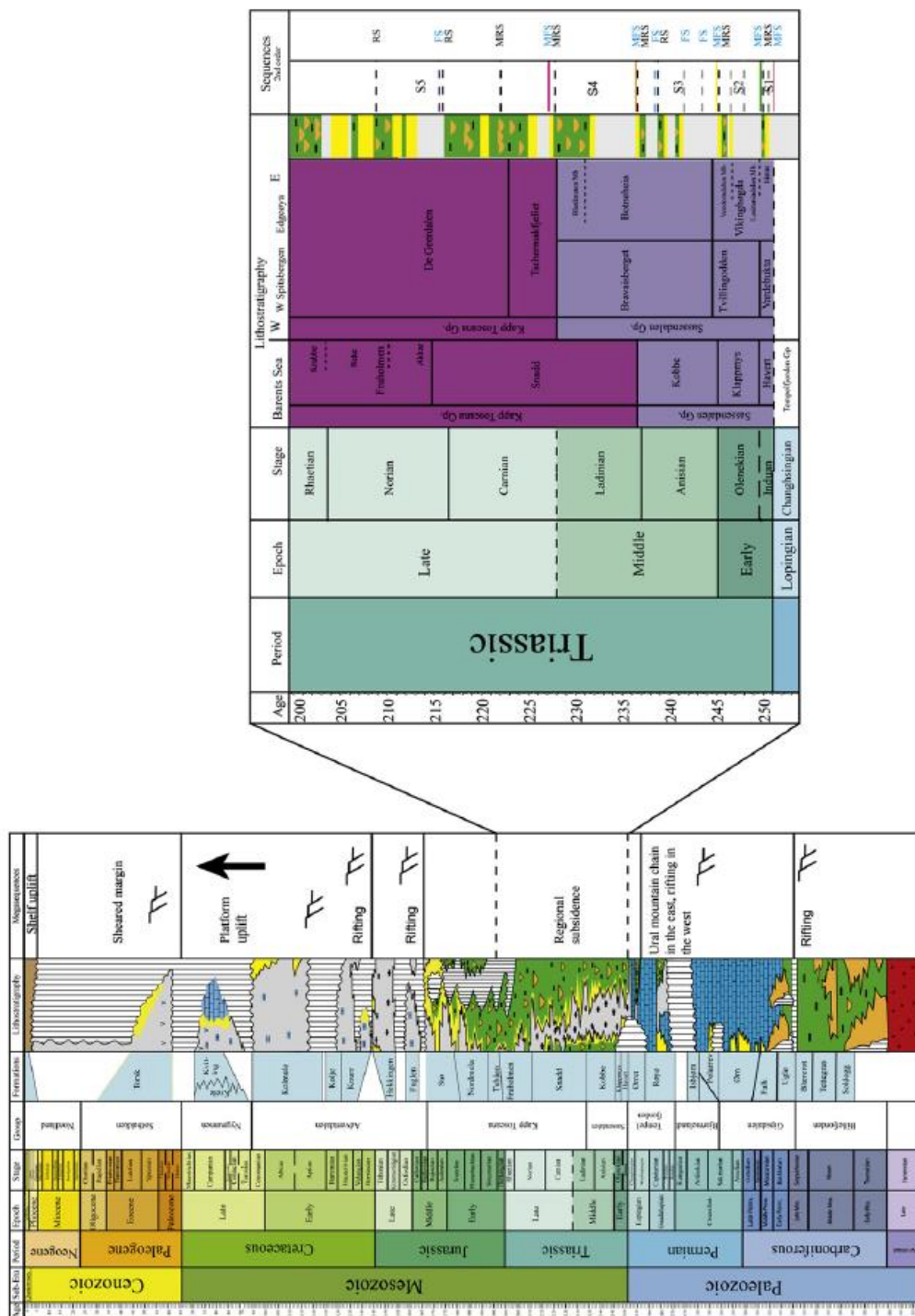


Figure 2.5: The Triassic lithostratigraphy and the Triassic sequence stratigraphic subdivision (2nd order) in the SW Barents Sea (Glørstad-Clark et al., 2010).

### **2.4.1 Sassendalen Group**

The Sassendalen Group consists of Early and Middle Triassic clastic sediments in the Barents Sea region and in Svalbard. The lithology is characterized by shales and siltstones with subordinate sandstones and minor amounts of carbonate rocks. Due to the Tertiary fold-thrust belt the group has been exposed on the western, eastern and central part of Svalbard as well as on Edgeøya, Barentsøya, southwestern Nordaustlandet and Bjørnøya and continues in the subsurface between these islands in the Barents Sea region to the Hammerfest Basin (Dallmann, 1999).

In western Svalbard the group shows coastal, deltaic to shallow sediments. The coastal sediments change into shelf mudstones to the east and south and the upper part of the succession is organic rich and phosphatic. Shallow to deep sediments were deposited in the SW Barents Sea. The Sassendalen Group shows stacked transgressive-regressive sequences and each formation being started with a regional transgression. These sequences can be outlined across the Barents Sea to Arctic Canada and Eastern Siberia (Mørk et al., 1989).

The Sassendalen Group is subdivided into ten formations, Vardebukta, Tvillingodden and Bravaisberget Formations on western Svalbard, Vikinghøgda and Botneheia Formations in central and eastern Svalbard, Urd Formation on Bjørnøya and Steinkobbe Formation on the Svalis Dome. Three formations are defined in the SW Barents Sea the Havert Formation, Klappmys Formation and Kobbe Formation (Dallmann, 1999).

#### **2.4.1.1 Kobbe Formation**

The Kobbe Formation is a part of the Sassendalen Group and the Ingøydjupet Subgroup with age of Anisian (Figure 2.6). The reference well of the Kobbe Formation is 7120/9-2 from 4245 m to 3962 m, the type well is 7120/12-2 from 3095 m to 2927 m. The thickness of the formation in the type well is 168 m and in the reference well is 283 m with 20 m thick shale succession, moves into interbedded shale, siltstone and carbonate cemented sandstone. The depositional environment has been interpreted as transgressive pulse which is marking the base of the sequence with clastic marginal regimes from the southern coastal areas. The base of the formation is marking the beginning of the phosphatic organic rich shales on Svalbard and in the Sverdrup Basin. This organic rich shale unit is represented by Botneheia Member of the Barentsøya Formation in central and eastern Svalbard. The Kobbe Formation presents

conformity to the Bravaisberget Formation in western Svalbard (Dalland et al., 1988, Worsley, 2008)

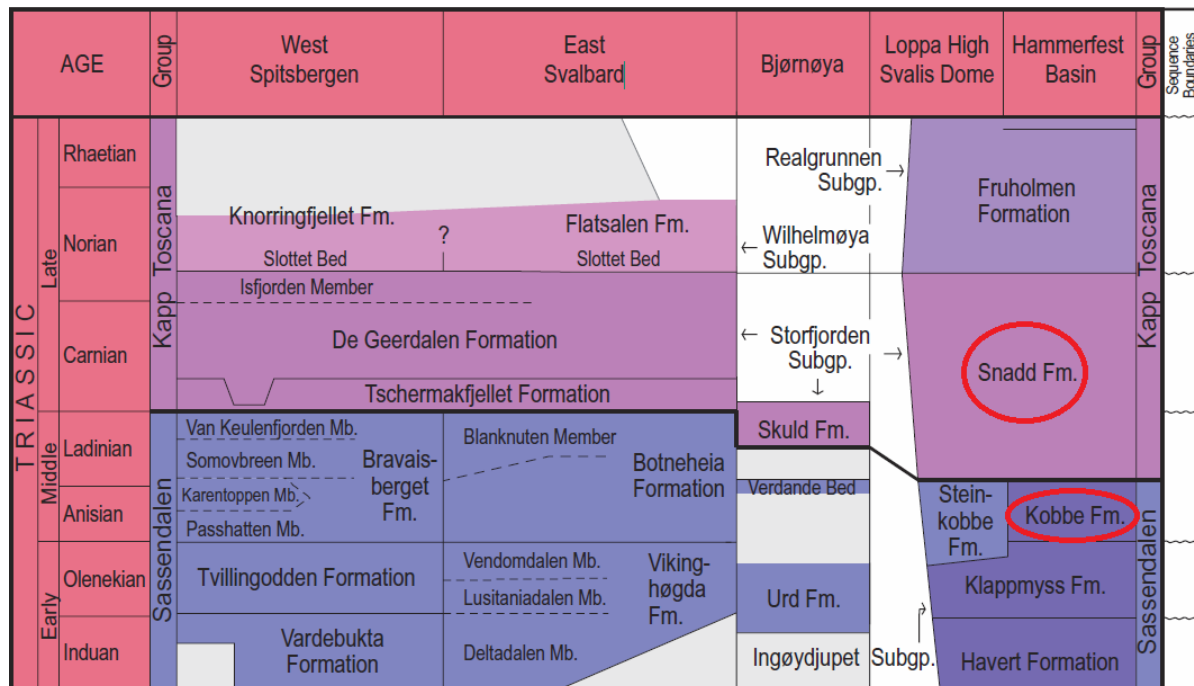


Figure 2.6: The Triassic lithostratigraphy in the Barents Sea and on Svalbard (red circle the studied formations) (Mørk et al., 1999).

## 2.4.2 Kapp Toscana Group

The Kapp Toscana Group consists of Late Triassic to Middle Jurassic shales, siltstones and sandstones in the Barents Sea and on Svalbard. The group represents grey shales of the Tschermakfjellet Formation at the base and it grades upward into the immature sandstones of the De Geerdalen Formation. This sequence consists of coarsening upward successions with increasing volumes of sandstone towards southwestern, north-eastern and eastern areas, while in central Svalbard shales are dominant. The upper part of the sequence shows a condensed clastic sedimentary succession on Svalbard and it is more developed towards the east areas (Wilhelmøya Subgroup). The Realgrunnen Subgroup in the Barents Sea represents relatively thick sequences, sandstones and shales are also dominant in the Barents Sea region (Dalland et al., 1988, Dallmann, 1999).

Due to the Tertiary fold-thrust belt the group has been exposed on the western, eastern and central part of Svalbard as well as on Edgøya, Barentsøya, Bjørnøya, Hopen and Kong Karls

Land and continues in the subsurface between these islands in the Barents Sea to the Bjarmeland Platform and the Hammerfest and Nordkapp Basins (Dallmann, 1999).

The depositional environment of the group has been interpreted as a generally nearshore, deltaic environment and is defined by shallow marine and coastal reworking of deltaic and fluviodeltaic sediments (Mørk et al., 1982).

The Kapp Toscana Group is subdivided into five formations in the Barents Sea region: Snadd Formation, Fruholmen Formation, Tubåen Formation, Nordmela Formation and Stø Formation (Dallmann, 1999).

#### 2.4.2.1 Snadd Formation

The Snadd Formation is a part of the Kapp Toscana Group and the Ingøydjupet Subgroup, has an age from Late Ladinian to Early Norian (Figure 2.6). The type and the reference well is the same for the Snadd Formation as for the Kobbe Formation and represents in the type well from 2927 m to 2354 m while in the reference well from 3962 m to 2552 m. The formation consists of grey shales at the base, coarsening upwards into shale units with interbedded grey siltstones and sandstones. The lower and middle part of the formation is characterized by limestones and interbedded calcareous sediments. The upper unit represents coaly lenses and the top of the unit red-brown shales occur. The depositional environment has been interpreted as distal marine environment with transgressive pulse that is submerged all structural highs and platform areas in the region. During Carnian large-scale progradation of deltaic systems took place over the whole region. The Snadd Formation has similarities with the Tschermafjellet and De Geerdalen Formations on Svalbard (Dalland et al., 1988, Worsley, 2008).

## 2.5 Source rocks in the Barents Sea

Source rock is a sedimentary unit, rich in organic matter (kerogen) from which hydrocarbon can be generated or is able to being generated by thermal conductivity of organic matter (Doré, 1995). It is an important part of the petroleum system with the total organic content of 1%. The petroleum system contains an active source rock, then oil and gas generate and all of the elements and processes are required for a petroleum accumulation to exist (Magoon and Dow, 1994). During burial and consequent heating, the kerogen breaks down to form



hydrocarbons resulted oil at lower temperature than gas. The terrestrial kerogen tends to generate gas, while the marine kerogen (algal material) is oil-prone (Doré, 1995).

Large scale of source rocks show up in the Barents Sea area, presented in Figure 2.7.

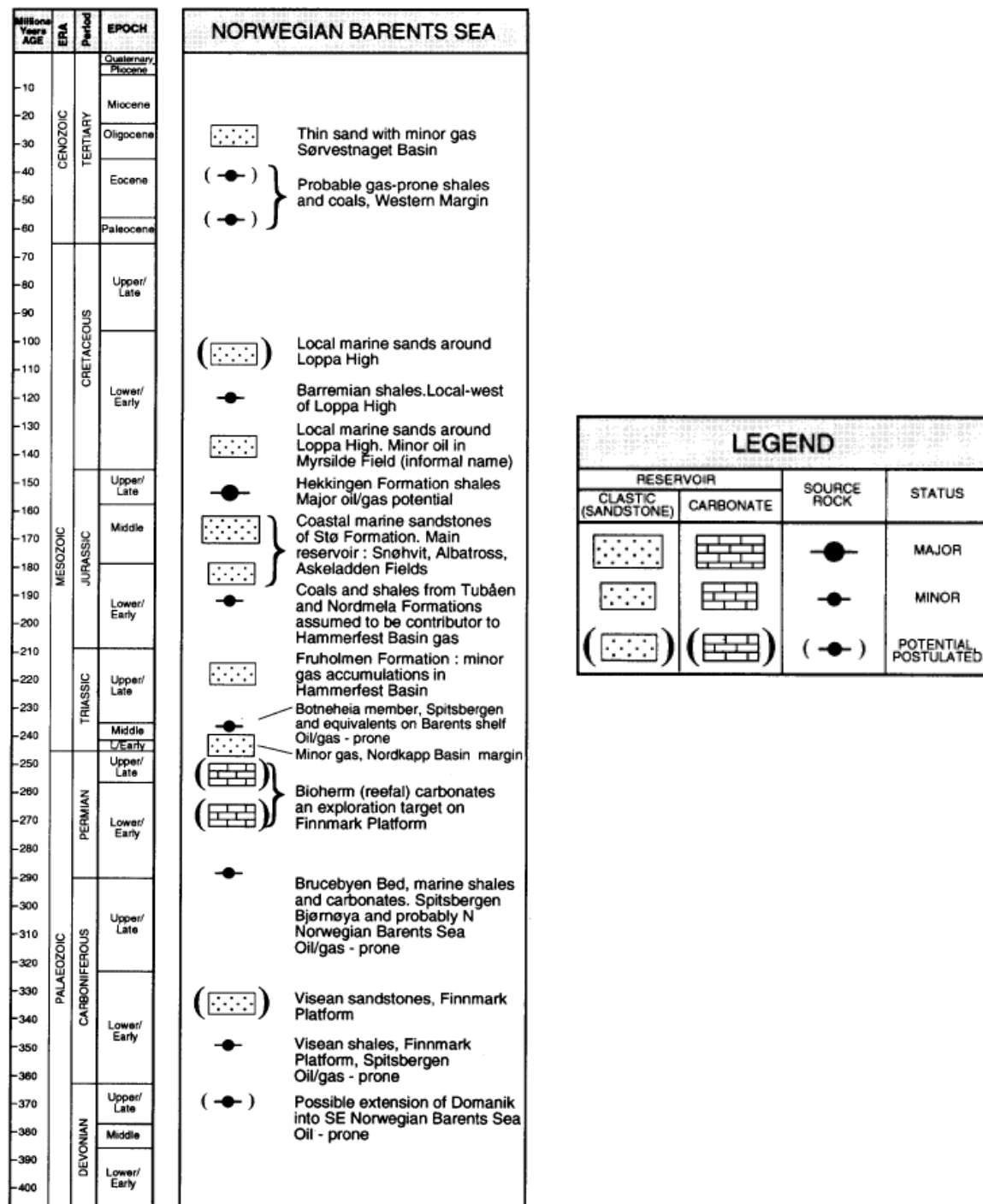


Figure 2.7: Time of deposition of proven and potential source and reservoir rocks in the Norwegian Barents Sea (Doré, 1995).



The source rocks in the Barents Sea are ranging in age from Silurian to Cretaceous and has been specified as a multisourced and overfilled petroleum system (Ohm et al., 2008, Henriksen et al., 2011b). The main source of the petroleum in the Norwegian Barents Sea is Late Jurassic dark, organic rich shales that are widespread over most of the Barents Sea region. Relatively the same shales give the source for most of the hydrocarbons in the North Sea and this unit is called the Hekkingen Formation in the Norwegian Barents Sea (Dalland et al., 1988, Doré, 1995). This unit is believed to be enough mature for oil and gas generation in a narrow belt at the western margin of the Hammerfest Basin and the Loppa High. Accumulation of the hydrocarbons in the Hammerfest basin was sourced from the Upper Jurassic but according to Larsen et al., (1993) most of the discovered gas extracts are from the underlying Lower Jurassic shales and coals. On Svalbard there is a Middle Triassic black phosphatic shale, called Botneheia Member and is known as a potential source rock for oil and gas (Bjørøy et al., 1979). The same unit has been identified during drilling in the southern Barents Sea which may be widespread but variable quality. This unit is mature for oil generation at several parts of the platform and gas-mature in the Hammerfest and Nordkapp Basins (Doré, 1995). The Upper Triassic shales may also be source rocks in the western part of the Barents Sea and contribute some of the Norwegian hydrocarbons but are not thought to be a major source (Johansen et al., 1992, Doré, 1995).

In the SW Barents Sea the Ladinian age marine and prodeltaic shale in the lower part of the Snadd Formation may be a potential source rock with high hydrogen index (HI) values of 400-500 mg/g TOC. In the middle Triassic the source rocks started to generate oil in the Barents Sea and achieved the maximum in oil generation in the Ladinian (Henriksen et al., 2011b).

## **2.6 Reservoir rocks in the Barents Sea**

Several reservoir rocks are presented in Figure 2.7. Reservoir rock is a term of a porous and permeable unit that is able to hold hydrocarbon. Porous sandstones, limestones and dolostones constitute the best reservoir rocks. The reservoir rocks in the Norwegian Barents Sea mainly are Jurassic sandstones. The major discoveries are Snøhvit, Albatross and Askeladden in the Norwegian sector and contain Lower-Middle Triassic sandstones. The Stø Formation has very good reservoir properties (porosity, permeability) and it was deposited in a coastal marine environment and moved into the Hammerfest Basin (Dalland et al., 1988, Doré, 1995). It has

been estimated that 85% of the petroleum reserves in the Norwegian Barents Sea lie within the Stø Formation (Larsen et al., 1993) and most of the resources are natural gas, except a thin oil leg in the Snøhvit Field (Figure 2.8). The Jurassic age traps in the Norwegian sector are

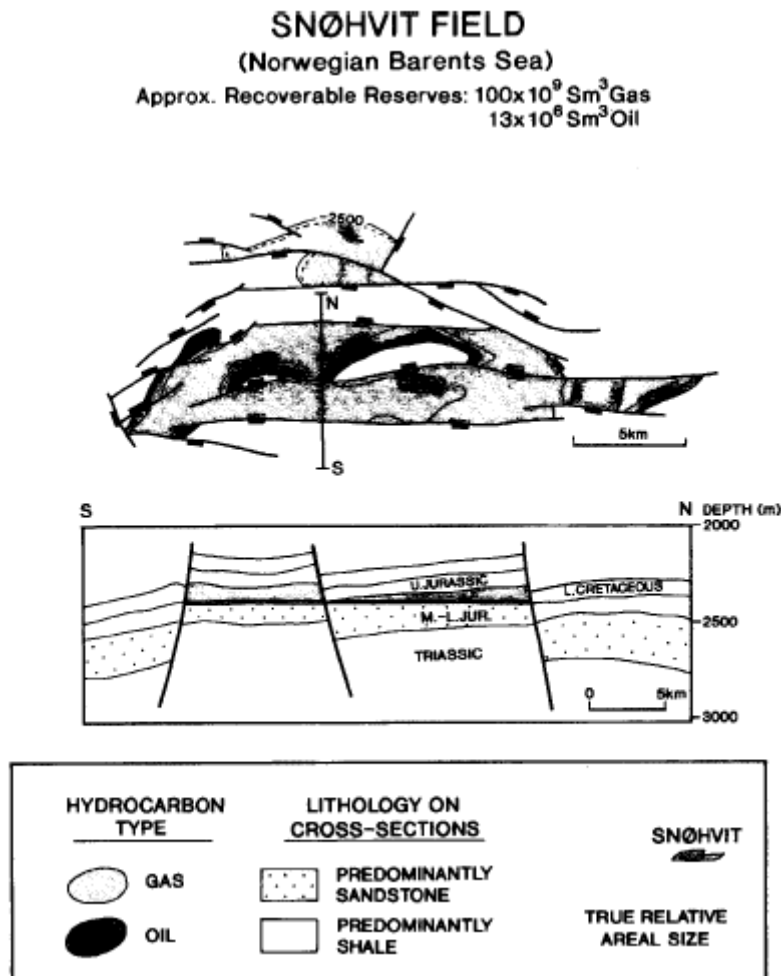


Figure 2.8: Geological cross-section of the Snøhvit Field, represents the fault bounded traps in the Norwegian sector (Doré, 1995).

usually fault-bounded positive blocks (Figure 2.8). The hydrocarbons are sealed by Upper Jurassic shales in the Snøhvit Field. The Triassic reservoirs in the Norwegian Barents Sea are sand-poor due to the distance from the terrestrial source. In the Hammerfest Basin and on the margin of the Nordkapp Basin gas accumulated in the Triassic. The Triassic reservoir rocks include fault-bounded and dome traps and sealed by intra-Triassic shales (Doré, 1995).

### 3. Theoretical background

The purpose of this chapter is to explain the factors that control reservoir quality in siliciclastic rocks. The most important reservoir properties are porosity and permeability. Other reservoir properties such as wetting properties of mineral surfaces and pore geometry have also influences on petroleum production. The properties of reservoir rock are greatly influenced by their origin, primary composition of sediments, the depositional environment of the reservoir rock and diagenesis near the surface and during burial (Bjørlykke and Jahren, 2015). Additionally the climatic factors influence the weathering of the rock and the mineralogical composition of sediments during transportation from source to the basin.

#### 3.1 Sedimentological effect on reservoir quality

Primary composition of sediments - that is function of transport, provenance and the depositional environment - is the most important element which is predicting reservoir quality (Figure 3.1) (Bjørlykke and Jahren, 2015).

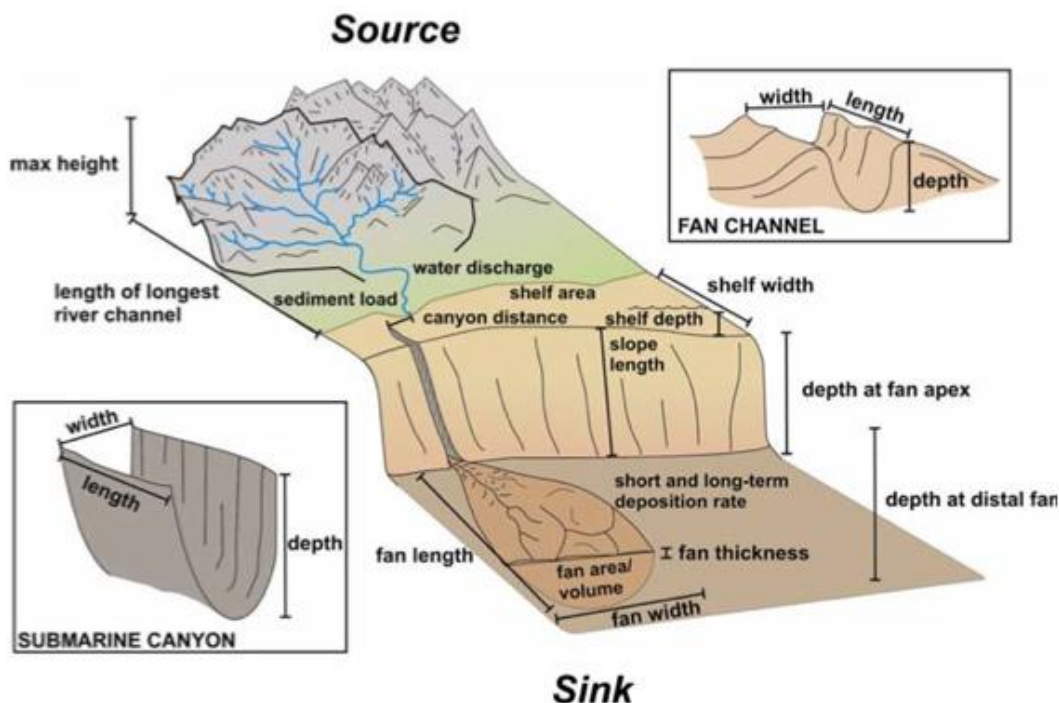


Figure 3.1: Key elements in sediment transport from the source to the basin (Martinsen et al., 2010).

Grain size, grain sorting, textural and mineralogical composition is very important factors to determine the source area of the sediments and interpret sequences during diagenetic processes until the sediments entered at their final position into the basin. This process is controlled by transport, provenance and mechanisms which take place in the depositional environment (Bjørlykke and Jahren, 2015). Tectonic movements play important role at the location of the sediments via basin formation, uplift, plate and fault movements. Climatic factors have also influence on reservoir quality due to source rock weathering, discharge of the rivers, sediment load, mineralogical composition of sediments and meteoric water flushing after deposition. Clay-sized particles have an important role in the mineralogical composition of the sediments during diagenetic processes in sandstones. Clays usually break down during weathering, erosion and transportation and develop or reproduce during burial diagenesis. In rocks clay minerals are allogenic or authigenic. Authigenic clays are formed in the sediment, in the basin, where the sediment was generated while allogenic clay minerals formed before deposition outside of the rock, being transported and became part of the rock. Allogenic clays have several types which occur in sandstones (Figure 3.2).

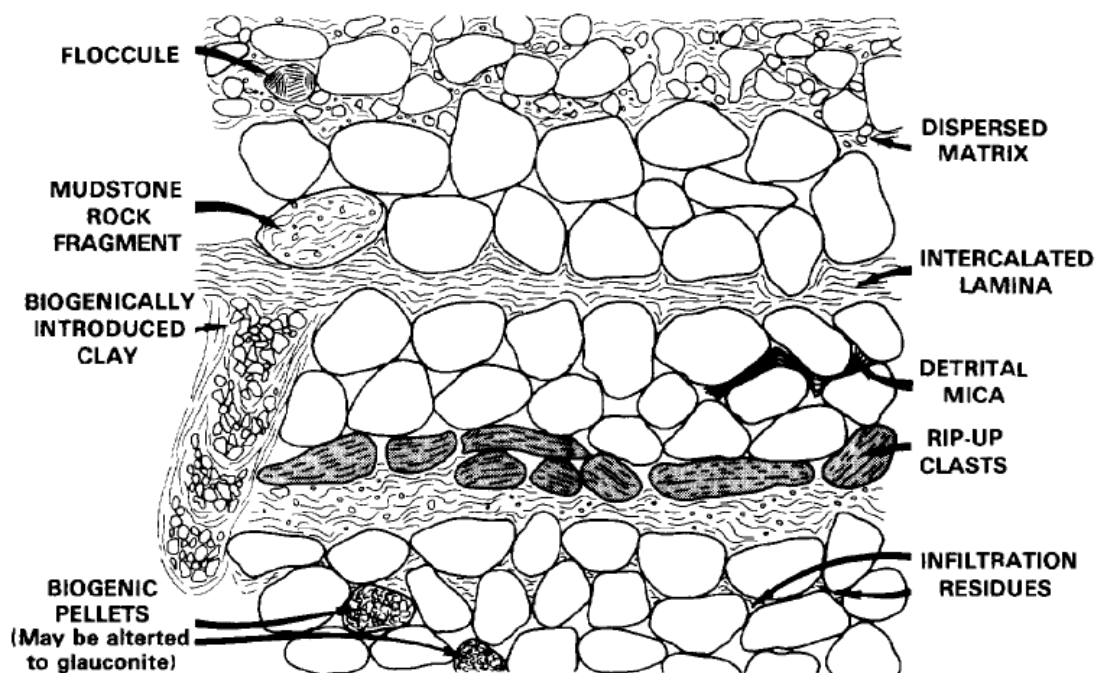


Figure 3.2: Occurrences of allogenic clays in sandstones (Wilson and Pittman, 1977).

Syn depositional clays deposited as matrix and thin laminae (e. g., clay flasers) in sandstones. Clay-sized particles from erosion of rocks and silt-sized matrix were deposited together with sand-sized debris. Detrital clays called “rip-up” clasts also build up in sandstones and contain

sand-sized or larger aggregates of clay minerals. They form during erosion. Clays or mud pellets form due function of biogenic organisms (Wilson and Pittman, 1977). Clays can develop sand-sized pellets due to flocculation (Pryor and Vanwie, 1971).

## **3.2 Diagenetic processes in sandstones**

Diagenesis is an open/closed system and it is sum of all processes which occur and cause changes in sediments after its deposition and before metamorphism. During diagenesis raw sediment converts to a sedimentary rock in an environment where pressure, temperature and chemistry are changing. These processes can modify porosity and permeability (Ali et al., 2010). This section distinguishes the different diagenetic processes from near surface to deep burial.

### **3.2.1 Early diagenesis**

Beneath the surface at depth <1-10 m the sediments react with atmosphere or meteoric water and diagenetic processes start to change the primary composition of the sediments. Diagenesis is an open system with add and remove solids in solution. Transportation of dissolved solids goes on by diffusion and fluid flow close to the surface, while diffusion takes place within 1 m of the seabed. The bulk composition of the sediments after deposition may change more likely at shallow depth due to the oxidizing conditions near the surface. During early diagenesis meteoric water flushing, biogenic activity, redox-driven processes and precipitation of authigenic clay minerals are reworked the primary composition of sediments (Bjørlykke and Jahren, 2015).

#### **3.2.1.1 Redox processes**

The redox boundary is at 1-20 cm beneath the seafloor and shows equilibrium between the supply of oxygen by diffusion and the consumption of the oxygen by the oxidation of organic matter. The concentration of oxygen and sulphate incline through the redox boundary and there is difference in ions solubility in oxidized seawater and in reduced seawater. In the porewater the oxygen concentration declines rapidly below the water/sediment interface. This process gives a concentration gradient for the diffusion of oxygen downwards into the sediments at the top. At deeper depth where there is no more dissolved oxygen in the

porewater the reduction of sulphates by sulphate-reducing bacteria produces pyrite (Bjørlykke and Jahren, 2015).

### 3.2.1.2 Biogenic activity

Biogenic activity changes the textural composition of sediments after deposition with destroying the primary lamination. Bioturbation has important role in reducing porosity and permeability due to mixing clay with clean sand. Bioturbation may increase the vertical permeability with destroying the clay laminae. The presence or absence of biogenic activity also has influence on the physical properties especially in velocity and resistivity.

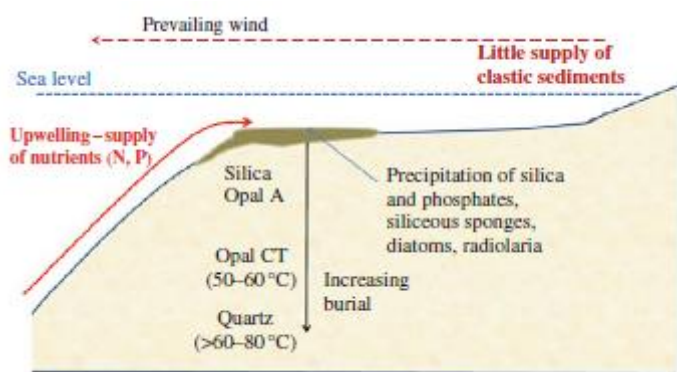


Figure 3.3: Biological precipitation of silica. Alteration of opal A to opal CT and then quartz (Bjørlykke, 2010b).

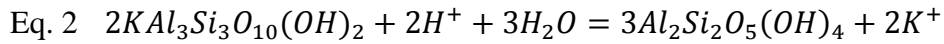
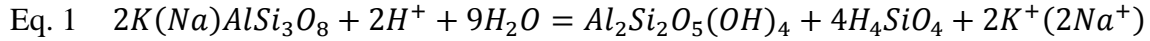
The source of carbonate cement is mainly from dissolution and reprecipitation of biogenic carbonate, especially from organisms made up of aragonite and it may form layers or concretions in sandstones. Aragonite is very unstable at shallow depth it will be dissolved and calcite will precipitate within the fossil or in the pore space

as cement between the grains. Siliceous organisms are also important in prediction of reservoir quality. Siliceous sponges or diatoms produce opal A which later at higher temperature will be replaced by opal CT and opal CT will be altered to quartz (Figure 3.3). It may be an important source of micro-quartz coatings on quartz grains at greater depth (Bjørlykke and Jahren, 2015).

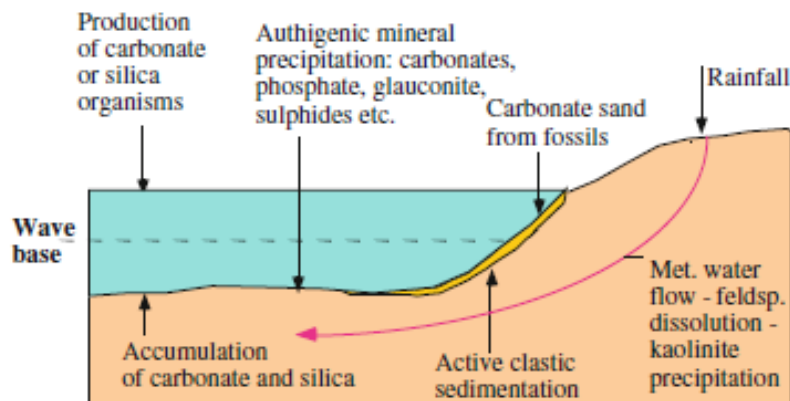
### 3.2.1.3 Meteoric water flow

Meteoric water means rainwater that penetrates into the ground and flows along the most permeable beds in the basin. Rainwater is somewhat acidic due to contain carbon dioxide and sulphur dioxide from the air and producing carbonic acid and sulphuric acid. CO<sub>2</sub> from root respiration is more important than rainwater due to accelerate the weathering process by humic acids made by decaying plants. The reaction between the rainwater and the surface has important role in weathering processes (Figure 3.4). Meteoric water flushing will first dissolve carbonates then unstable minerals such as feldspar and mica and will precipitate

authigenic clay minerals mostly kaolinite. Equation 1 shows the reaction between dissolution of feldspar and precipitation of kaolinite, while equation 2 shows dissolution of mica and precipitation of kaolinite.



Dissolution of feldspar and mica produce secondary pore space (secondary porosity). In these pore spaces kaolinite precipitation presence and it reduces the porosity because there is a little net gain in the pore space. Pore-filling authigenic kaolinite also reduces the permeability. The pore space in between the kaolinite grains is too small to be filled with oil due to high capillary entry pressure, so the oil saturation will be reduced in sandstones which are rich in kaolinite. Authigenic kaolinite consists clusters, oil can flow between the clusters and around the densely kaolinite cemented pore spaces (Bjørlykke and Jahren, 2015).



**The primary clastic composition is modified by:**

- 1) Meteoric water leaching and precipitation of kaolinite.
- 2) By addition of biogenic carbonate and silica.
- 3) By precipitation of authigenic minerals on the seafloor.

Figure 3.4: Meteoric water flushing and other diagenetic processes in shallow marine environment (Bjørlykke and Jahren, 2015).

### 3.2.2 Mechanical compaction

Mechanical compaction takes place down at 1.5-2 km depth and it is function of the vertical effective stress and compressibility of the mineral framework (Figure 3.5) (Bjørlykke et al., 2015). The main factors that influence the mechanical compaction are mineralogy, grain size, grain sorting, shape of the grains and packing. The mechanical compaction results porosity loss due to rearrangement and packing of the grains. Well sorted, fine-grained sand compact less as compared to coarse-grained sand due to in coarse-grained sand the per grain contact is less to hold the vertical effective stress (Figure 3.6). The sufficient per grain contact divides stress on each grain equally which reduces grain crushing and rearrangement of the grains (Chuhan et al., 2002). Little quartz cement (2-4%) may stop the mechanical compaction due to rearrangement of the grains. The mechanical compaction is critical in the case of determining the intergranular volume (IGV), which is porosity before starting quartz cementation (Bjørlykke et al., 2015). Due to high effective stress, the fictional sliding, rotation and the grain crushing cause mechanical compaction (Zhang et al., 1990).

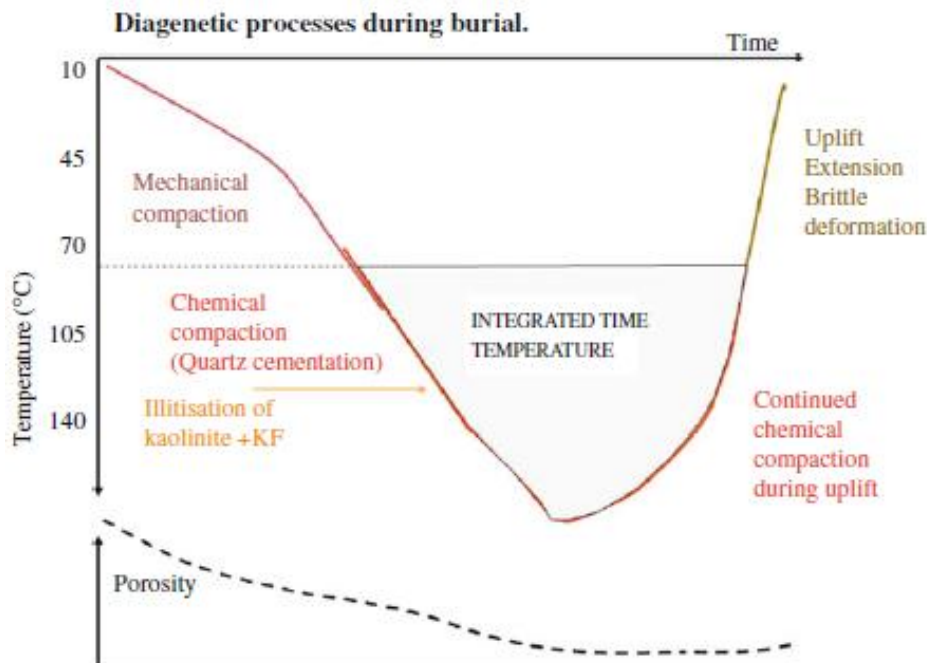


Figure 3.5: Mechanical and chemical compaction during burial (Bjørlykke and Jahren, 2015).



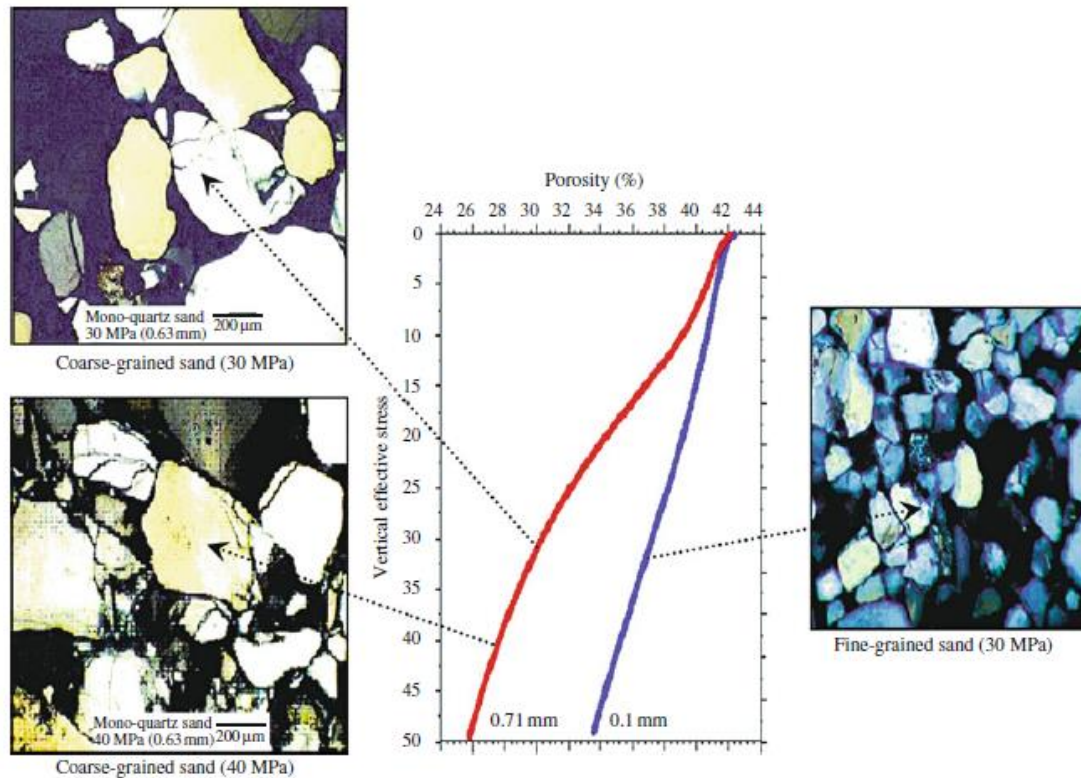


Figure 3.6: Compaction of coarse-grained and fine-grained sand (Chuhan et al., 2002).

### 3.2.3 Chemical compaction

Chemical compaction takes place after 2 km depth and the temperature is the main factor that influences compaction processes (Figure 3.5). Chemical compaction driven by thermodynamics and kinetics and it is a chemically closed system. The effect of vertical effective stress reduces due to temperature controlling chemical compaction zone, where dissolution and precipitation of quartz appears. The quartz precipitates as overgrowth on the surface of detrital grains into the pore space and the vertical effective stress has no longer effect on it. Grain coating may stop or block the quartz cementation, but grain fracturing may represent uncoated fresh grain surfaces for further quartz cementation and it will reduce the porosity (Bjørlykke et al., 2015).

#### 3.2.3.1 Intermediate depth (2-3.5 km, 65-120°C)

Both mechanical and chemical compaction takes place at intermediate depth in reducing the porosity. Due to quartz cementation at 2-3 km depth and 70-100°C temperature, strengthens

of the rock increasing, this area is called the transition zone. Mechanical compaction acts until a little quartz cement appears, it can stop the mechanical compaction and further mainly chemical compaction will act but mechanical compaction may continue if coatings stop or restrict the quartz cementation results that grain fracturing may represent fresh grain surfaces for further quartz cementation and it will cause further porosity reducing (Bjørlykke and Jahren, 2015).

Albitisation is replacement of K-feldspar or plagioclase by albite. Albitisation is often in sandstones which are buried to about 3 km or more depth. At this depth albite is more stable than K-feldspar or other feldspar minerals because sodium is the dominant cation in the porewater. Albitisation of plagioclase will discharge  $Ca^{2+}$  and it may be the source of calcite cement. Albitisation does not have strong influence in changing reservoir qualities in sandstones. In some muddy and volcanic sandstone which were exposed to meteoric water flushing smectite may be present. At 70-80°C smectite dissolves and precipitate mixed-layer minerals and illite. Sandstones which are contain smectite have poor reservoir quality (Bjørlykke and Jahren, 2015)

### 3.2.3.2 Deep burial (>3.5-4 km, >120°C)

Quartz cementation starts at 70-80°C and will continue until all the porosity is lost and remains at slower rate during uplift and basin inversion in sandstones. The controlling factor is the temperature. The porosity and the permeability are reducing very sharply in deeply buried sandstones and it is due to quartz cementation and diagenetic illite. The quartz cementation is increasing by a factor of 1.7 for every 10°C temperature increase (Walderhaug, 1996). The process is controlled by the surface area available for quartz cementation and the precipitation in the pore space which may

decrease the surface area available for further quartz overgrowth. Quartz cementation is insensitive to effective stress. At grain contacts and along stylolites dissolution of silica goes on. The dissolved silica is transported towards the grain surfaces where quartz overgrowth

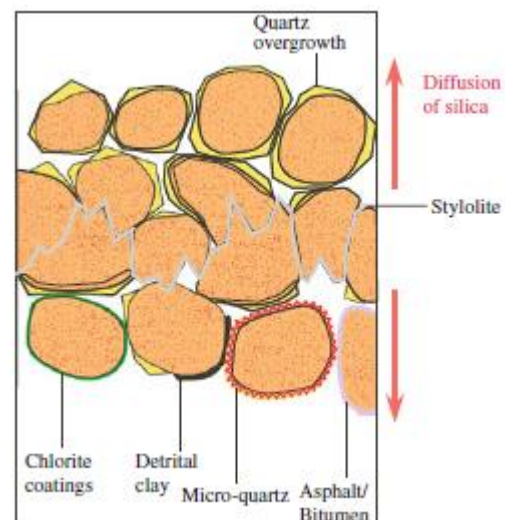
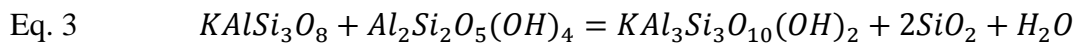


Figure 3.7: Dissolution of quartz along stylolites (Bjørlykke and Jahren, 2015).

forms (Figure 3.7). If coating appears on the grain surfaces (e.g. clay, petroleum, bitumen) quartz overgrowth could be stopped or blocked by grain coating (Bjørlykke and Jahren, 2015).

Authigenic illite can form from smectite, feldspar and kaolin minerals as illitization requires potassium and occurs at 70°C temperature from smectite and 130°C temperature from kaolinite. Authigenic illite has hair-, plate-like form and it reduces the permeability in rocks. In smectite rich sandstones presence of illite may improve the reservoir quality due to illite has a lower specific surface area than smectite. In sandstones which are moderately well-sorted the source of illitization are kaolinite or dickite (Bjørlykke and Jahren, 2015). Equation 3 shows illitization of kaolinite and K-feldspar.



### 3.2.4 Porosity preservation

Porosity preservation is important in oil production due to valuable oil flow from the reservoir as a result of low porosity and permeability.

#### 3.2.4.1 Authigenic clays

Authigenic clays form in the sediment, in the basin where the sediment was generated and include neoformed and regenerated clays (Figure 3.8). Pore lining clay minerals or grain coating (e.g. authigenic and detrital clay, bitumen, micro-quartz) may prevent the quartz cementation due to reduce the surface area available for quartz cementation and results high porosity values in reservoirs (Figure 3.7) (Wilson and Pittman, 1977). Authigenic chlorite coating is an important process for preserving porosity during deep burial (Aagaard et al., 2000). Chlorite has Mg/Fe content which may identify the depositional environment. Mg-rich chlorite forms in continental environments at high temperature and is typical in metamorphic rocks, while Fe-rich chlorite forms authigenically at shallow depth in marine environments (Bjørlykke, 2010a). Pore filling clays reduce the primary porosity in sandstones due to little net gain in the pore space and also reduce the permeability because the pores in between the clay crystals are too small to be filled with oil due to high capillary entry pressure and it results decreasing in oil saturation (Bjørlykke and Jahren, 2015). Fracture filling clays occur seldom and change the primary porosity. Replacement clays modify the primary

mineralogical composition of detrital grains by completely or moderately replacement of grains (Wilson and Pittman, 1977).

#### 3.2.4.2 Formation of overpressure

Presence of overpressure reduces the effective stress and will then preserve porosity due to stopping or reducing mechanical compaction. Expansion of overpressure depends on the fluid flux and on the permeability of the rocks. Mechanical compaction may not cause high overpressure due to reduced effective stress while transportation of fluids from deep burial may cause high overpressure at shallow depth. At greater depth (>2 km) and at higher temperature (80-100°C) chemical compaction and quartz cementation reduce the porosity and the permeability both in sandstones and shales. Therefore high sedimentation and subsidence rate will decrease the rate of compaction-driven flux and the rate of permeability reduction in seals resulting overpressure (Bjørlykke, 2015).

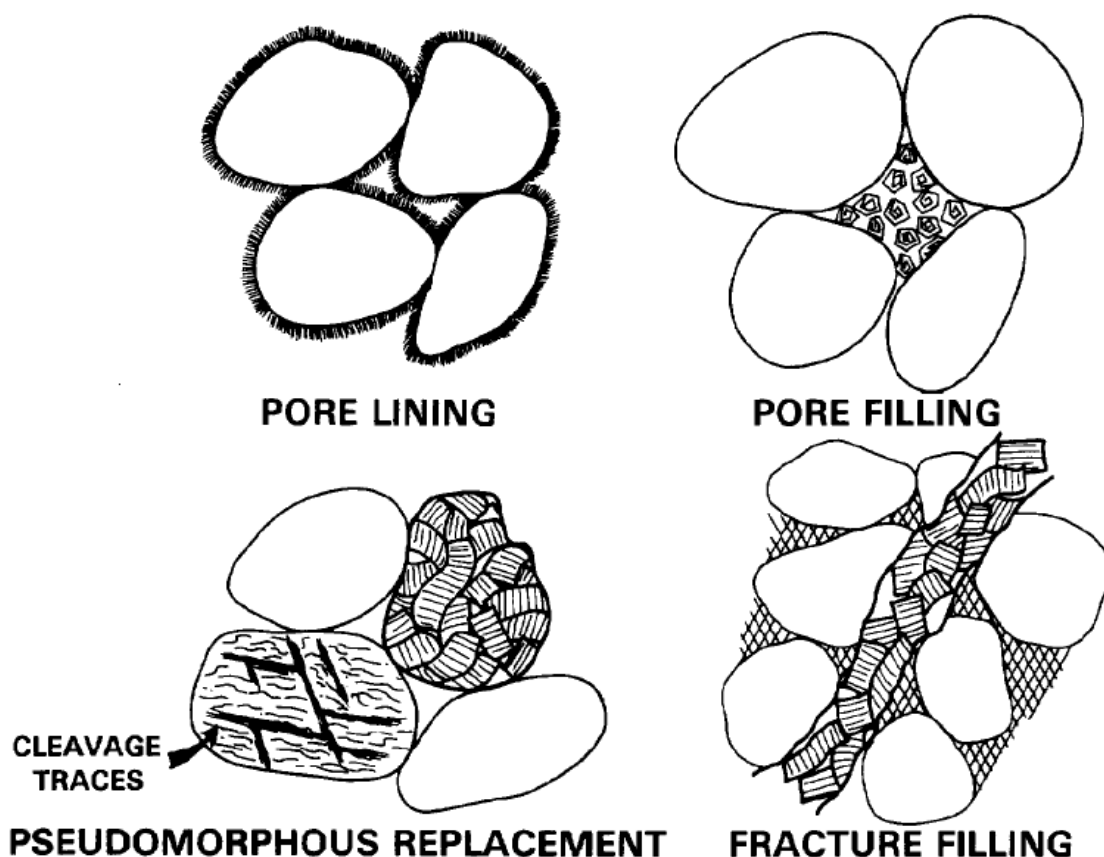


Figure 3.8: Occurrence of authigenic clays in sandstones from Wilson and Pittman, (1977).

## 4. Methodology

### 4.1 Sedimentological logging

The sedimentological logging of core 7222/11-1 was carried out from 10 to 11 May 2016 at Norwegian Petroleum Directorate in Stavanger. The core was logged on the D-cut of the core (Figure 4.1) and on logging sheet at scale of 1:50 cm for both Kobbe and Snadd Formations and was digitalized by using SedLog 3.0 and Adobe Illustrator CS6. During the logging the core observation was made up of lithology description, grain size and different sedimentary structures determination. The core photos and sedimentological logs were used to interpret the facies and the depositional environment.

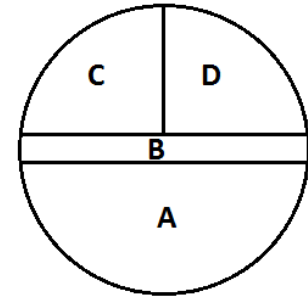


Figure 4.1: Location of the different cuts of a core. Logging on the D-cut.

### 4.2 Mineralogical and Petrographic analysis

Mineralogical and petrographic analysis of the samples was done by using optical thin-section observations, scanning electron microscopy (SEM) analysis on the selected samples, clay fraction analysis and X-ray diffractometry (XRD) on the bulk composition of the rock samples.

#### 4.2.1 Thin section analysis

The observation gives information about texture, mineralogy, lithology, structure, average grain size, grain shape and sorting of the rocks. 30 samples were chosen from well 7222/11-1, 10 thin-sections from Kobbe Formation and 20 thin-sections from Snadd Formation were analysed by using Nikon Optiphot-Pol petrographic microscope. All thin-sections were polished down to 30µm thickness and the porosity was filled with blue epoxy. During the analysis all of the thin-section were examined under plane polarized light (ppl) and cross polarized light (xpl). The grain size was determined by measuring the longest axis of the grains at three different points of the thin-sections and calculating the average value. Grain

sorting was determined by using the classification scheme by Compton (1962) (Figure 4.2) and roundness of the grains was observed by using Powers' terminology (1953) (Figure 4.3).

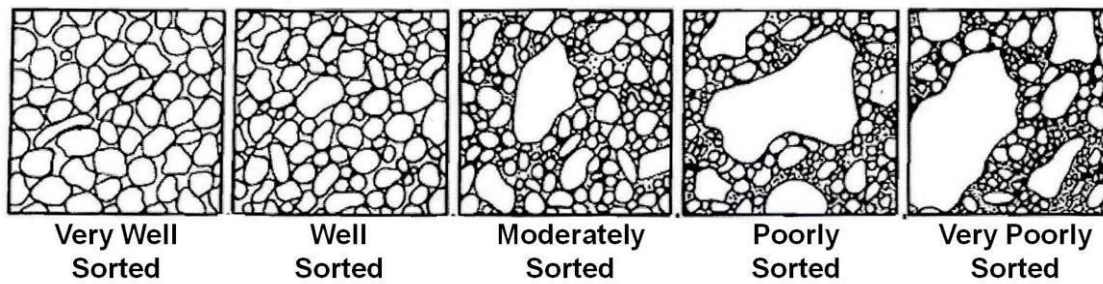


Figure 4.2: Classification scheme of grain sorting (Compton, 1962).

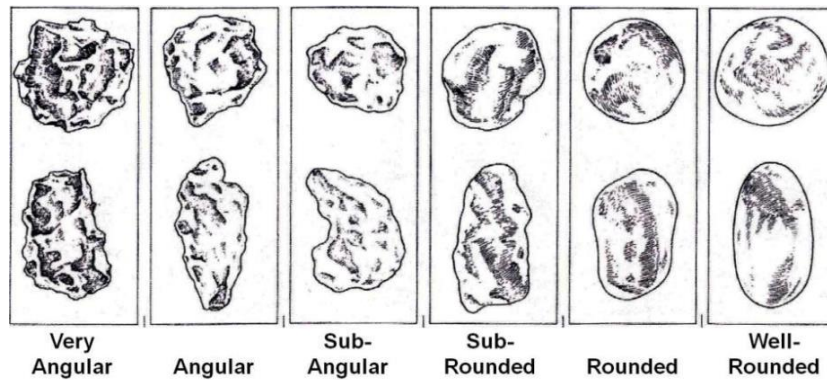


Figure 4.3: The roundness of detrital grains (Powers, 1953).

The preservation of detrital grains such as feldspar and mica may use to show the weathering and leaching intensity in the depositional environment. During the optical microscopy observation the identification of feldspar grains based on the degree of weathering and referred into 5 categories, where category 1 represents fresh grains, which have not been subjected to weathering and twins are fully preserved. Category 2 shows grains, which have been subjected some weathering but twins still very well preserved, while category 3 shows grains with sericitization and twins hardly seen. Category 4 represents grains with very rough surface and high degree of sericitization, twins are difficult to observe. In category 5 very difficult to identify K-feldspar and plagioclase, some part of the grains are preserved and very high degree of sericitization is observed. Twins are absent. Identification of mica grains based on the intensity of deformation and alteration and referred into 3 categories, where category 1





The IGV is function of the grain size, shape, sorting and mechanical compaction. IGV decreases with burial depth due to effective stress and overburden. Sandstones with less than 50% IGV reduction classified as loosely packed, while more than 70% IGV reduction classified as tightly packed (Santin et al.)

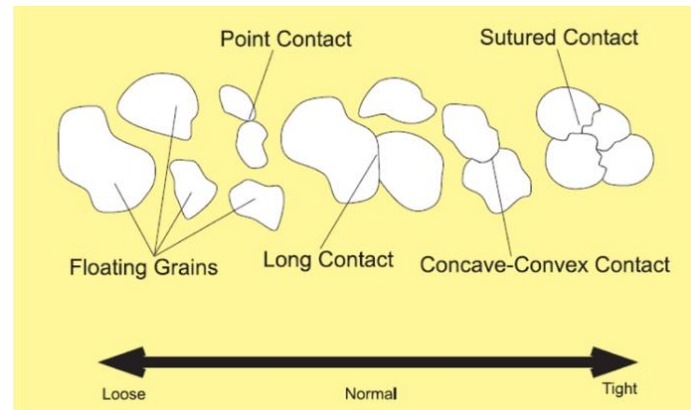


Figure 4.5: The figure represents the different grain contacts that have been recognized during textural analysis (Santin et al.).

#### 4.2.2 X-ray diffractometry (XRD)

XRD analysis was done at the Department of Geosciences at University of Oslo for examination of mineralogical composition of rocks. X-ray diffractometry is very useful to determine crystal structures because minerals have crystal properties. It can be used in significant studies and when minerals are too small to identify under optical microscope. Furthermore XRD used for identify different polymorphic forms and crystalline material, quantify the percent crystallinity of a sample and dividing between amorphous and crystalline material. X-rays are generated by a cathode ray tube, clarified to produce monochromatic radiation and guided towards the sample. When Bragg's Law ( $n\lambda = 2d \sin \theta$ ) prevails the cooperation between the rays and the sample produces constructive interference. This law describes the wavelength ( $\lambda$ ) of the incident X-rays to the diffraction angle ( $\theta$ ) between the incident rays and atomic planes and the atomic spacing ( $d$ ) in the crystalline lattice. First X-rays are detected then processed and counted. All diffraction directions of the mineral lattice should be detected during scanning through  $2\theta$  angles because the powdered material has random direction. Due to transformation of the diffraction peaks to  $d$ -spacing minerals become definable because each mineral has a characteristic  $d$ -spacing (Table 4.1). Identification of minerals is got by comparison of  $d$ -spacing with standard reference pattern (Moore and Reynolds, 1989).



Table 4.1: Characteristic d-spacing of the common minerals.

Mineral	d-spacing	Mineral	d-spacing
Quartz	4.26 Å	Kaolinite	7.0 Å; 3.58Å
Plagioclase	3.19 Å	Chlorite	7.0 Å; 3.54 Å
K-feldspar	3.24 Å	Illite	10.0 Å
Muscovite	10.01 Å	Calcite	3.03 Å

#### 4.2.2.1 Bulk analysis

30 samples were prepared for bulk XRD analysis, where the aim was to get information about the mineralogical composition of the samples. First the samples were crushed by a slinging mill to separate the minerals. During this process the grain size reduced to 500 µm, mostly to 100-200 µm. In the next step 3 g of each rock powder was weighed out and mixed with 9 ml ethanol in a small box with 48 pieces of agate, then put into the micronizer machine and run for 12 minutes and reduced the grain size to 10 µm. After that the micronized samples were placed into an oven at temperature 40-50 °C and left them for drying. The dried samples were placed carefully into pellets and run through XRD.

#### 4.2.2.2 Clay fraction analysis

15 samples were selected for clay fraction analysis, 5 samples from the Kobbe Formation and 10 samples from the Snadd formation. First the samples were crushed by a hammer to 1-2 mm size then put into beakers and filled with 200 ml Na<sub>2</sub>CO<sub>3</sub>, and then it was mixed for 1 minute and put in an ultrasonic bath for 10 minutes. After the sonic bath the solution was stirred again for 1 minute and left them for 24 hours rest. After 24 hours the samples were placed in the ultrasonic cleaner again for 10 minutes, afterwards stirring for 1 minute and filled with Na<sub>2</sub>CO<sub>3</sub> up to 600 ml. Then left them for 6.5 hours rest, later on the top 8.5 cm of the suspended material was juiced into a plastic box. The samples were run in 4 rounds through XRD. After the first round air-dried samples were analysed. The samples were treated with ethylene-glycol vapour and placed in an exsiccator for 1 night to analyse swelling clays before the second round. In the third run the samples were heated up to 350 °C. In the fourth round the samples were heated up to 550°C, at this temperature kaolinite becomes amorphous to X-rays. The difference between the EG-treated and the 550 °C samples may give information about presence and absence of kaolinite.

DiffraXt.eva software was used to identify the mineralogical composition of the samples.

#### **4.2.3 Scanning electron microscope (SEM)**

Scanning Electron Microscopy used to identify the smallest minerals and consider the distribution of these minerals in the pore space. A JEOL JSM-6460LV Scanning Electron Microscope with LINK INCA Energy 300 (EDS) was used for sample analysis. Both thin-sections and stubs were studied in the electron microscope to get information about mineralogical composition focusing on authigenic minerals and preserve grains. The thin-section samples were coated by carbon and the stub samples were coated by gold. Backscatter electron (BEI) X-rays were used during thin-section analysis while secondary electron (SEI) X-rays was used during stubs analysis. SEM Petrology Atlas was utilized for elemental analysis by identifying spectrum peaks (Welton, 1984).

### **4.3 Petrophysical analysis**

Petrophysical analysis is performed by using available geophysical logs. Before analysis standard log check was implemented and not any significant correction in the log data was required. The petrophysical interpretation is performed by using Interactive petrophysics (IP) software. Gamma ray log, sonic log, neutron log and density log are used in petrophysical analysis.

#### **4.3.1 Shale volume estimation**

##### **4.3.1.1 Shale volume from gamma ray log**

Gamma ray log measure the natural radioactivity of the rocks. The main radioactive elements present in rocks are Uranium, Thorium and Potassium. In sedimentary rocks shales contain higher radioactivity because of abundance of Uranium. Therefore the gamma ray log is always higher in shales lithology. In pure sandstone the gamma ray value is always lower but presence of heavy minerals and K-Feldspar can cause high gamma ray signature in sandstone.

Besides qualitative use to discriminate lithology, gamma ray log is used for quantitative calculation of shale volume. The shale volume is calculated by linear relation of gamma ray

index  $I_{GR}$  and  $V_{sh}$ . The shale volume from gamma ray index is calculated by using Eq 4 & 5 by defining clean sand line and shale line. The equation is defined by Mondol, (2015).

Eq. 5 
$$V_{sh} = I_{GR}$$

Eq. 6 
$$I_{GR} = \frac{GR_{log} - GR_{min}}{GR_{max} - GR_{min}},$$

where  $I_{GR}$  – gamma ray index,  $GR_{log}$  – gamma ray log in area of interest,  $GR_{min}$  – minimum gamma ray log reading in clean sand,  $GR_{max}$  – maximum gamma ray reading in clean shale.

The linear relation of gamma ray index and shale volume has no scientific assumption therefore correction is required (Mondol, 2015). The linear relation of gamma ray index and shale volume overestimates shale volume in most scenarios. The correction is applied by using different equations suggested by different authors (Table 4.2)

Table 4.2: Commonly used non-linear equations for shale volume estimation (Rider and Kennedy, 2011).

Author(s)	Equations
Larinov (1969) Younger rocks	$V_{sh} = 0.083 \times (2^{3.71} I_{GR} - 1)$
Larinov (1969) Old rocks	$V_{sh} = 0.33 \times (2^{I_{GR}} - 1)$
Steiber (1970)	$V_{sh} = I_{GR} \div (3 - 2 \times I_{GR})$
Clavier et al. (1971)	$V_{sh} = 1.7 - [3.38 - (I_{GR} + 0.7)^2]^{1/2}$

#### 4.3.1.2 Shale volume from neutron-density

Another approach for calculation of shale volume is using combination of neutron-density log. The approach is useful in data where picking of clean sand line is difficult because of high GR value. The shale volume is calculating by defining clean sand line and clay line in neutron-density cross plot (Figure 4.6).

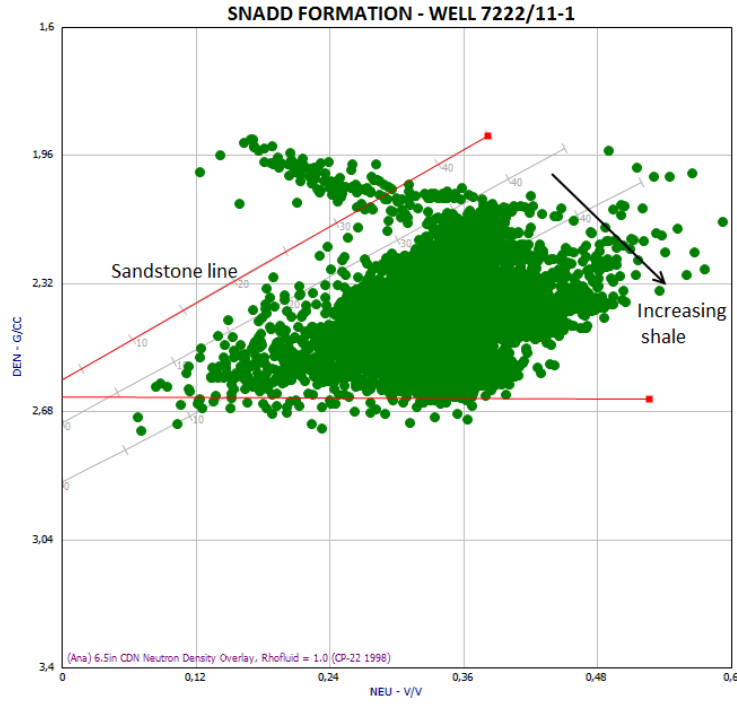


Figure 4.6: Neutron-density cross plot from Snadd Formation. The cross plot is used to define clay line and sand line for shale volume estimation.

### 4.3.2 Porosity estimation

Porosity is defined as ratio of volume of pore spaces to the total volume of rock. In petrophysical analysis various logs are used for porosity estimation, such as neutron porosity, sonic porosity and density porosity. But each log contain some limitations and uncertainties, therefore alternative approach is required for reliable porosity calculation. In industry practice the most common method is using average porosity of neutron porosity and density porosity. The following equation is often used:

$$\text{Eq. 7} \quad \Phi = \sqrt{\frac{\Phi^2 N + \Phi^2 D}{2}},$$

where  $\Phi_N$  is porosity from neutron log and  $\Phi_D$  is density porosity.

The neutron log measure porosity as a function of hydrogen present in rock pore spaces. In rock pore spaces water or hydrocarbon contain hydrogen which is measured by neutron logging tool and alternatively porosity. In shales the hydrogen is present in clay mineral

structure therefore neutron tool overestimates the porosity in shales. On the other hand gas in pore spaces contain less hydrogen as compared to water and oil that leads to underestimation of porosity in gas sand.

The density log measure porosity as function of rock matrix density and pore fluid density by following equation:

$$\text{Eq. 8} \quad \Phi_D = (\rho_{ma} - \rho_b)/(\rho_{ma} - \rho_{fl}),$$

where,  $\rho_b$  – formation bulk density,  $\rho_{ma}$  – matrix density and  $\rho_{fl}$  – fluid density.

The accurate porosity calculation is from core sample but core samples are not always available. By using geophysical logs average porosity is the most reliable.

### 4.3.3 Permeability estimation

Permeability is ability of the rocks to transmit fluids in porous media. The capacity to transmit fluids in porous media depends on the grain size with smaller, fewer or less interconnected pore spaces. A rock with high porosity may have low permeability due to fine-grained particles in the pores and a rock with low porosity may have high permeability due to fractures in the sample. Permeability is one of the most important parameter in reservoir quality. Porosity is the main factor influencing permeability but pore throat size and shape, wetting angle, capillary pressure and clay mineral distribution have also effect on permeability in rock samples. The unit used for permeability called Darcy (D) or milidarcy (mD). Most accurate permeability can be calculated from core samples; alternatively indirect measurement is by using well log data. Permeability is calculated from well log data based on porosity estimation and water saturation. Different empirical equations such as Tixier's, Timur's and Coates' equations are used to calculate permeability from well log data (Torskaya et al., 2007). Wyllie and Rose (1950) proposed a general empirical equation for permeability calculation based on porosity estimation and water saturation.

$$\text{Eq. 9} \quad k = a \frac{\phi^b}{S_{wi}^c},$$

where  $k$  is permeability,  $\Phi$  is porosity,  $S_{wi}$  is irreducible water saturation and  $a, b, c$  are model parameters. In this study Timur's equation (Timur, 1968) was used for permeability calculation:

$$\text{Eq. 10} \quad k = 8.58 \frac{\Phi^{4.4}}{S_{wi}^2}$$

#### 4.3.4 Net-to-Gross ratio and pay zone

The net-to-gross ratio is the ratio of total thickness of formation to thickness of clean reservoir. Gross is the total thickness of reservoir while net is the thickness of interval with sufficient reservoir properties. The reservoir cut-off value is used to find the net-to-gross ratio. In this study to find net-to-gross ratio by using petrophysical logs the cut-off value used for porosity is 0.1 and shale volume is 0.3.

#### 4.3.5 Estimation of the uplift in the study area

The tectonic evolution of the sedimentary basin causes subsidence and/or uplift of the rocks. The subsidence and/or uplift affect rock physical properties. The rock physical properties increase with depth and expected to follow a certain trend with burial depth. In a sedimentary basin the transition from mechanical compaction (MC) to chemical compaction (CC) zone occur when temperature reach to 70 – 80 °C. This temperature corresponds to depth of 2 – 2.5 km with geothermal gradient of 35 – 40 °C/km. After the onset of the chemical compaction sudden increase in velocity occur due to grain stiffening after early precipitation of the quartz cement. During uplift estimation the distinguishing between MC and CC zones is useful. The common technique used for uplift estimation is plotting of the velocity-depth data with one of the several published curves. The published reference curves like Mondol et al, (2009) Kaolinite-Silt 50:50 are acquired by studying the mixture of the kaolinite and silt under vertical effective stress. The plotted velocity-depth data from well log is believed to follow the published reference curve in mechanical compaction zone. The mismatch of data from curve in MC zone shows the area is uplifted. In following study the reference curve from Mondol et al, (2009) and Storvoll et al, (2005) are used to estimate uplift of the study area. The following equation is used to estimate the geothermal gradient:

$$\text{Eq. 11} \quad G = \left( \frac{BHT - SBT}{TVD} \right) * 100,$$

where BHT-bottom hole temperature; SBT-sea bottom temperature (4°C) and TVD-total vertical depth. The bottom hole temperature was not accessible for well 7222/11-1, thus the bottom hole temperature has been interpolated from the neighbouring well 7222/11-2.

#### 4.4 Sources of error

Experience of the interpreter is very important during thin section analysis. Clay minerals can be hard to recognize and identify. K-feldspar and plagioclase (albite) grains were difficult to separate from quartz grains. Quartz overgrowth may not be interpreted due to lack of dust rims on the quartz grains. During point-counting analysis 400 points were counted, which means only selection of points were counted for representation of the entire sample. The possible source of error during SEM analysis is contamination of samples during the preparation and misinterpretation of elemental analysis due to size of the minerals and closeness to other minerals. Misinterpretation during XRD analysis may be due to size and orientation of the samples and due to cracks on the samples' surfaces.

Petrophysical analysis using well logs contains uncertainties because such measurements are not directly obtained from rock samples. Each geophysical log used for analysis contains uncertainties.

For shale volume estimation gamma ray log and neutron-density log were used. Sources of error by using gamma ray log to calculate shale volume is the high amount of potassium minerals in sandstones gives high  $GR_{min}$  value for sand. Due to such high value overestimation of the shale volume is expected in potassium rich sandstone. Spectral gamma ray log can be used to identify these anomalies in such case. Further if there is any caving in the borehole, the gamma ray response may be lower and it can be corrected by using caliper log. Another source of error is drilling mud, if it is high density mud e.g. barite based, it can underestimate the shale volume, while it is low density mud e.g. potassium chloride, it can overestimate the shale volume. Uncertainties by using neutron-density response to calculate shale volume is if the sandstone contains other minerals than quartz will result an extra separation between the neutron and density curves, for example gas zone and dolomite separation do not develop shale (Mondol, 2015).

Neutron-density log was used to estimate porosity. Due to fractures and gas in the borehole or in the formation porosity may show high values. Drilling with heavy mud may cause incorrect density data and porosity from density log depends on fluid density.



## **5. Sedimentology**

The sedimentological analysis of the Triassic Snadd and Kobbe Formations has been done to interpret the depositional environment and its effects on the maturity of the sediments. The description was made of the 7222/11-1 well on a logging sheet in scale 1:50 by core logging, which are presented in Figure 5.2 and Figure 5.3. The legend for the sedimentological logs is present in Figure 5.1. The formations have been subdivided into facies, based on characteristic properties and described in section 5.2. The different depositional environments are described in section 5.3.

### **5.1 Description of the core**

#### **5.1.1 Core 7222/11-1**

The total core length is 75.8 metres and contains Core 1, Core 2, Core 3, Core 4 and Core 5 cores. The core consists of sediments from Snadd and Kobbe Formations, described below. The core is incomplete because 479.9 metres from the Snadd Formation is missing and between Snadd and Kobbe Formations there is a 910 metres gap. Smaller sections are also missing in the core. The whole section represents a coarsening upwards succession.

##### **5.1.1.1 Kobbe Formation**

For the Kobbe Formation Core 4 and Core 5 were logged in a 1:50 scale log sheet. Core 4 is cut from 2209.5 m to 2227.7 m and Core 5 is cut from 2227.7 m to 2243.5 m. The lower part of Core 5 contains a 1 meter thick laminated mudstone layer. The next succession contains approximately 10 m thick very fine- to fine-grained sandstone with current ripples. The upper part of Core 5 and the lower part of Core 4 contains more mud with interbedded very fine- to fine-grained sandstone and represents heterolithic deposits. This succession starts with flaser bedding and towards to the top of Core 5 and the bottom of Core 4 becomes more muddy, wavy- and lenticular bedded deposits take place with minor bioturbation. Above the 1.5 m layer contains of fine- to very fine-grained sandstone. The lower part of this unit is characterized by moderate bioturbation, while the upper part is calcite cemented and represents planar cross bedding. The next 4.5 meters describes an alternating mud and sand layers unit with minor bioturbation. The upper part of Core 4 starts with very fine-grained

sandstone with planar cross bedding going into silt-clay sized deposits with intensive bioturbation. The uppermost 4 m thick succession represents horizontal laminated mudstone (Figure 5.2).

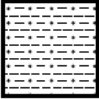





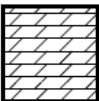


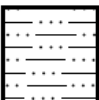



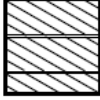


Lithologies		Symbols	Base Boundaries
	Mudstone	 Horizontal planar lamination	 Sharp
	Sandstone	 Intraclasts	 Gradational
	Carbonate	 Mudclasts	 Erosion
	Siltstone	 Current ripple cross-lamination	
		 Minor bioturbation	
		 Moderate bioturbation	
		 Planar cross bedding	
		 Intense bioturbation	
		 Roots	

Figure 5.1: Legend for the logged sections of the Kobbe and Snadd Formations in well 7222/11-1, representing on Figure 5.2 and Figure 5.3.

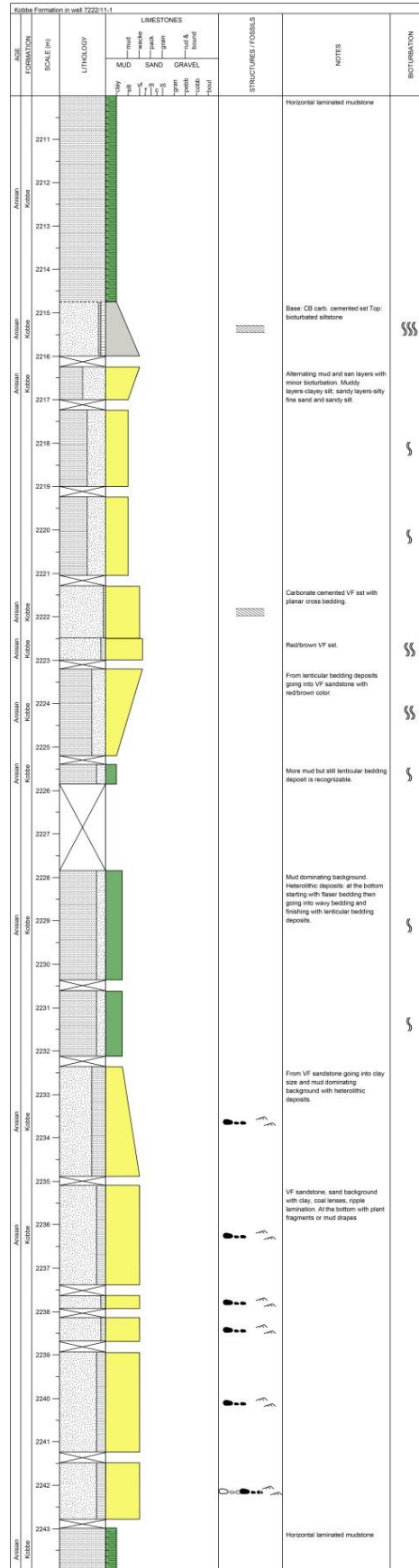


Figure 5.2: The logged section for the Kobbe Formation in well 7222/11-1.

#### 5.1.1.2 Snadd Formation

For the Snadd Formation Core 3, Core 2 and Core 1 were logged in a 1:50 scale log sheet. Core 3 is cut from 1287 m to 1299.5 m; Core 2 is cut from 798.5 m to 807.1 m and Core 1 from 778 m to 798.8 m. The lowest part of Core 3 represents mudstone with intensive bioturbation. The next 7 meters are dominantly sandstone with interbedded shale and containing dolomite, ankerite and calcite cement. The lowermost 3.5 m of this succession contains more carbonate and the lower part is showing high bioturbation while the upper part is horizontal laminated with minor bioturbation. The uppermost 3.5 m contains less carbonate. The lower part of this unit is more muddy and contains red clasts with moderate bioturbation and the upper part is less muddy with coal lenses and low grade of bioturbation. After this succession there is an erosional surface and the uppermost 5 meters represents very fine- to fine-grained and medium-grained sandstone with planar cross bedding. The whole Core 3 unit is showing a coarsening upwards succession.

The lowermost 1.5 m thick unit of Core 2 contains palaeosol with interbedded sandstone, rootlets and intensive bioturbation. The middle part of Core 2 represents fine- to medium-grained sandstone at the bottom and clay-silt sized deposits at the top, and then is going into a siltstone deposit with sand lenses and moderate bioturbation. After the siltstone in Core 2 more sand presents with heterolithic deposits. The unit is starting with lenticular bedded deposits, then the amount of sand is increasing and the wavy and flaser bedded deposits take place with low bioturbation and then this succession turns into palaeosol again with interbedded sandstone, rootlets and high grade of bioturbation. The upper part of Core 2 represents fine-to medium-grained sandstone with horizontal lamination at the bottom and with structureless massive sandstone at the top. Core 1 represents medium-grained sandstone with planar cross bedding at the bottom and with structureless, massive sandstone at the top. The mid-part of Core 1 contains very fine- to fine-grained sandstone with calcite cement and planar cross bedding (Figure 5.3).

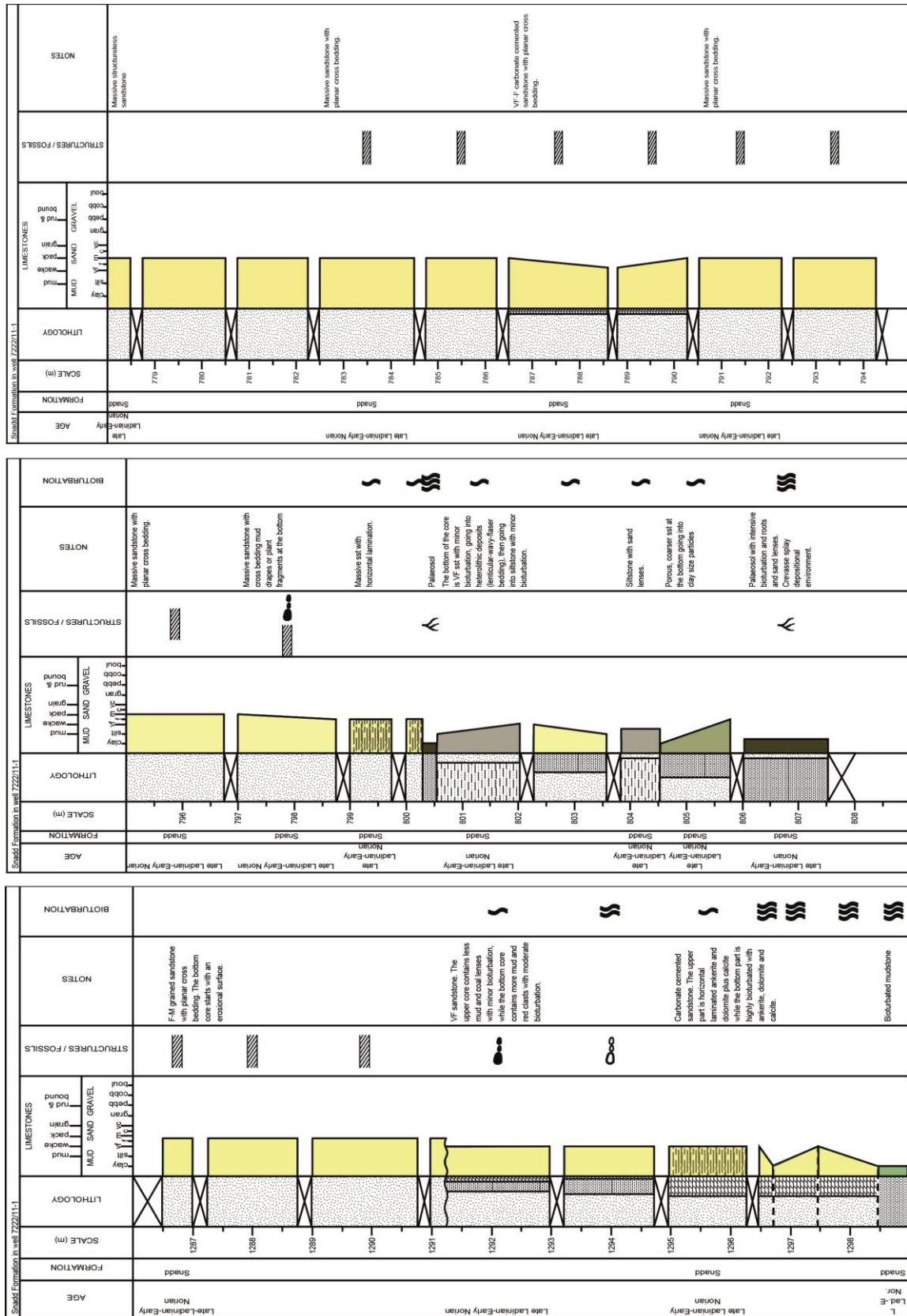


Figure 5.3: The logged section for the Snadd Formation in well 7222/11-1.

## 5.2 Facies description

During the sedimentological analysis of the 7222/11-1 core, 8 different facies have been defined with different subfacies. The facies association and the depositional environment are described in section 5.3.

### **Facies 1: Massive sandstone**

This facies is found only at the uppermost and lower-middle part of the Snadd Formation and divided into 4 subfacies described below.

#### *Facies 1A: Structureless massive sandstone*

The uppermost 4 m of the Snadd Formation represents this subfacies. Three 1-2 m thick fine- to medium-grained packages of structureless sandstone were observed within the core. The subfacies is underlain by cross-bedded massive sandstone and carbonate cemented sandstone unit (Figure 5.4 A).

#### *Facies 1B: Cross-bedded massive sandstone*

The subfacies occur below the structureless sandstone and represents 15 m thick unit with 1 m thick interbedded carbonate cemented sandstone (F5C) at the upper part of the core and a 4 m thick unit at lower-middle part of the core. Nine 1-2 m thick fine- to medium-grained sandstone packages were observed with planar cross bedding. The succession is underlain with a massive sandstone unit with mud flakes (Figure 5.4 B).

#### *Facies 1C: Massive sandstone with coal flakes*

The bottom part of the cross-bedded massive sandstone unit represents this subfacies and it is underlain by a massive sandstone unit with minor bioturbation and horizontal coal lamination. The succession is 0.2 m thick fine-grained sandstone with coal flakes which are showing the current flow (Figure 5.4 C).

#### *Facies 1D: Massive sandstone with bioturbation*

The subfacies is found at the lowermost 1 m of the massive sandstone succession. The fine-grained unit is characterized by minor bioturbation and horizontal coal lamination. The lamination of the sandstone is not well-observed due to bioturbation but some part of the core

section is well-seen. The section is underlain by palaeosol and very fine- to fine-grained sandstone with heterolithic deposits (Figure 5.4 D).

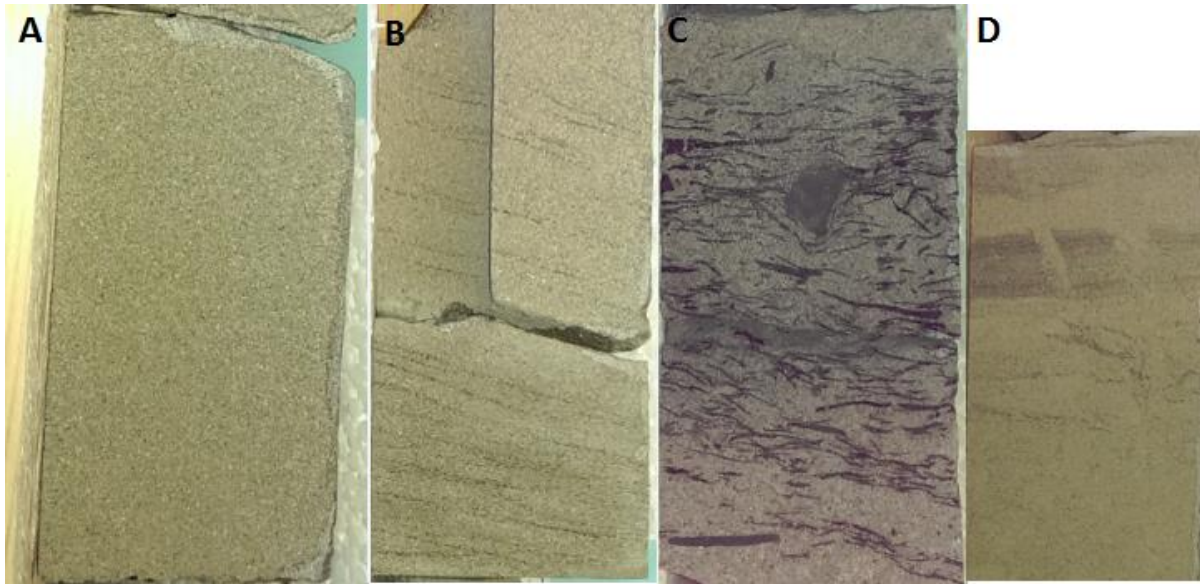


Figure 5.4: Massive sandstone facies with the 4 different subfacies in the Snadd Formation. A: Structureless massive sandstone at 780 m depth; B: Cross-bedded massive sandstone at 783 m depth; C: Massive sandstone with coal flakes at 798 m depth; D: Massive sandstone with bioturbation at 799 m depth.

## **Facies 2: Siltstone**

The siltstone facies show up in the middle part of Snadd Formation under the massive sandstone unit and above the very fine- to fine-grained sandstone package with heterolithic deposits, while in the Kobbe Formation it is found in the upper part of the core. The facies is subdivided into 2 subfacies described below.

### *Facies 2A: Siltstone with sand lenses*

The section represents 0.25 m thick unit in the middle part of the Snadd Formation. The mud/sand ratio is high; the background of the unit is mud with interbedded sand lenses (Figure 5.5 A). The subfacies is underlain by very fine- to fine-grained sandstone with heterolithic deposits and overlain by bioturbated siltstone.

### *Facies 2B: Siltstone with bioturbation*

The subfacies presents in both Kobbe and Snadd Formation. The section is found in the middle part of the Snadd Formation and the upper part of the Kobbe Formation and characterized by minor bioturbation and red colour in the Snadd Formation, while in the Kobbe Formation this subfacies represents intensive bioturbation and greyish colour. The thickness of the unit is 0.25 m in the Snadd and 0.5 m in the Kobbe Formation (Figure 5.5 B-C). The succession is overlain by a thin layer of palaeosol and underlain by the siltstone unit with sand lenses in the Snadd Formation. In the Kobbe Formation it is underlain by the carbonate cemented sandstone unit and overlain by the horizontal laminated mudstone facies.

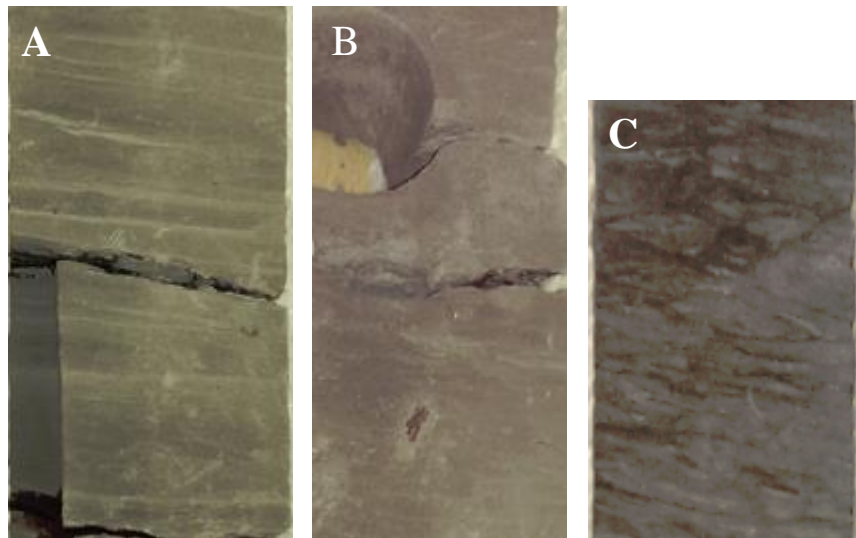


Figure 5.5: Siltstone facies in the Snadd and Kobbe Formation. A: Siltstone with sand lenses at 800-800.5 m depth in the Snadd Fm; B: Bioturbated siltstone at 800-800.5 m depth in the Snadd Fm; C: Highly bioturbated siltstone in the Kobbe Fm at 2214.5 m depth.

### **Facies 3: Heterolithic deposits**

The facies consists of mixed layers of mud and sand with differing mud/sand ratio and occur in both Snadd and Kobbe Formation in the middle part of the core. The facies is divided into three subfacies flaser-, wavy-, and lenticular-bedding described below. The wavy and the lenticular-bedding subfacies are the most dominant sedimentary structure in this unit. In the Snadd Formation the facies is starting with lenticular-bedding then going into wavy- and flaser-bedded deposits, so the sand/mud ratio increases towards shallower depth, while in the Kobbe Formation the facies occurs reversed. All three subfacies is characterized by minor



bioturbation. The facies is underlain and overlain by a siltstone and palaeosol unit in the Snadd Formation. In the Kobbe Formation the succession is underlain by very fine- to fine-grained ripple-laminated sandstone and overlain by very fine- to fine-grained sandstone with moderate bioturbation.

*Facies 3A: Flaser bedding*

Flaser bedding represents at the top of the heterolithic deposits facies as change from wavy bedding to flaser bedding in the Snadd Formation, while in the Kobbe Formation the facies is starting with flaser bedding and going into wavy-bedded deposits. Sand is the dominant grain size and mud occurs as drapes in the succession. Minor bioturbation occurs in the subfacies (Figure 5.6 A; Figure 5.7 A).

*Facies 3B: Wavy bedding*

This subfacies characterized by continuous mud and sand layers very close to the lenticular-bedded deposits. Current ripples can be seen in the sand lenses in the Snadd sample. Low grade of bioturbation shows up in the unit (Figure 5.6 B; Figure 5.7 B).

*Facies 3C: Lenticular bedding*

The lenticular-bedded deposits represent at the bottom of the facies in the Snadd Formation with a change into wavy bedding, while in the Kobbe Formation the subfacies occurs at the top of the facies with a change from wavy bedding to lenticular bedding. The mud is the dominant grain size and the sand occurs as isolated sand lenses with current ripples within the mud. Minor bioturbation occur within the succession (Figure 5.6 C; Figure 5.7 C).

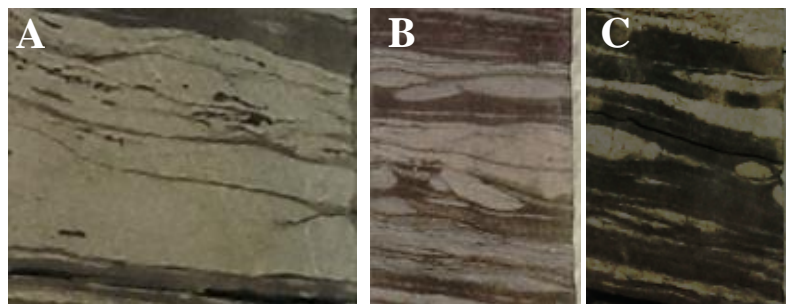


Figure 5.6: Heterolithic deposits in the Kobbe Formation. A: Flaser bedding at 2231 m depth; B: Wavy bedding at 2229 m depth; C: Lenticular bedding at 2225 m depth.

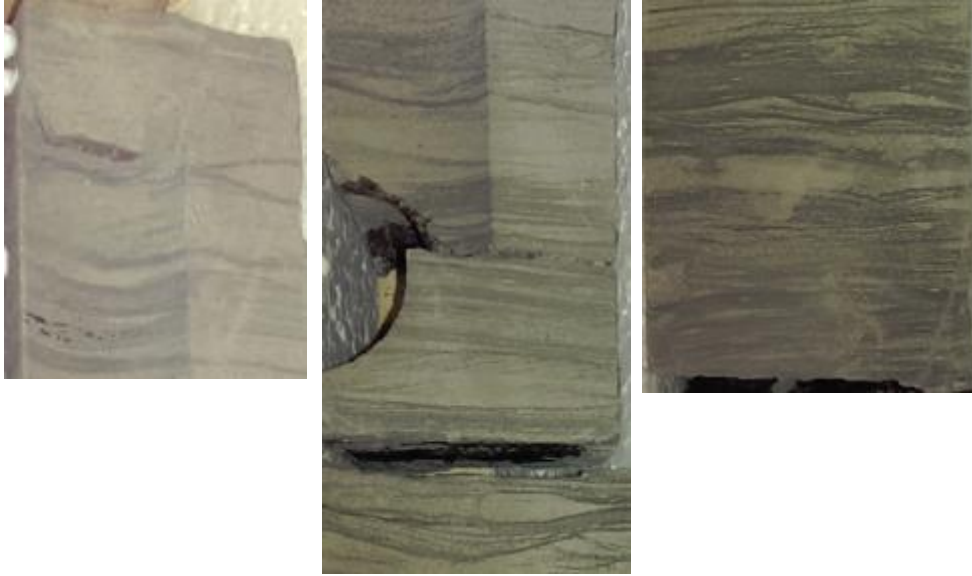


Figure 5.7: Heterolithic deposits in the Snadd Formation. A: Flaser bedding at 801 m depth; B: Wavy bedding at 801.5 m depth; C: Lenticular bedding at 802 m depth.

#### **Facies 4: Palaeosol**

This facies represents only in the middle part of the Snadd Formation. There is a thin layer of palaeosol at 799.5-800 m depth and a 1.5 m thick package of palaeosol with interbedded sand lenses at 805.5-807 m. The palaeosol layer is found under and above the massive sandstone unit with interbedded siltstone, sandstone and heterolithic deposits facies. The facies associated to intensive bioturbation and rootlets. The colour of the palaeosol is changing between black and grey with light coloured interbedded sand lenses and few part of the soil consists of soft sediments. A little calcite cement is present in the sample (Figure 5.8)



Figure 5.8: Palaeosol represents in the Snadd Formation.

## **Facies 5: Carbonate cemented sandstone**

The facies can be divided into three subfacies based on the dominating sedimentary structures and is found in both Snadd and Kobbe Formations. In the Snadd Formation all three subfacies are presented and most abundant is the dolomite and ankerite cemented sandstone. Less abundant the calcite cemented sandstone, in the Kobbe Formation only the calcite cemented sandstone is present.

### *Facies 5A: Horizontal lamination*

The dominant characteristic of this subfacies is that the carbonate cement mainly consists of dolomite and ankerite and a little amount of calcite. The sandstone is highly carbonate cemented with horizontal lamination and minor bioturbation (Figure 5.9 A). The succession is underlain by Facies 5B and overlain by calcite cemented sandstone.

### *Facies 5B: Bioturbation*

The cement is the same as in Facies 5A, ankerite and dolomite is the most abundant in this unit with moderate calcite cement. The difference between Facies 5A-5B is that this subfacies associated with intensive bioturbation (Figure 5.9 B). The dolomite-ankerite sandstone is overlain by Facies 5A and underlain by the horizontal laminated mudstone.

### *Facies 5C: Cross-bedded calcite cemented sandstone*

In the Snadd Formation this succession is found in between the cross-bedded massive sandstone unit with 1 m thick very fine- to fine-grained sandstone package at 788-789 m depth. The subfacies occur in the middle and in the upper part of the Kobbe Formation. The uppermost subfacies is 0.75 m thick fine- to very fine-grained sandstone going into siltstone, underlying by alternating mud and sand layers. The lowermost unit is very fine-grained porous sandstone with planar cross bedding, overlying by alternating mud and sand layers and underlying very fine- to fine-grained, red coloured sandstone with moderate bioturbation (Figure 5.9 C1-C2).

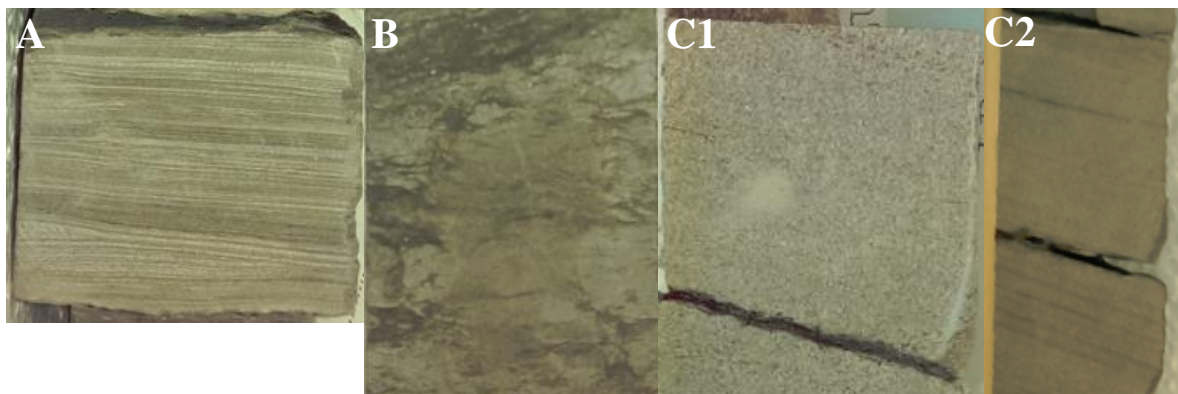


Figure 5.9: The sample represents carbonate cemented sandstone with the different subfacies. A: Horizontal lamination in the Snadd Fm at 1296 m depth; B: Bioturbation in the Snadd Fm at 1298 m depth; C1: Cross-bedded sandstone in the Snadd Fm; C2: Cross-bedded sandstone in the Kobbe Fm.

### **Facies 6: Mudstone**

The facies is found in both Snadd and Kobbe Formation and subdivided into 2 subfacies described below.

#### *Facies 6A: Mudstone with bioturbation*

The subfacies represents 0.5 m thick layer in the lowest part of the Snadd Formation with intensive bioturbation at 1299 m depth. The mudstone is black coloured and contains interbedded sand lenses. The mudstone is overlain by dolomite-ankerite cemented sandstone (Figure 5.10 A).

#### *Facies 6B: Horizontal lamination*

This subfacies is present at the deepest and at the shallowest part of the core giving a frame for the Kobbe Formation. The deep layer is found at 2243 m, it is 1 m thick and is overlain by ripple-laminated sandstone, while the top layer 4-4.5 m thick and underlying by bioturbated siltstone. The mudstone has black-greyish colour (Figure 5.10 B).

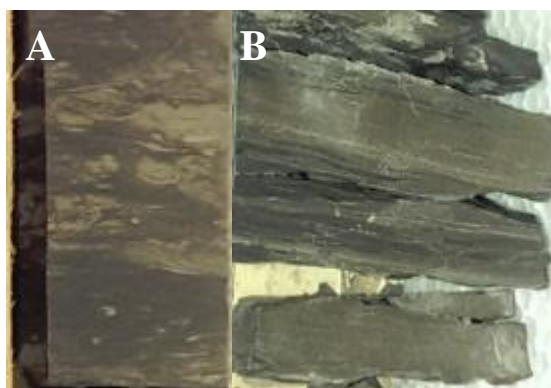


Figure 5.10: A: Bioturbated mudstone in the Snadd Formation; B: Horizontally laminated mudstone in the Kobbe Formation.

### **Facies 7: Very fine – Fine-grained sandstone**

The facies represents in both Snadd and Kobbe Formations and divided into 2 subfacies. The facies is found at the lowermost part and at the middle part of the Kobbe and Snadd Formations.

#### *Facies 7A: Very fine – Fine-grained sandstone with bioturbation*

This subfacies represents at the middle part of the Kobbe and Snadd Formations. The sandstone layer from the Kobbe Formation core is red coloured while the unit from the Snadd Formation core is grey coloured. The bioturbation in the Kobbe sample is more intensive than in the Snadd sample (Figure 5.11 A-B). The subfacies is underlain by lenticular-bedded deposits and overlain by carbonate cemented sandstone layer in the Kobbe Formation and in the Snadd Formation is underlain by siltstone with sand lenses and overlain by lenticular- and wavy-bedded deposits.

#### *Facies 7B: Ripple-laminated sandstone*

The subfacies occurs only in the lowermost part of the Kobbe Formation and it is underlain by horizontal laminated mudstone and overlain by flaser- and wavy-bedded deposits. Sand is the dominant grain size in the 9 m thick very fine – fine-grained sandstone with several coal lenses. The current ripple laminae are mostly horizontal (Figure 5.11 C).

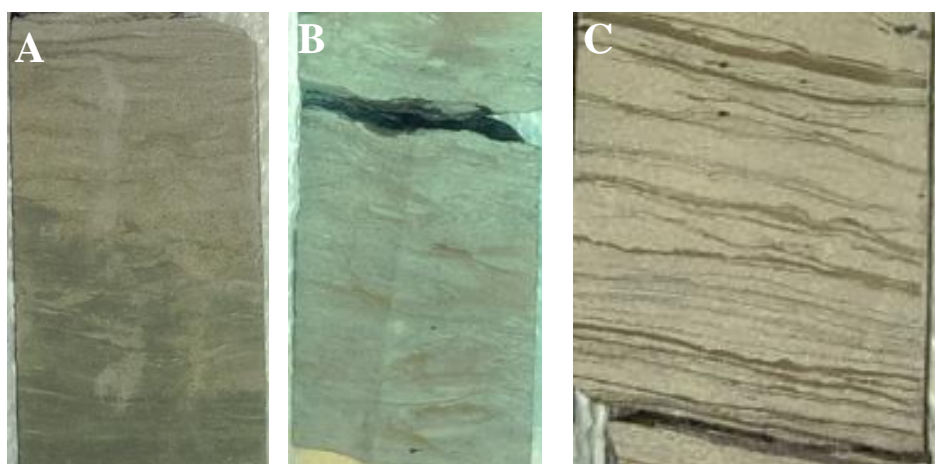


Figure 5.11: A: Vf-f-grained sandstone with bioturbation in the Snadd Formation at 803 m depth; B: Vf-f-grained sandstone with bioturbation from the Kobbe core at 2223-2224 m depth; C: Vf-f-grained sandstone with current ripples in the Kobbe Formation at 2239 m depth.

### **Facies 8: Alternating mud and sand layers**

The facies is found only in the Kobbe Formation at 2217-2221 m depth. Black-grey coloured muddy layers (silty clay) varying with light-coloured sandy layers with some sand lenses. The sandy layers are changing silty fine sand to fine sandy silt (Figure 5.12). The facies is situated in between the carbonate cemented sandstone units. Bioturbation is also present in the succession with low grade.

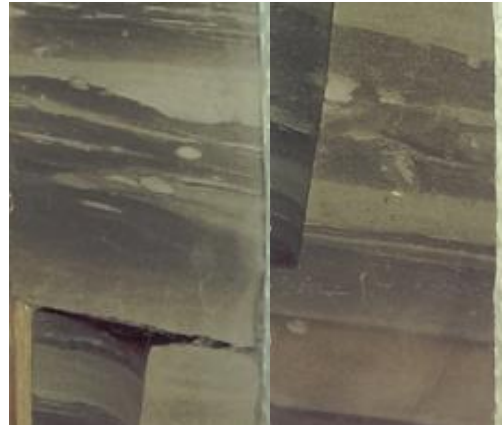


Figure 5.12: Alternating mud and sand layers in the Kobbe Formation.

### 5.3 Facies association

Four possible depositional environments have been defined by using the core and the facies descriptions (Table 5.1). All facies associations submit a tidal influenced delta as depositional environment with several subenvironments.

Table 5.1: The interpreted facies association with the depositional environments and subenvironments.

<b>Facies association</b>	<b>Depositional environment</b>	<b>Subenvironment</b>	<b>Geological features</b>	<b>Included facies</b>
FA1	Delta plain/Coastal plain	Tidal channels, tidal creeks, distributary channels, mouth bars, inter- to supratidal flats	High sand: mud ratio; Cross bedding is visible; No sign of reworking; Carbonate cement; Horizontal lamination;	F1, F5, F7
FA2	Muddy shelf, prodelta, delta front, intertidal zone		High mud: sand ratio; Interbedded sandstone; Intense bioturbation	F4, F6
FA3	Interdistributary areas on the delta plain	Crevasse splays, crevasse channels, levees, bays	Interbedded mud and silt; Heterolithic deposits; Moderate bioturbation	F2, F3, F4, F7
FA4	Delta plain	Tidal flat (mud flat, mixed flat)	Heterolithic deposits; Lower sand: mud ratio; Alternating sand and mud	F3, F8, F4



## 6. Petrographic analysis

### 6.1 Snadd Formation

#### 6.1.1 Lithology and texture

The deeper samples of the Snadd Formation (1287-1299.5 m) contain well-sorted very fine-grained sandstone with high clay and carbonate content. The shallowest part of the Snadd Formation (778.80-807 m) is well-sorted very fine- to fine-grained and medium-grained sandstone with lower clay and carbonate content. The grains are dominantly subangular and the contact between the grains is mostly tangential and long (Figure 6.1).

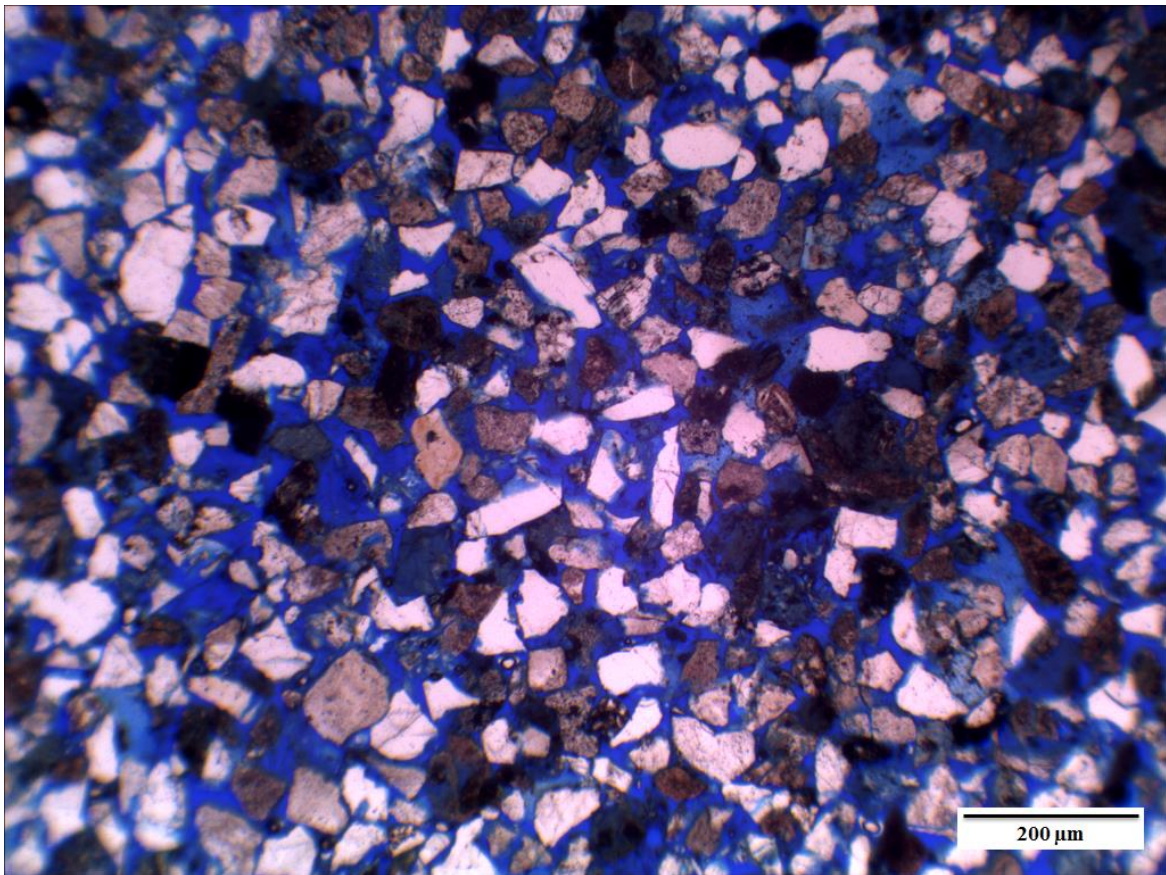


Figure 6.1: Well-sorted very fine- to fine-grained quartz-rich sandstone at 784.10 m depth. The white grains are quartz, the white to dusty brown grains are feldspar and the dark brown black grains are rock fragments.



### 6.1.2 Detrital grains

Quartz is the most abundant detrital mineral in the Snadd Formation (Table 6.1). The quartz grains are mostly monocrystalline but polycrystalline grains are also found in the formation with volume ranging from 2 to 10%. The amount of quartz in the Snadd Formation is ranging between 28-51%.

K-feldspar as microcline present in all samples with sample volume of 0,3-4,25%. The microcline grains are showing twinning and some of them are partially or totally dissolved. Plagioclase feldspar is also seen in all samples with volume of 2,9-8,2% (Table 6.1). Some grains show albite twinning, while some grains are heavily sericitized and preservation of albite twinning is not possible. Grains with low sericite-grade also show albite twinning. Little plagioclase feldspar is partly or totally dissolved.

Rock fragments are found in all samples including quartz and mica rich rock fragments, mica schist, volcanic rock fragments, mud rock fragments and cherts. Rock fragments account for 12,5-25,5% of sample volumes (Table 6.1).

Both muscovite and biotite are present in the Snadd Formation. The mica grains are dominantly compressed and folded around the other detrital grains. Some of the grains have been partly or totally dissolved and replaced by chlorite. Chlorite grains appear in the samples and have been defined as detrital grains (Figure 6.4 C).

Heavy minerals are also found in the formation, including zircon, staurolite, rutile, apatite, monazite and sphalerite.

### 6.1.3 Authigenic minerals

#### *Quartz*

Quartz overgrowths only occur in trace amounts (0,3-1,3%) in the samples, due to chlorite coating almost all the grain surfaces. The quartz overgrowth generally observed where calcite cement and chlorite coating are incomplete (Figure 6.2 A).

#### *Kaolinite*

Kaolinite occurs as a pore-filling mineral filling the voids of dissolved minerals as well as intergranular pore spaces. In the intergranular pore spaces kaolinite represents blocky

pseudohexagonal booklets together with vermicular structure. The kaolinite booklets are linked to microporosity and pore-filling chlorite. Kaolinite was also observed replacing mica and feldspar. Kaolinite account for 1,25-6,6% of sample volumes in the Snadd Formation (Figure 6.2 B,D).

### *Chlorite*

Chlorite is an abundant authigenic minerals in all samples as well as pore filling minerals and grain coating. Pore filling chlorite develops fibrous grains and partially or totally replacing mica. Pore filling chlorite is mostly associated with kaolinite and chloritized mica. Where chlorite coating is present quartz overgrowth is absent in the samples. Chlorite is covering almost all grains as grain coating mineral in the Snadd Formation. The pore filling chlorite is ranging between 0,5-8,25%, while grain coating chlorite from 3,9 to 8,1% in the formation (Figure 6.2 A,C).

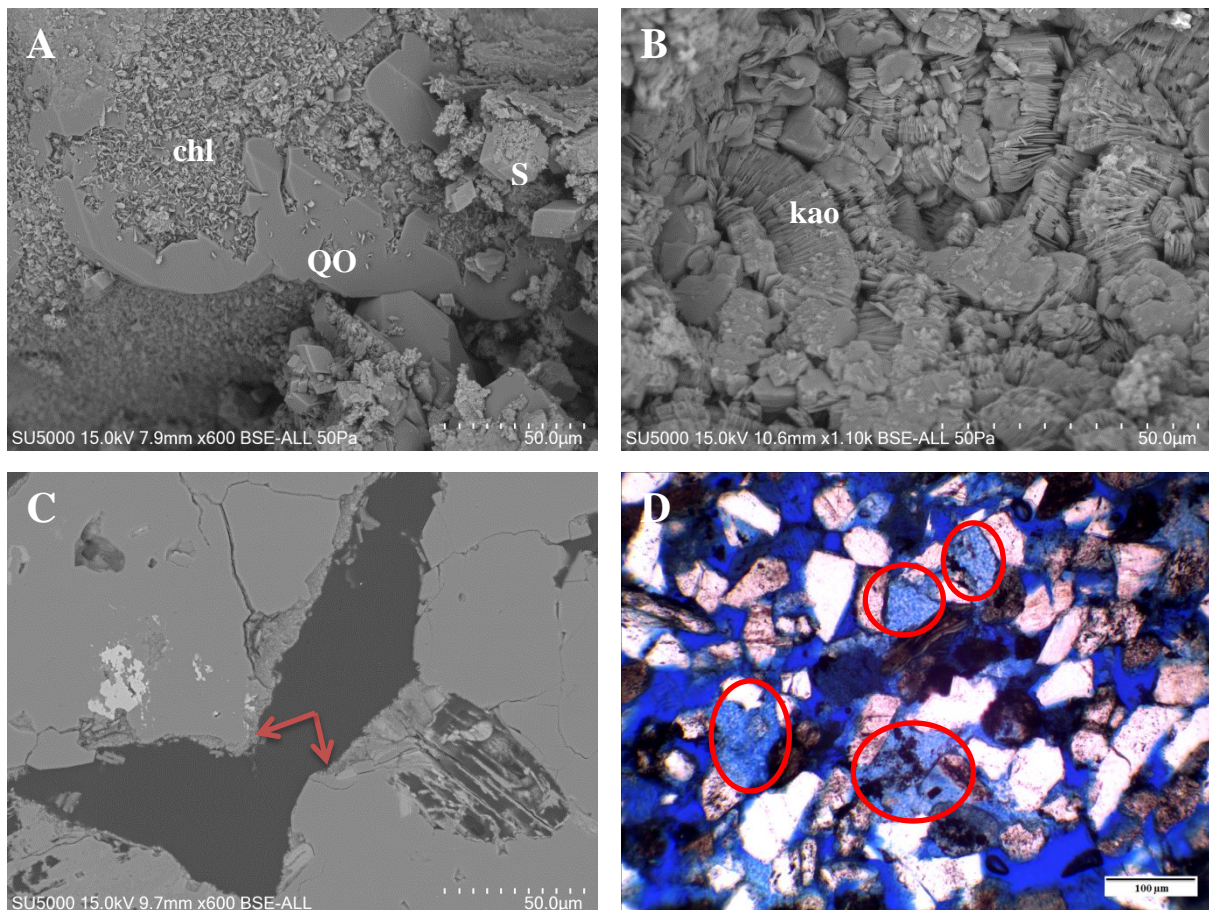


Figure 6.2: A: The sample represents quartz overgrowths (QO), chlorite coating (chl) and rhombic siderite (S) grains at 797.60 m depth in 3D, picture taken by SEM; B: Authigenic pore-filling kaolinite at 780.50 m depth in 3D, picture taken by SEM; C: Chlorite coating (red arrows) in a 2D-view at 784.10 m depth, picture taken by SEM; D: Pore-filling kaolinite (red circles) as viewed through plane polarized light (ppl) at 782.70 m depth.

## Siderite

Two types of siderite cement are seen in the Snadd Formation. The siderite forms brown rhombic grains (Figure 6.2 A; Figure 6.3 A,C,D) and represents within the clay clasts and mica grains and occurs as complete cement at 797,60 m depth together with pyrite and calcite cement (Figure 6.3 B). The other type of siderite appears as spherulitic patches in the samples and they are generally dissolved mostly in the crystal cores. These dissolution pores usually filled by authigenic chlorite. The rhombic-shaped siderite occurs at shallower part of the formation, while the spherulitic siderite patches appear only at 1293,80 m depth in the formation.

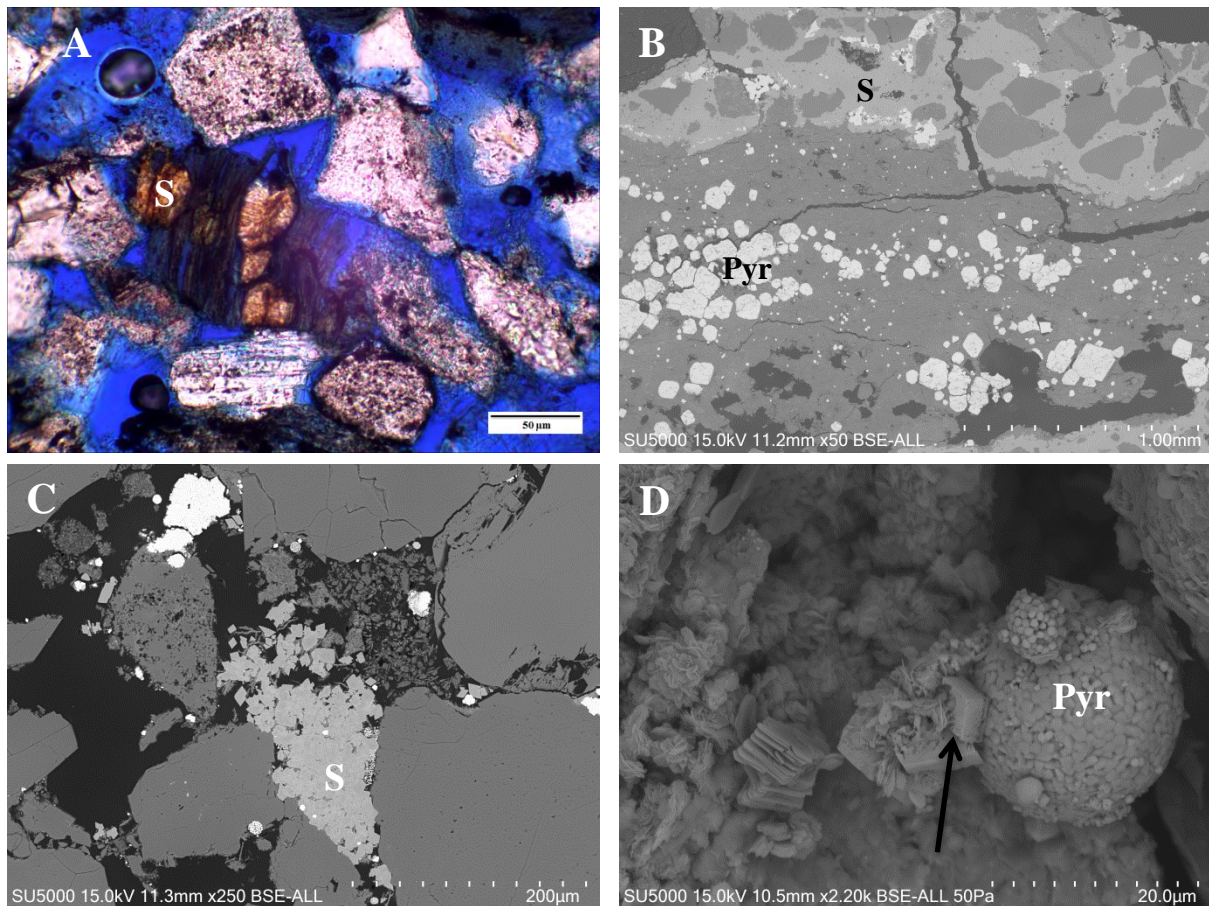


Figure 6.3: A: The sample represents rhombic siderite grains within expanded biotite at 782.70 m depth (ppl); B: Siderite cement (S) together with blocky pyrite crystals (Pyr) in mica rich matrix at 797.60 m depth (SEM 2D); C: Rhombic siderite grains (S) filling the pore space at 797.60 m depth (SEM 2D); D: 3D-view of rhombic siderite grains (indicating with black arrow) and framboidal pyrite grains (Pyr) at 797.60 m depth (SEM).



### *Ankerite and dolomite*

Ankerite and dolomite are found at the deepest part of the Snadd Formation. In the core samples they occur with red-brown colour with horizontal lamination and intensive bioturbation. Fibrous chlorite is also present in the pore space (Figure 6.4 A,B).

### *Calcite*

Calcite cement occurs in the pore space as pore filling cement and it is dominant in the middle part and at the bottom of the Snadd Formation (Figure 6.4 A,C,D). Cementation does not take place 100% in the samples there are several pore spaces which filled by clays or just presenting porosity. The calcite cement is replacing detrital grains, usually feldspar grains (Figure 6.4 C).

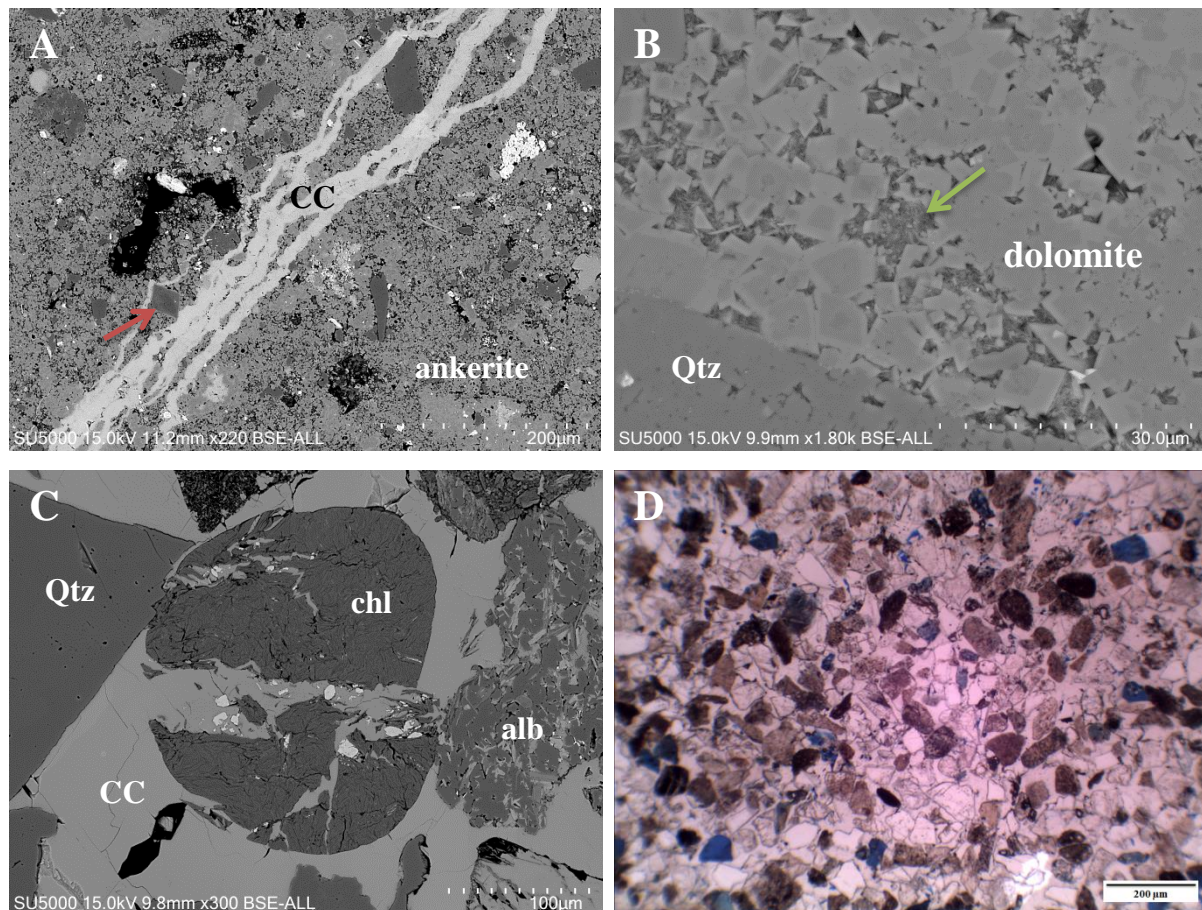


Figure 6.4: A: The sample contains mainly ankerite with calcite veins (CC), red arrow indicates dolomite grain at 1297.60 m depth (SEM 2D); B: The sample consists of dolomite, quartz (Qtz) and pore-filling chlorite (green arrow) at 1292.15 m depth (SEM 2D); C: Calcite cement replacing chlorite and albite grains at 788.42 m depth (SEM 2D); D: Calcite cemented sandstone (788.42 m) (ppl).

## *Pyrite*

Both framboidal and blocky pyrite crystals (Figure 6.3 B-D) are observed in the samples. The pyrite crystals were recognized only by using scanning electron microscope. Pyrite cement was observed together with siderite and calcite cement at 797,60 m depth under scanning electron microscope (Figure 6.3 B-D; Figure 6.5).

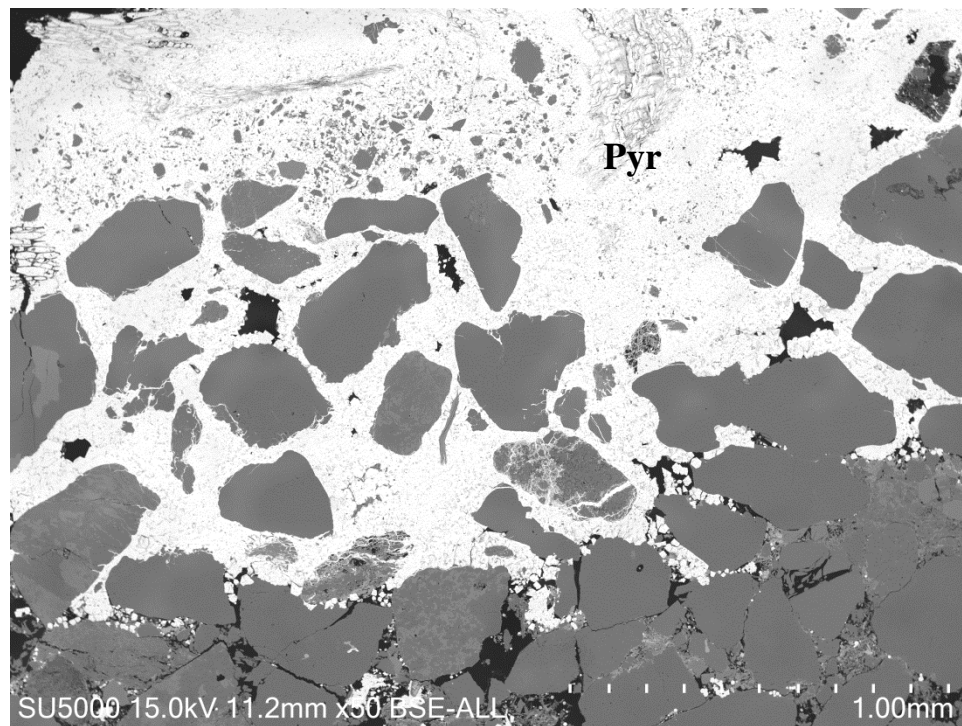


Figure 6.5: Pyrite cement (Pyr) at 797.60 m depth in the Snadd Formation.



## 6.2 Kobbe Formation

### 6.2.1 Lithology and texture

The samples of the Kobbe Formation contain moderately-sorted very fine-grained sandstone with moderate to high clay content (Figure 6.6).

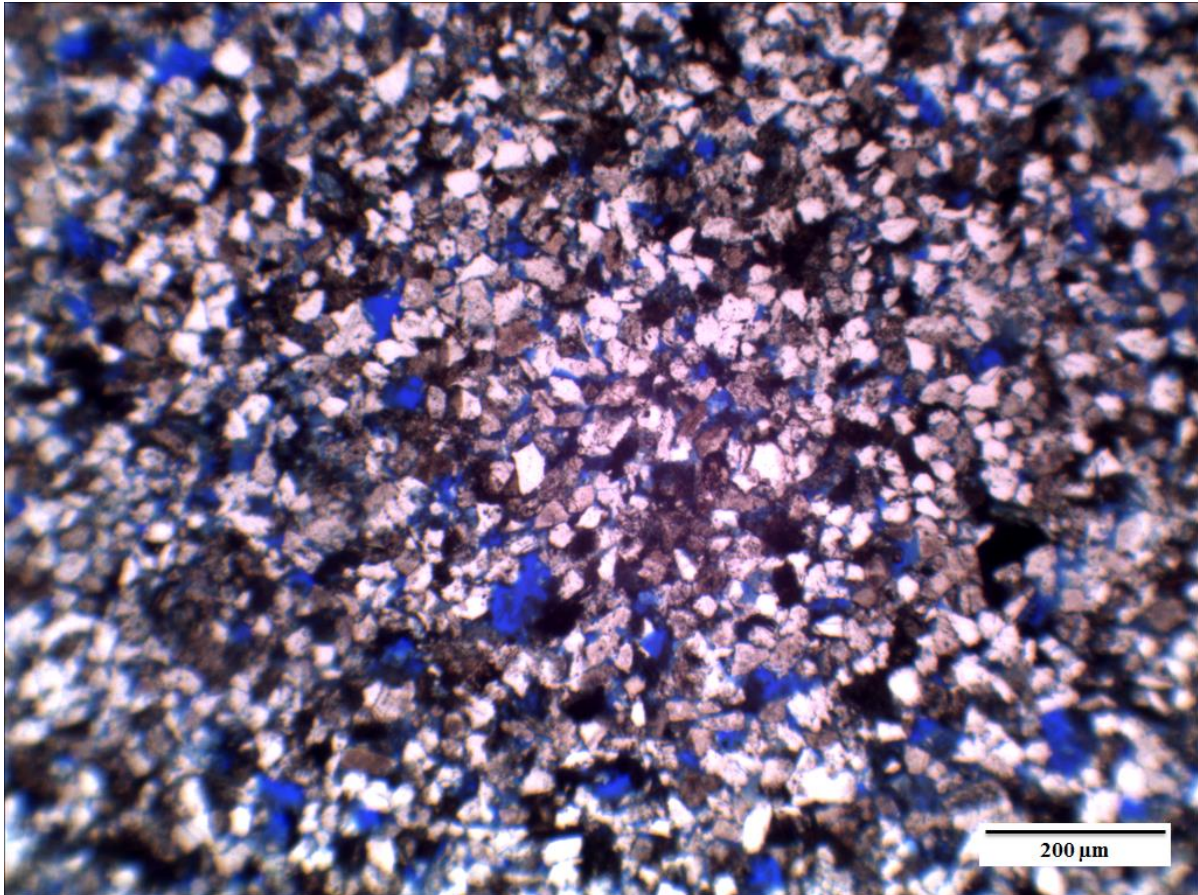


Figure 6.6: Well-sorted very fine-grained quartz-rich sandstone at 2237.65 m depth in the Kobbe Formation

### 6.2.2 Detrital grains

Quartz is the most abundant detrital mineral in the Kobbe Formation, including mostly monocrystalline grains but polycrystalline grains are also present (2,5-9%). The amount of quartz is ranging between 24,5-56% in the Kobbe Formation (Table 6.1).

K-feldspar is not present in the Kobbe Formation but the volume of the plagioclase feldspar is ranging from 6 to 11,5% (Table 6.1). Some of the plagioclase grains show albite twinning,

some of them contains high amount of sericite. Grains with low amount of sericite also show albite twinning. Several grains are partly or totally dissolved.

Rock fragments are also present in the formation with volume of 11,5-34% (Table 6.1), including cherts, mica and quartz rich rock fragments, mica schists, volcanic rock fragments and mud rock fragments.

Both muscovite and biotite are observed in the samples in trace amounts. The mica grains are mostly crushed and folded around the other minerals and few of them are partially or totally dissolved and replaced by chlorite. Detrital chlorite was observed at depth 2241.65 meter (Figure 6.8 E).

Heavy minerals are also present in the formation, including zircon, monazite, rutile and apatite. Carbonate fossils developed at shallower part of the formation in trace amount and it may be a source of the carbonate cement.

### **6.2.3 Authigenic minerals**

#### *Quartz*

Quartz overgrowths are present with volume of 0,2-1% in the Kobbe Formation. Quartz overgrowth is commonly seen where calcite cement and chlorite coating are absent (Figure 6.7 C,E,F). Slightly more quartz overgrowth represents in the Kobbe Formation than in the Snadd Formation.

#### *Kaolinite*

The kaolinite is present in the samples as pore filling mineral, filling the voids of dissolved grains as well as intergranular pores. In the pore space kaolinite builds up blocky pseudo-hexagonal booklets together with vermicular patterns. The pore filling kaolinite is associated with microporosity and pore filling chlorite. The chlorite fills the space between the kaolinite booklets. Kaolinite was observed replacing feldspar and mica. Kaolinite account for 0,7-3,25% of sample volumes (Figure 6.7 B-F).

### *Chlorite*

Chlorite is present both as pore filling and grain coating authigenic mineral in the Kobbe Formation. The pore filling chlorite account for 0,5-7,1% of sample of the volumes, while grain coating chlorite is ranging between 1,5-3%. Chlorite coating in the Kobbe Formation is not so developed as in the Snadd Formation. The chlorite coating is not continuous. Where chlorite coating is missing quartz overgrowths take place. The pore filling chlorite builds up fibrous grains and partially or totally replacing mica grains. Fibrous chlorite mostly linked to kaolinite and chloritized mica (Figure 6.7 A-F).

### *Siderite*

The spherulitic siderite cement commonly observed in the shallower samples while the rhombic-shaped siderite is present at deeper depths within expanded mica grains. The core of spherulitic siderite grains is mainly dissolved and the pores are usually filled by authigenic chlorite (Figure 6.7 A, Figure 6.8 A-D).

### *Calcite*

Calcite is present as pore filling cement in the Kobbe Formation and it is dominant at shallower part of the Kobbe Formation (Figure 6.8 A-B). The cementation does not fill the pore space 100%, there are few voids left which filled by clays or preserving porosity. The calcite cement is replacing detrital grains, generally feldspar grains.

### *Pyrite*

Both framboidal and blocky pyrite crystals are observed in the formation. The pyrite crystals were recognized only by using SEM.



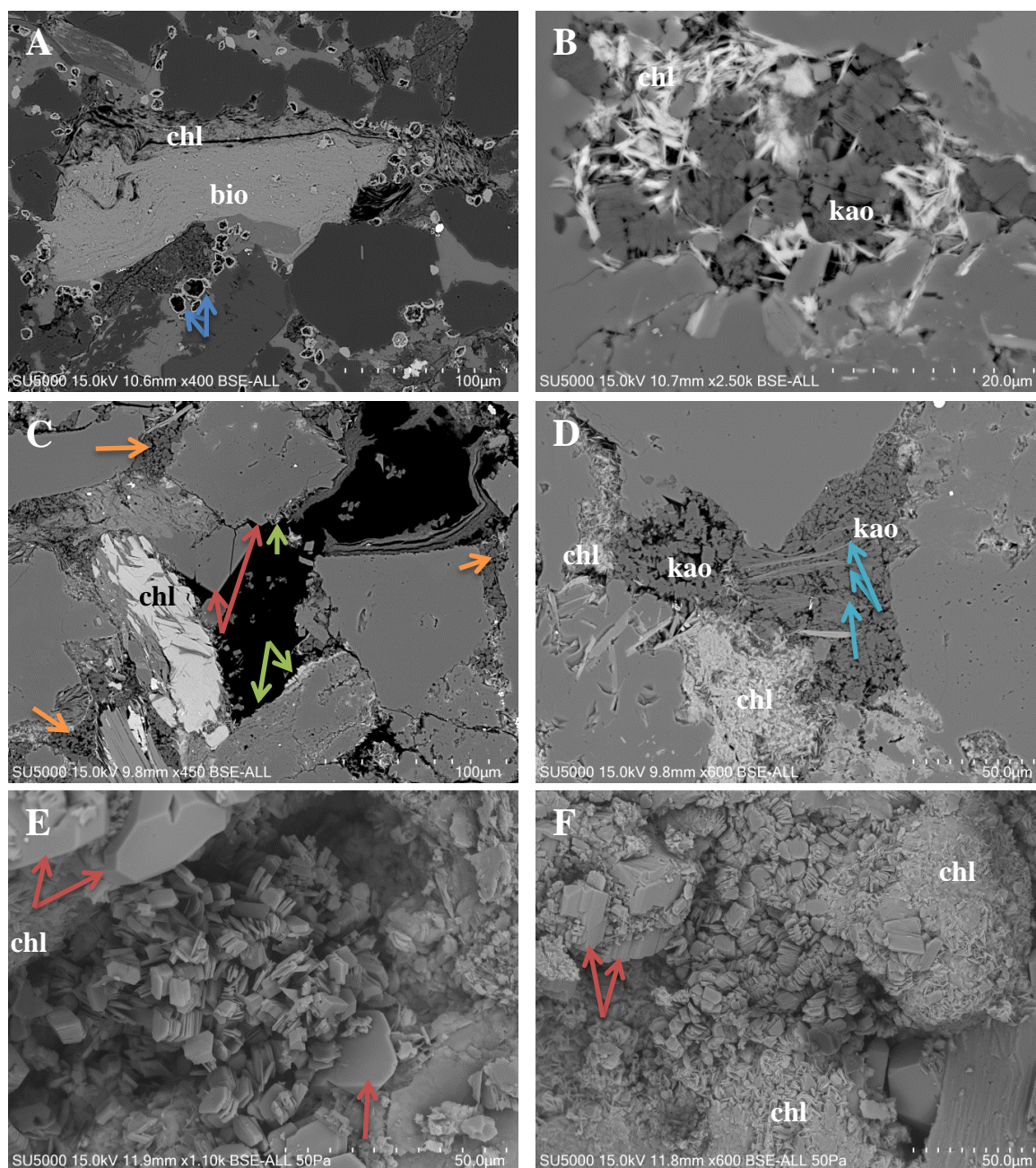


Figure 6.7: A: The sample represents biotite (bio) grain being replaced by chlorite (chl), blue arrows showing siderite cement at 2214.75 m depth (SEM 2D); B: Pore-filling authigenic chlorite (chl) and kaolinite (kao) at 2230.60 m depth (SEM 2D); C: The sample represent chlorite coating (green arrows), where the coating is incomplete quartz overgrowths are present (red arrows). Authigenic kaolinite is present in the pore space (orange arrows). Chlorite (chl) is replacing mica grain at 2233.60 m depth (SEM 2D); D: Pore-filling authigenic kaolinite (kao) is replacing muscovite (blue arrows) at 2241.65 m depth (SEM 2D); E-F: Pore-filling authigenic kaolinite with chlorite coating (chl) and where the coating is absent quartz overgrowths appear (red arrows) at 2241.65 m depth (SEM 3D).



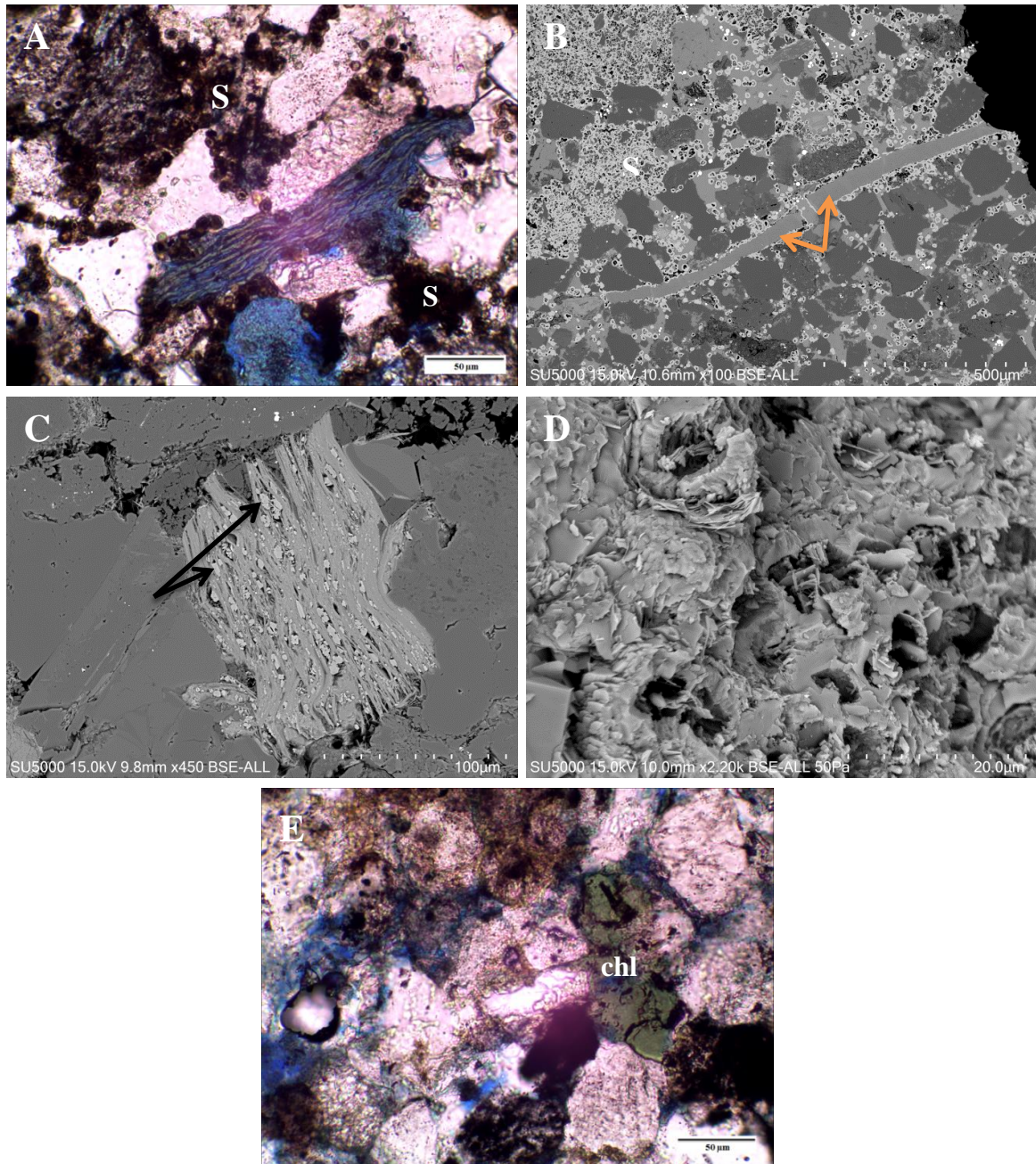


Figure 6.8: A-B: Calcite cemented sandstone at 2214.75 m depth. Siderite cement (S) scattered all over the sample. Carbonate fossil is presented by orange arrows; C: Rhombic siderite grains (black arrows) within expanded biotite grain at 2241.65 m depth; D: Siderite cement patches in 3D view at 2214.75 m depth (SEM); E: Detrital chlorite grain (chl) is present at 2241.65 m depth.

### 6.3 Modal analysis

The results of the modal analysis are presented in Table 6.1. The purpose of the modal analysis was to compare the maturity of both Kobbe and Snadd Formation. The results do not show difference between the 2 formations, both sandstone have been interpreted as lithic arenite and plotted in the QFR-diagram (Figure 6.9). The Snadd and Kobbe formations are mineralogical immature sandstones.

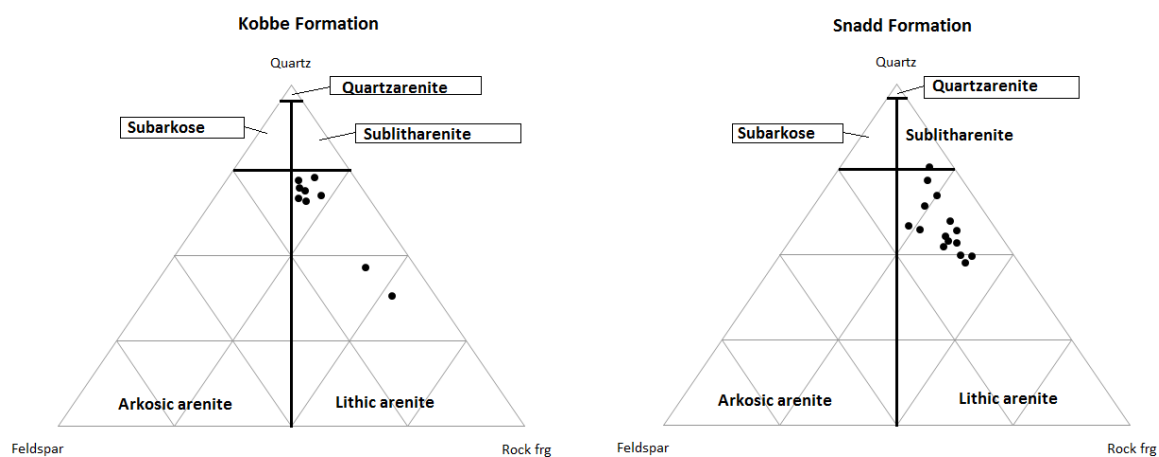


Figure 6.9: The figure shows the sandstone composition for the Kobbe and Snadd Formation in the 7222/11-1 well. All samples represent lithic arenite sandstones.

Table 6.1: Modal analysis of the Snadd (left) and Kobbe Formations (right) in well 7222/11-1.

Sample	Depth (m)	Quartz		Feldspar		Rock fr.		Porosity		Qtz overgr.		Chlorite		Kaolinite	Siderite	Carbonate	IGV	Matrix
		Monocrystalline	Polycrystalline	Plg	Kfs			Primary	Secondary			Coating	Pore-filling					
S1	778.80	31,25	5,75	8,2	2,3	17,2		12,25	4,25	1,3		4,3	5,8	5,3	-	-	30,95	2
S2	780.50	24,2	5	4,25	2,75	25,2		10,5	5,2	1,2		5,9	6,9	6,6	-	-	33,2	2
S3	782.70	28,7	2	5,4	1,6	24,2		8,75	6,75	0,3		8,1	6,8	3,5	-	-	31,15	3,7
S4	784.10	30	5,5	5,5	2	21,2		10,72	9,98	0,75		5,75	4,25	2,25	-	-	25,72	2
S5	787.60	26,2	4	4	1,5	25,5		13,7	7	1,25		4,25	5,5	4,5	-	-	31,7	2,5
S6	788.42	24,4	9,6	6,25	4,25	13,7		0,25	3,75	-		-	0,5	-	-	34,7	37,95	2,5
S7	790.70	31,2	6,8	4,7	1	23		9,25	7,25	-		5,5	5,5	3	-	-	25,95	2,7
S8	792.65	30,2	9	5,2	2	14,7		13,7	9	-		4,6	4,4	4,2	0,5	-	29,6	2,2
S9	794.65	25	10	5,7	2,5	22,7		10,14	8,4	-		3,9	4,9	3,4	0,3	-	24,6	2
S10	796.65	42,25	6,25	2,9	0,3	12,5		21,2	7	-		6,5	0,5	-	-	-	28,7	0,5
S12	799.20	32,5	4,5	4	1,5	20,2		11,2	8,5	1		6,75	6	1,25	-	-	28,7	2,5
S14	804.60	28,2	5,5	5	2,5	21,5		6,5	8	0,5		6,25	7,75	3,5	-	-	29,2	4,7
S16	1287.40	45,6	4,6	3,9	1,3	14,5		11,5	6,2	-		5,25	5,25	-	-	-	23,7	1,7
S17	1290.70	37,5	7,2	3,5	1,5	16,7		8,7	9,5	0,75		4,5	8,25	-	-	-	23,9	1,7
S19	1293.80	29,5	4,5	4,25	2,25	23,2		4,9	6,3	-		5	5	-	-	7,7	29,9	7,2

Samples	Depth (m)	Quartz		Feldspar		Rock fr.		Porosity		Qtz overgr.		Chlorite		Kaolinite	Siderite	Carbonate	IGV	Matrix
		Monocrystalline	Polycrystalline	Plg	Kfs			Primary	Secondary			Coating	Pore-filling					
K1	2214.75	21	3,5	6	-	34		1,5	1,7	-		-	1	-	-	21,5	33,7	9,7
K3	2221.50	34,2	2,5	8,5	-	34		3,5	1,2	0,2		1,6	7	-	1,1	-	19,5	6
K4	2230.60	42	9	9,2	-	13,7		0,5	1	-		-	0,5	0,75	-	19,25	25	4
K5	2233.60	46,4	4,8	10,7	-	15,7		1,3	2,4	-		1,5	6,1	1,7	-	-	19,6	9,2
K6	2235.65	49	3,2	10	-	12,7		5,2	3	0,7		1,7	7,1	1	-	-	21,9	6,2
K7	2237.65	48,5	5	9,2	-	11,5		4	4,5	0,25		3	6	3,3	-	-	21,2	4,7
K8	2239.65	46,8	4,7	11,5	-	14,2		2,7	2,5	1		1,75	3,5	3,25	-	-	20,2	8
K9	2240.65	50	6	6,5	-	14,5		4,3	2,2	0,5		1,5	5,5	0,7	-	-	20,65	8,2
K10	2241.65	46,6	6,9	7,7	-	18		1,75	1,75	0,25		2	5,75	2,5	-	1	18,95	5,7

### 6.3.1 Porosity and Intergranular volume (IGV)

The point counted porosity varies between 1,5-8,5% in the Kobbe Formation, while in the Snadd Formation it varies between 4-28,2% (Figure 6.10). The average porosity value is 5% for the Kobbe Formation and 17% for the Snadd Formation. The intergranular volume is ranging from 23,7 to 37,95% in the Snadd Formation while in the Kobbe Formation it is ranging from 18,95 to 33,7% (Figure 6.10). The average IGV of the Snadd Formation is 29% and it is 22% for the Kobbe Formation.

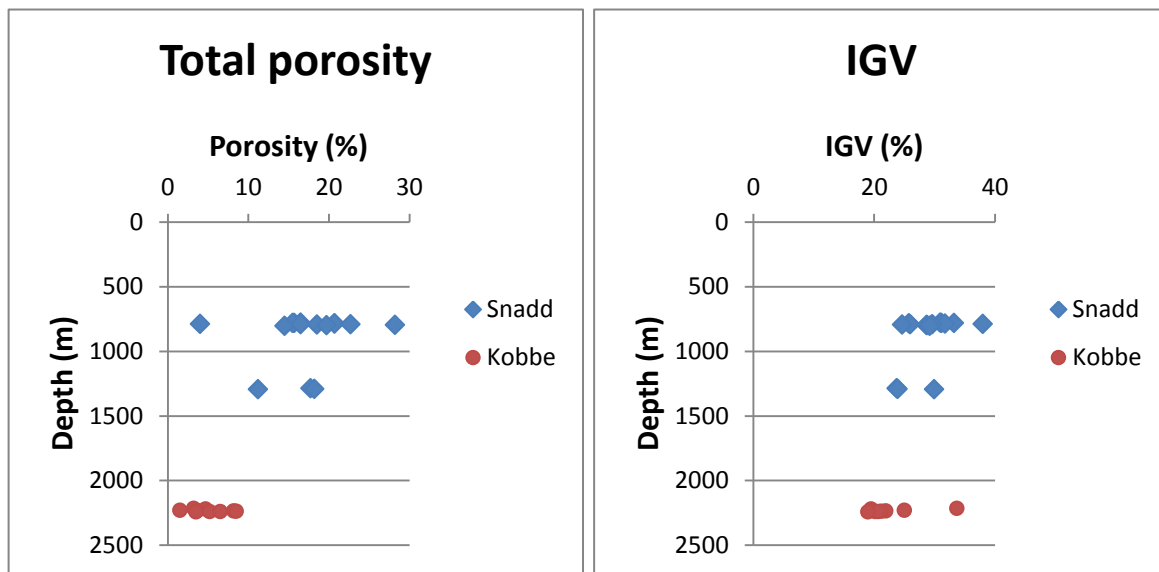


Figure 6.10: Total porosity and IGV for Snadd and Kobbe Formation.

The Snadd Formation shows higher porosity than the Kobbe Formation because the mechanical compaction has less effect on the sandstone due to low clay content and the lower amount of rock fragments than in the Kobbe Formation. Chlorite coating is more developed in the Snadd sandstones than in the Kobbe sandstones, preventing quartz cement and preserving higher porosity. The pore system in both sandstones generally consists of primary intergranular macropores. Due to mechanical compaction and precipitation of authigenic chlorite, kaolinite, carbonate cements and quartz overgrowth the original size of the pores has been changed. Micropores are mostly associated with authigenic kaolinite and chlorite and account for considerable part of the total porosity. Dissolution of feldspar and other detrital grains build up secondary porosity, but no net gain in porosity is documented as the volume dissolved, it is equal to the volume precipitated as cement.

## 7. Petrophysical analysis

In this chapter the results of the petrophysical analysis are presented. The reservoir properties such as volume of shale, porosity, water saturation, net-to-gross and permeability are calculated by using the geophysical logs. The uplift in the area is also calculated and results are presented in this chapter. The results are presented for Kobbe and Snadd Formations separately. The separate subheading is used for uplift estimation result.

### 7.1 Snadd Formation

In the well 7222/11-1 approximately 1372 m thick strata for Snadd Fm is encountered. The thickness and formation top information is provided by NPD. Considering the entire Snadd Formation the average shale volume calculated by using combination of the neutron-density log is 46 to 51 %. To calculate net-to-gross ratio, cut-off value used for porosity is 0.1 and  $V_{sh}$  is 0.3. All the results for petrophysical analysis of the Snadd Formation are shown in Table 7.1.

Table 7.1: The results of the petrophysical analysis of the Snadd Formation.

Well	Formation	Vsh	$\Phi_t$	$\Phi_e$	$S_w$	Gross (m)	Net (m)	N/G
7222/11-1	Snadd	0.46	0.15	0.13	0.90	1372	795	0.58

The results obtained by using geophysical logs are comparable with results obtained from thin section analysis. The thin clean reservoir interval approximately 21 m thick is observed from well 7222/11-1 (Figure 7.1). The clean sand interval is proven to be hydrocarbon saturated. Towards the top of the Snadd Formation small clean sand intervals, 1-2 m thickness are also observed from neutron-density crossover. Below the depth of the 1750 m depth (MDKB), the Snadd Formation contains usually shale with interbedded sandstones, siltstones and palaeosol.



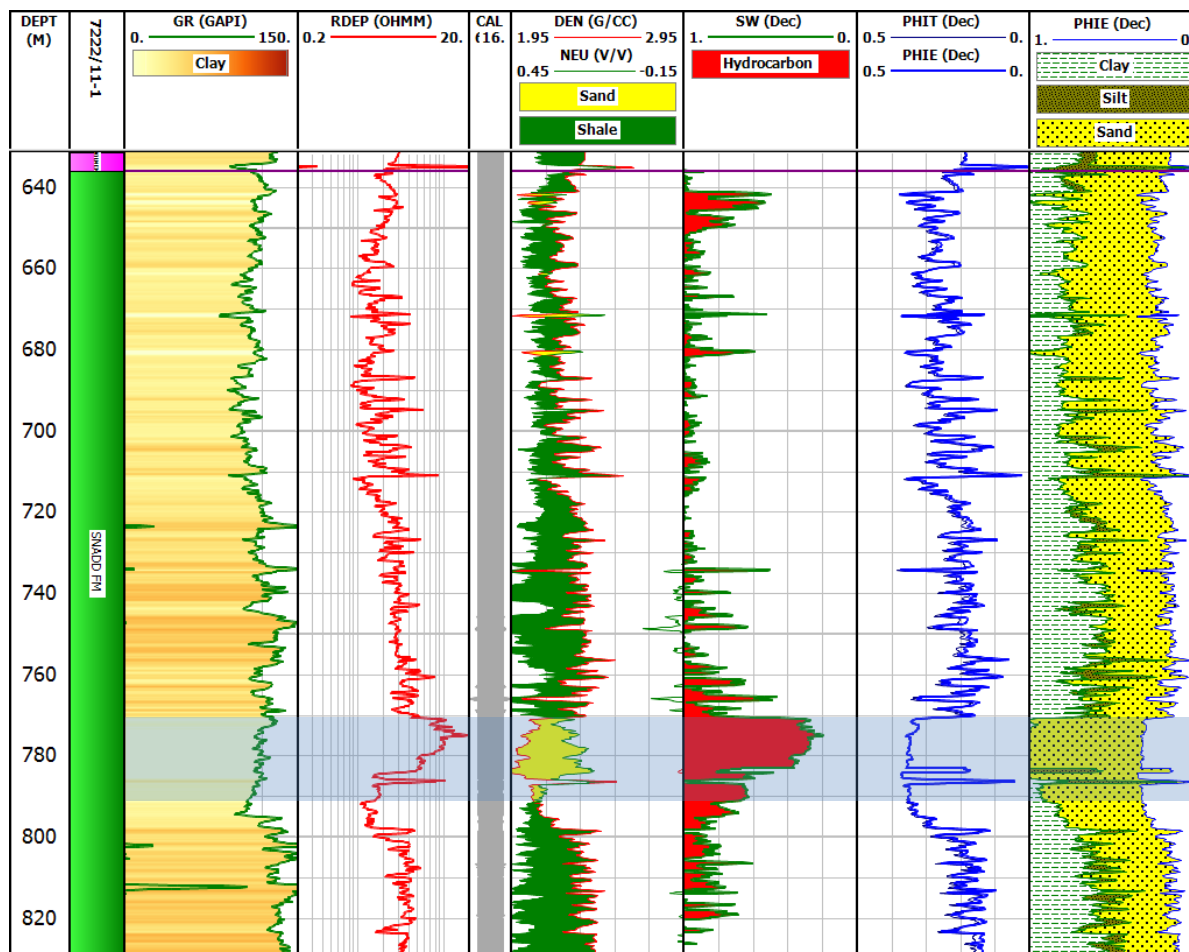


Figure 7.1: The composite log section of the Snadd Formation in well 7222/11-1. The clean reservoir interval marked with light blue shading. GR-gamma ray log; RDEP-deep resistivity log; DEN-density log; NEU-neutron log; SW-water saturation; PHIT-total porosity; PHIE-effective porosity.

## 7.2 Kobbe Formation

Approximately 73 m thickness of the Kobbe Fm is encountered in well 7222/11-1. The reservoir properties of the Kobbe Formation are comparatively bad in the following well. To calculate net-to-gross ratio cut-off value used for porosity 0.1 and shale volume is 0.3. The petrophysical results are shown in Table 7.2. The shale volume is calculated by combination of the neutron-density log. The average shale volume for this well is 62 %. The Kobbe Formation contains generally shale with interbedded sandstones and siltstones, with few clean sandstone packages which are highly carbonate cemented; therefore the formation has poor reservoir quality.

Table 7.2: The petrophysical results for the Kobbe Formation.

Well	Formation	Vsh	$\Phi_t$	$\Phi_e$	$S_w$	Gross	Net	N/G
7222/11-1	Kobbe	0.62	0.07	0.06	0.99	73	0.15	0.002

### 7.3 Porosity versus permeability

The average total porosity of the Snadd Formation in the studied well (estimated from neutron-density combination) is 15% and the average effective porosity (from neutron-density combination considering shale) is 13%. The average permeability is 7.7 mD in the Snadd Formation. The average total porosity (estimated from neutron-density log combination) is 7.7%, the average effective porosity is 7% in the Kobbe Formation in well 7222/11-1 and the average permeability is 0.12 mD (Figure 7.2).

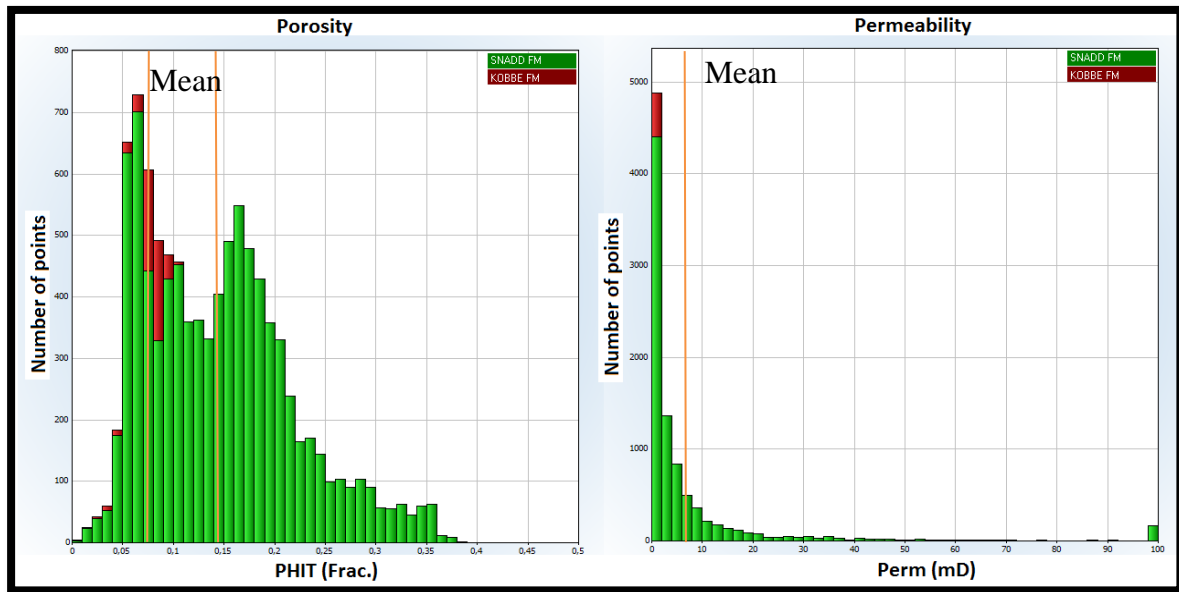


Figure 7.2: Total porosity and permeability in the Snadd and Kobbe Formations. Kobbe Formation shows low permeability and porosity values comparing to the Snadd Formation.



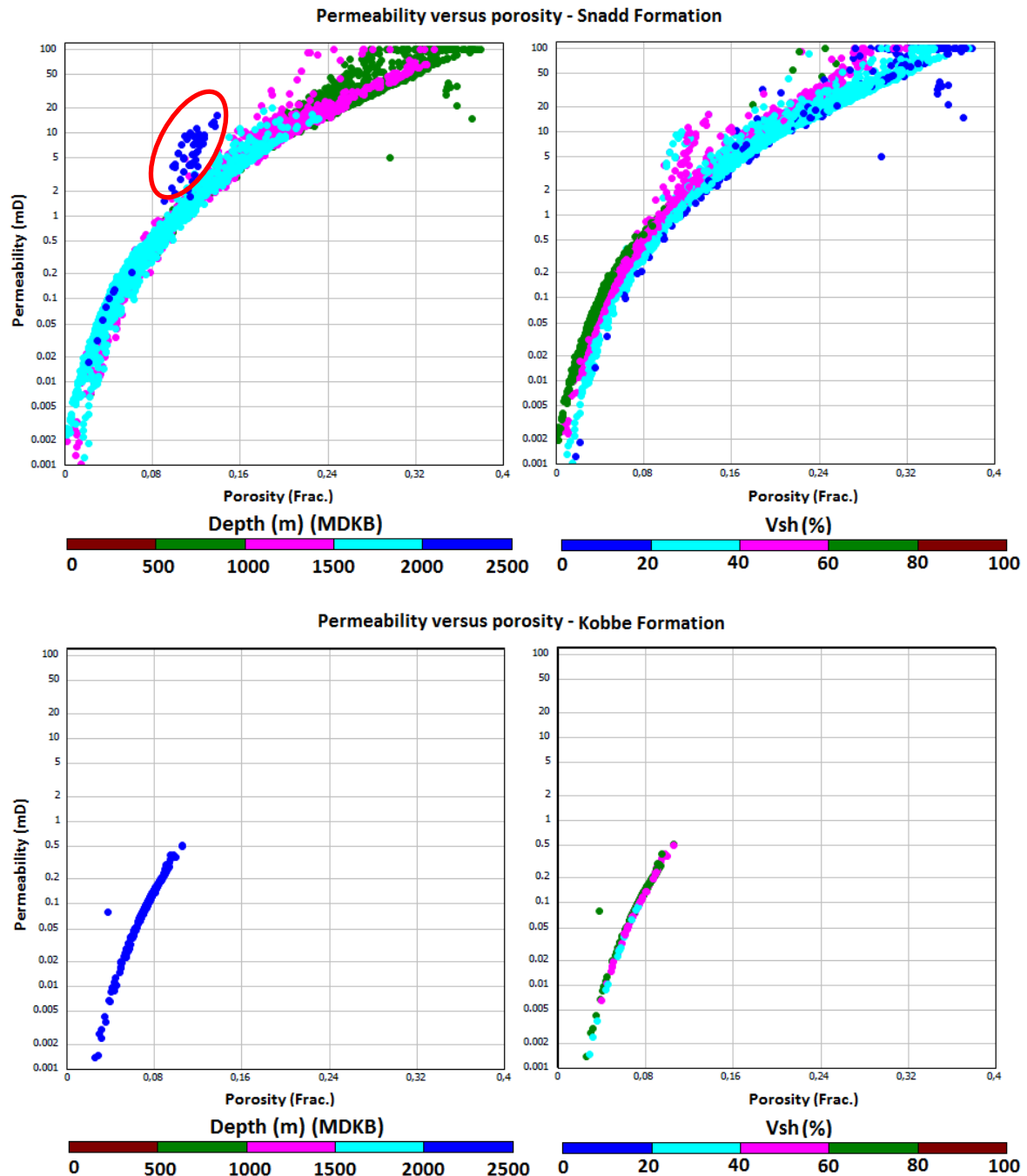


Figure 7.3: The figure represents porosity versus permeability according to depth (m) and shale volume (Vsh%) in both formations in well 7222/11-1.

The relation between porosity and permeability is showing on Figure 7.3. The porosity and the permeability are decreasing with increasing depth. At deep burial depth high temperature is favourable for quartz cementation, which is main porosity predator. The points highlighted with red ellipse in upper left figure shows high porosity at deeper depth. The possible reason for high porosity at deep depth is presence of chlorite coating, which preserves porosity and

hinders quartz cementation. Additionally with increasing shale volume, decrease in permeability can be observed on Figure 7.3. Shale acts as barrier for fluid flow and causes permeability reduction. Also fine clay particles settle in pore spaces and decrease permeability due being extremely microporous. The Kobbe Formation consists of mainly shale with minor interbedded sandstone and siltstone, thus has very low porosity and permeability. At the shallowest part of the Snadd Formation comprises clean sandstone unit with good porosity and permeability (Figure 7.3).

## 7.4 Uplift estimation

In this study, uplift estimation has been done by comparing the observed velocity-depth trends from the following authors Storvoll et al. (2005) and Mondol (2009). The transition zone was estimated from the complete velocity dataset and uplift estimation has been carried out for data representing shale. The gamma ray log has been applied to estimate the shale volume.

According to Storvoll et al. (2005) compaction curve, 1300 m approximate uplift has been interpreted in well 7222/11-1 and 1600 m by using Mondol (2009) kaolinite:silt 50:50 compaction curve (Figure 7.4)

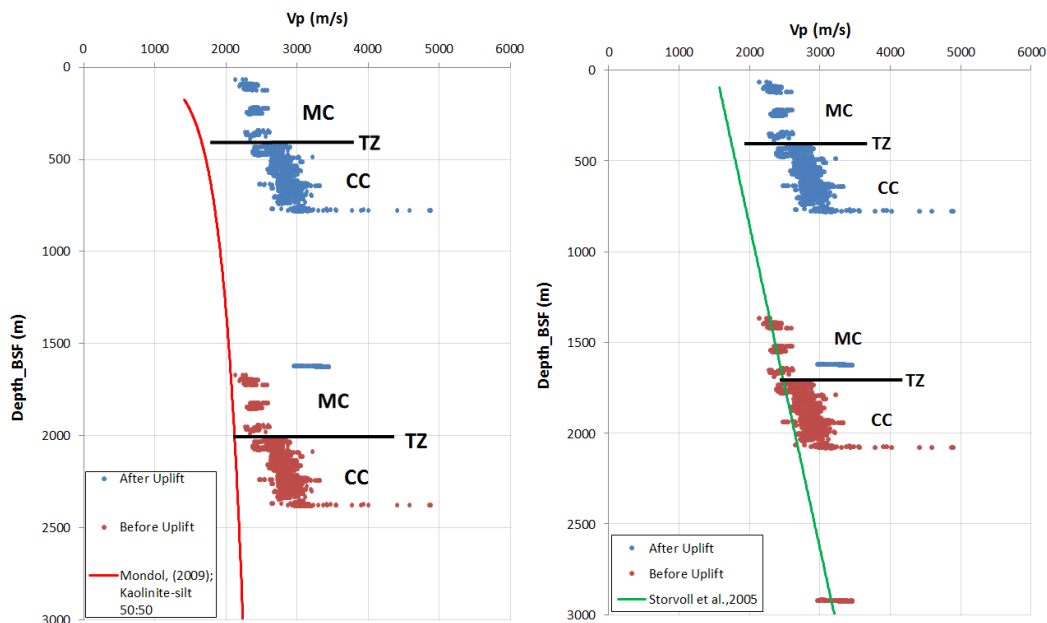


Figure 7.4: The approximate estimated uplift by using Storvoll at al. (2005) and Mondol (2009) compaction curves in the study area; MC-Mechanical compaction zone; CC-Chemical compaction zone; TZ-Transition zone.

The current transition zone between the mechanical and chemical compaction zones has been estimated approximately 400 m, before exhumation the transition zone has been interpreted at 1700 m depth by using Storvoll et al. (2005) compaction curve and 2000 m by Mondol (2009) compaction curve. The results are presented in Table 7.3.

Table 7.3: Estimated uplift, geothermal gradient (G) and transition zone (TZ) depths in well 7222/11-1. The bottom hole temperature has been interpolated from the neighbouring well 7222/11-2 (87.8°C).

Compaction	Uplift (m)	G (°C/km)	Current TZ (m)	TZ before uplift (m)
Storvoll et al.	1300	32	400	1700
Mondol (2009)	1600	32	400	2000

The study area has been exposed to significant uplift, therefore the sandstone reservoirs have been subjected to deeper depth than which they are now. As a result of uplift the degree of compaction and consolidation of sandstones could be much higher than it is expected from the present depths and temperature gradients.

Table 7.4: The maximum burial depths and the maximum temperature according to the estimated uplift and the geothermal gradient in well 7222/11-1. The bottom hole temperature has been interpolated from the neighbouring well 7222/11-2 (87.8°C).

Estimated	Geothermal	Kobbe Formation		Snadd Formation	
		Max. burial	Max.	Max. burial	Max.
1600 m	32	3800	120-125	2900	90-100
1300 m	32	3500	110-115	2600	80-90

The maximum burial of the Kobbe Formation is 3800 m by using Mondol (2009) compaction curve and the maximum temperature is 120-125 °C from estimation of geothermal gradient. The temperature did not exceed 130 °C before uplift. The maximum burial depth of the Snadd Formation is 2900 m and the maximum temperature is 90-100 °C (Table 7.4).

After Storvoll et al. (2005) the maximum burial depth of the Kobbe Formation is 3500 m and the maximum temperature is 110-115 °C. The maximum burial of the Snadd Formation is 2600 m and the maximum temperature the formation has been exposed to is 80-90 °C (Table 7.4).

## **8. Discussion**

This chapter tries to build an understanding of sandstone composition, provenance and depositional environment, outline the diagenetic processes related to authigenic minerals and discuss the reservoir quality of the Kobbe and Snadd Formations according to sedimentological, petrographic and petrophysical results.

### **8.1 Composition of the sandstones and provenance**

The Snadd Formation sandstones are well-sorted, very fine- to fine- and medium-grained quartz rich sandstones with moderate clay and carbonate content. Plagioclase feldspar is present in all samples with volumes of 3-8,2%, while K-feldspar is less common than plagioclase. The amount of K-feldspar in the samples is ranging between 0,3-4,25%. The detrital clay content of the Snadd sandstones is low. The amount of rock fragments is ranging between 12-26%.

The sandstones in the Kobbe Formation are moderately-sorted, very fine-grained quartz-rich sandstones. The grain size of the samples is finer and the clay and carbonate content is higher in the Kobbe Formation than in the Snadd Formation. The presence of carbonate fossil may be the source of the calcite cement. K-feldspar is not present in the Kobbe Formation, while plagioclase has volume ranging from 6-11%. The amount of rock fragments is higher (11-35%) than in the Snadd sandstones.

The petrographic and mineralogical studies of the Kobbe and Snadd Formations show lithic arenite sandstones with high amount of rock fragments, including cherts, volcanic rock fragments, metamorphic quartz-rich rock fragments, recycled grains and mica schists. The high amount of metamorphic rock fragments indicates a source area rich in metasediments with some volcanic particles for both sandstones. The plagioclase may come from basaltic rocks (Bergan and Knarud, 1993). Both formations contain zircon, apatite, rutile, monazite, but only the Snadd Formation contains staurolite that is common in metamorphic rocks and indicate a source area with metasediments (Deer et al., 1992). The difference in the feldspar composition and metamorphic components may indicate a source area from Caledonides, Baltic Shield area and from Uralides, containing mafic rocks (Figure 8.1 and Figure 8.2).

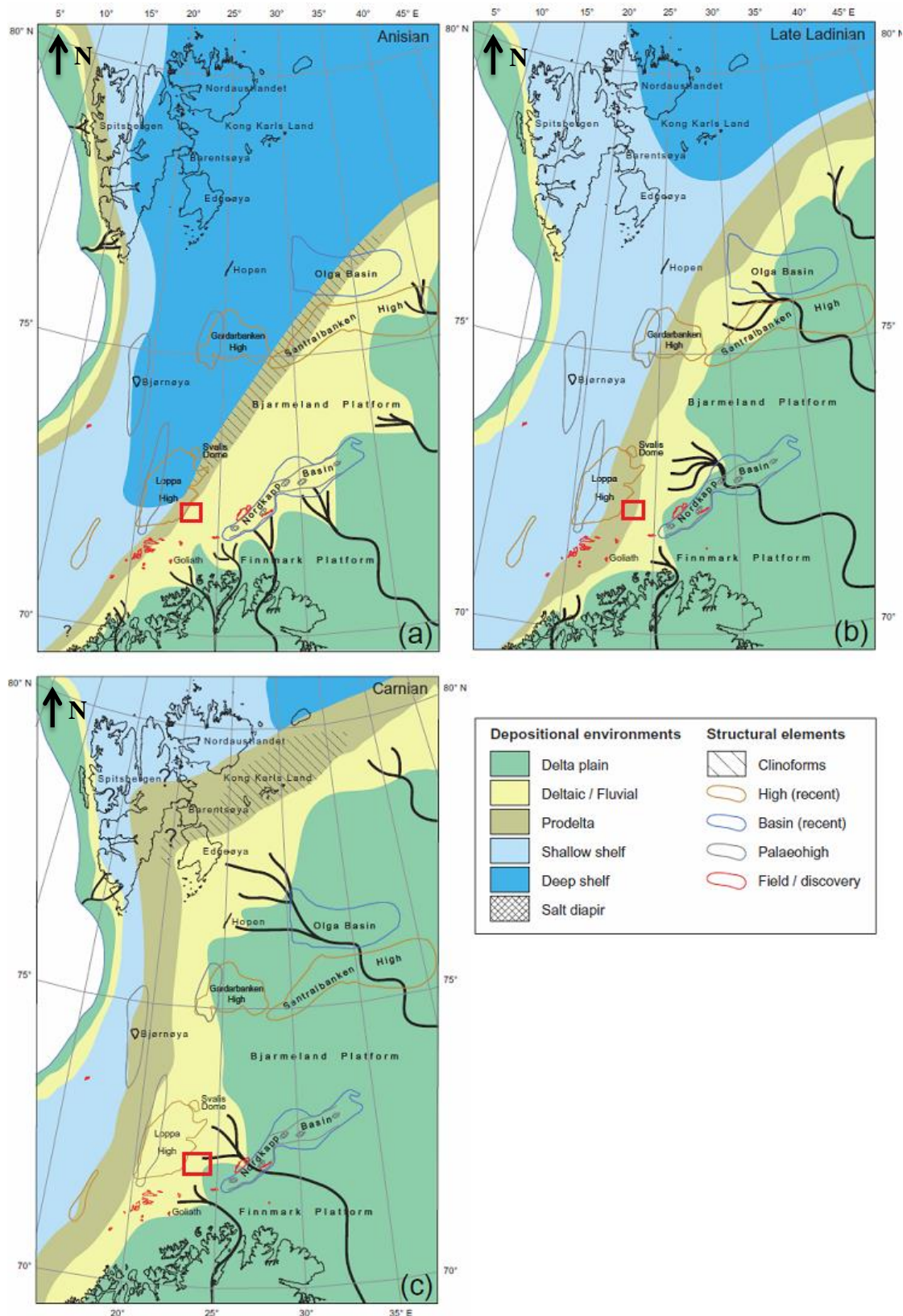
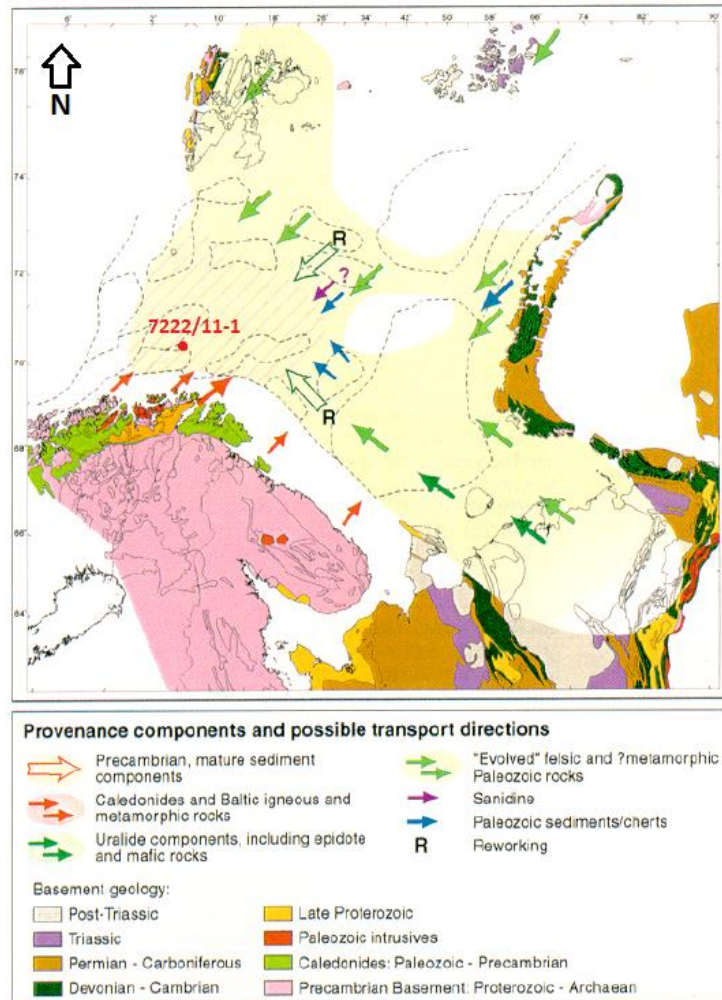


Figure 8.1: The map is showing the progradation of the deltaic system from Middle (a-b) to Late Triassic-Carnian (c) in the Barents Sea. The study area is marked by red rectangle. Modified from Riis et al., (2008).



Figure 8.2 is representing the possible provenance and transport directions in the Barents Sea area according to Mørk, (1999), the study area marked with red dot. There is no significant difference in sandstone composition but the difference in sandstone texture could have several interpretations. Changing the depositional environment could cause different sorting, grain size and clay content in sandstones. As mentioned above in the Kobbe Formation, the sandstones are moderately-sorted, very fine-grained and contain more clay and carbonate than the Snadd



sandstones; therefore the Kobbe Formation may be deposited on muddy shelf, prodelta, delta front

Figure 8.2: The possible interpreted provenance and transport directions in the Barents Sea. The study area marked with red dot. Modified from (Mørk, 1999).

environment with interbedded thin sandstones and siltstones (Figure 8.1). Changing the energy levels in the depositional environment also could result different sandstone texture and composition. Due to erosion of the different type of rocks the sandstones with various compositions and texture could come from the same source area. Furthermore changes in climate could increase the influence of weathering and result more quartz-rich sediments (Fruholmen and Tubåen Formation in Upper Triassic) (Bergan and Knarud, 1993, Mørk, 1999). Previous studies represent that sandstones with high amount of rock fragments have eastern source areas (Uralides), while sandstones with high quartz content sourced from Scandinavia (Mørk, 1999). Thus the lithic arenites Kobbe and Snadd Formation are likely sourced from the eastern areas. Mica schists and metamorphic rock fragments are common in both formations, indicate provenance from Caledonides and the Baltic areas, but the main

source area is from the Uralides (Figure 8.2). Zircon age data of Triassic sediments from Svalbard also show eastern (Uralides) provenance for the formations (Bue and Andresen, 2014).

## 8.2 Depositional environment

The depositional environment has been interpreted as tidally influenced delta system with several subenvironments for both Kobbe and Snadd Formations (Figure 8.3).

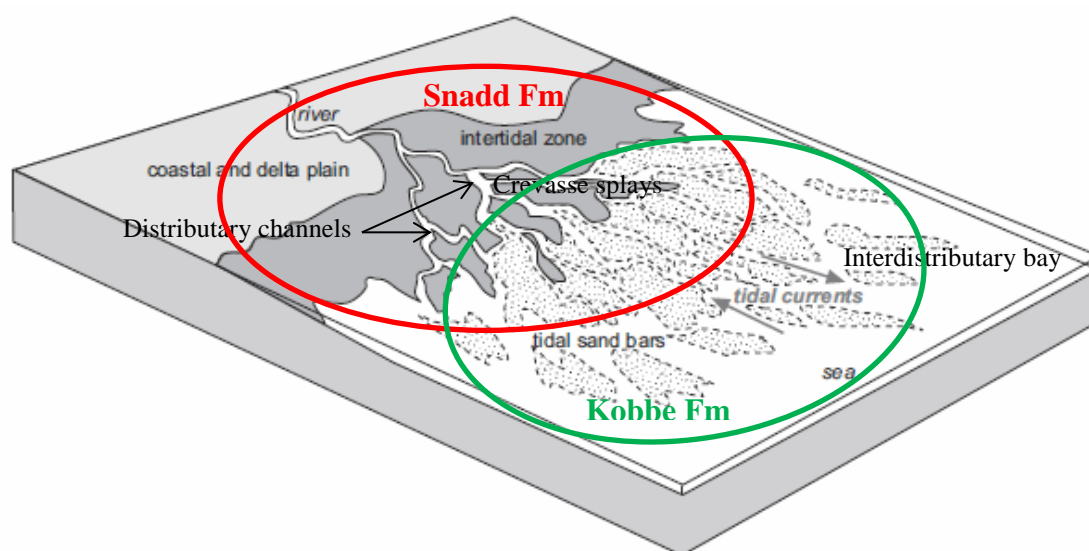


Figure 8.3: Tidally influenced delta system with subenvironments, modified from (Nichols, 2009). The red circle represents the depositional environment for the Snadd Formation and the green for the Kobbe Formation.

The 7222/11-1 core is containing repeated successions which represent deltaic cycles with shifting of delta lobes in the tide-dominated delta environment.

The lowermost part of the core represents the Kobbe Formation with 3 coarsening upwards units and one fining upward unit. The coarsening upward units are representing delta plain/interdistributary areas on the delta plain depositional environments with several subenvironments. The sand packages with sedimentary structures in the coarsening upward units indicate tidal channels, tidal mouth bars, distributary channels and crevasse splays as subenvironments on the delta plain. Tidal sedimentary structures such as heterolithic deposits (flaser-, wavy-, lenticular-bedding) and alternating mud and sand layers represent tidal flat depositional environment with minor bioturbation. The fining upward unit at the top of the

Kobbe Formation represents a tidally less influenced succession and intertidal zone as depositional environment (Figure 8.3 and 8.4).

The Snadd Formation consists of big package of coarsening upward succession with smaller coarsening and fining upwards units. The fining upward unit is representing less tidal-dominated unit such as the palaeosol units in the middle part of the formation. The less tidally influenced environment indicates deposition in the intertidal zone, in mid/upper delta plain. The Snadd Formation starts with mudstone deposited in prodelta environment, then a thick package of carbonate cemented sandstone with dolomite, ankerite and calcite, represents inter- to supratidal environment on the delta plain. Tidal sedimentary structures such as flaser, wavy, and lenticular bedding are present in the middle part of the formation and indicate tidal flat depositional environment with some minor bioturbation. The massive sandstone package at the top of the Snadd Formation indicates coastal deltaic depositional environment and the sand may be deposited in tidal channels, tidal mouth bars and distributary channels (Figure 8.3 and 8.4).

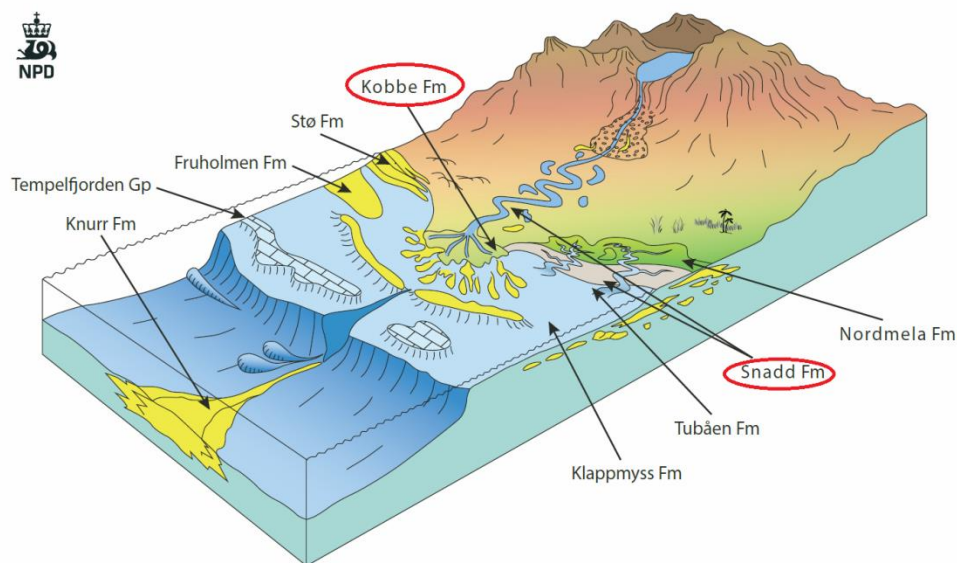


Figure 8.4: The depositional environment for the studied formations, marked with red circle modified from (Halland et al., 2014).

The two coarsening upward sequences of the Snadd Formation and the three coarsening upward sequences in the Kobbe Formation may represent prograding lobes within the tide-influenced delta system (Figure 8.1).



### 8.3 Diagenetic evolution of the sandstones

Authigenic minerals such as chlorite, kaolinite, pyrite, carbonate cement and quartz overgrowth are very important factors in sandstone diagenesis and reservoir quality. This chapter summarizes the diagenetic processes from early diagenesis to deep burial.

#### 8.3.1 Early diagenesis

Authigenic kaolinite is present as pore-filling mineral, filling the voids of dissolved grains as well as intergranular pore spaces. Formation of kaolinite is related to leaching of feldspar, mica and rock fragments where the meteoric water flushing leaching the  $K^+$  from feldspar and mica grains and precipitating authigenic kaolinite. The pore-filling kaolinite is associated with microporosity which leads to reduce permeability in sandstones.

A thin layer of coating is present in the sandstones. It is observed from SEM analysis that this thin layer of coating contains Fe and it may be the precursor for the grain coating chlorite in the sandstone samples (Figure 8.5). The chlorite occurs as coating and pore-filling mineral in both sandstones. The formation of chlorite requires Fe and Mg, found in detrital biotite or rock fragments (Bjørlykke, 1998).

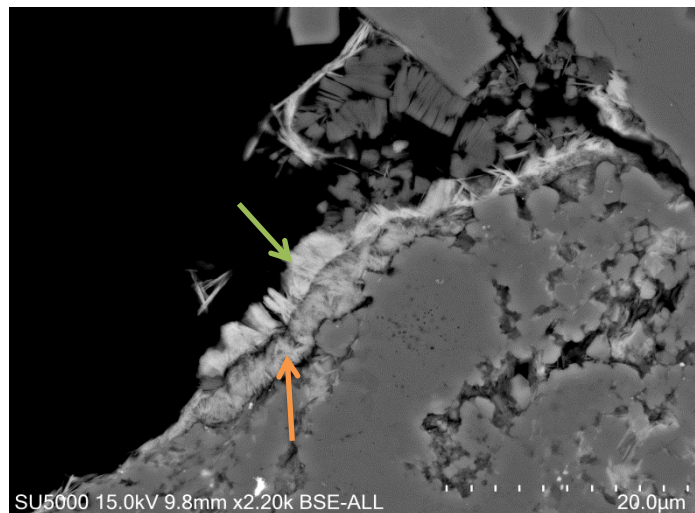


Figure 8.5: Two generations of grain coating chlorite. The precursor coating (orange arrow) covers the grain's surface and authigenic chlorite coating (green arrow) overlays the precursor coating at 2241.65 m depth in the Kobbe Formation.

The chlorite coating was formed before quartz cementation because chlorite coatings on the detrital grains preventing quartz overgrowth precipitation (Figure 8.6).

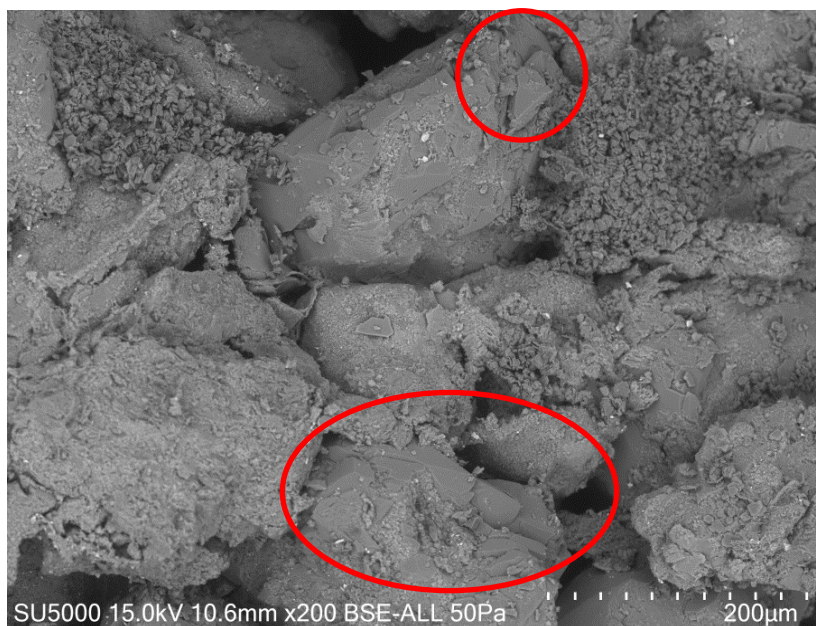


Figure 8.6: Chlorite coatings covering all grains preventing quartz overgrowths, where chlorite coating is incomplete quartz overgrowths presence (red circles), Snadd Fm, 780.50 m depth.

Carbonate cement is including siderite, calcite, ankerite and dolomite and represents as cement in the pore space or small spherulitic patches in the sandstones (Figure 8.7).

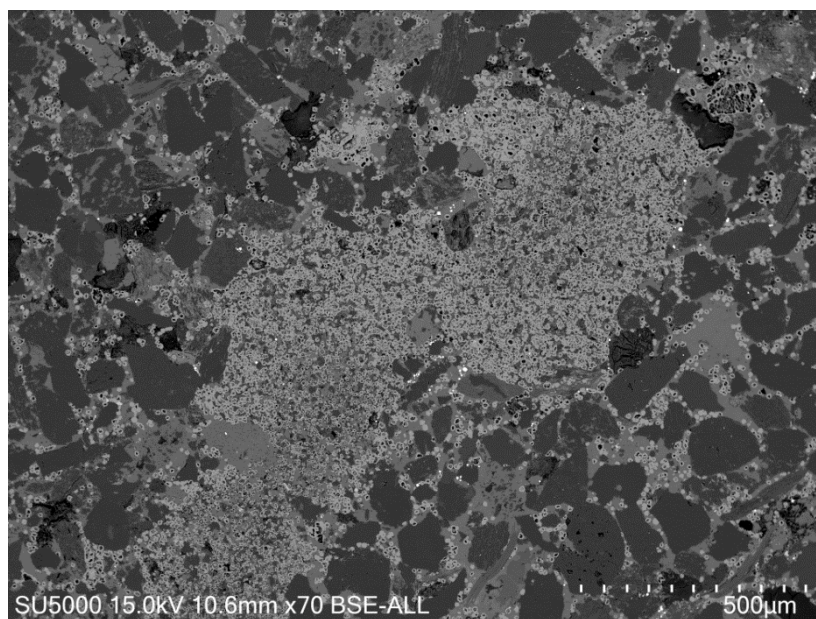


Figure 8.7: Pore-filling calcite cement and siderite cement occurs as spherulitic patches in the Kobbe Formation at 2214.75 m depth.

The pore-filling calcite is engulfing chlorite, siderite and pore-filling kaolinite. This indicates calcite recrystallization in the sandstone samples. Where calcite cement occurs quartz overgrowths are absent but there is some samples where minor quartz overgrowths are present, which means some calcite recrystallization took place after start of quartz cementation. Siderite has been interpreted as early diagenetic mineral while ankerite is generally a late diagenetic mineral forming at elevated temperature (80-125°C) but it also could present as a near-surface mineral (Morad et al., 1996, Mozley, 1989, Berner, 1980, Berner, 1981). The formation of the siderite is considered to an depositional environment where the river water transports iron into marine water, where the iron particles flocculate with saline water (Ehrenberg, 1993). In the studied sandstones ankerite represents early diagenetic mineral due to folded mica grains around the ankerite cement explains that ankerite probably preceding mechanical compaction and the maximum temperature has been calculated 100°C in the Snadd Formation, which may not indicate a late diagenetic ankerite. The formation of ankerite is linked to a depositional environment where there is an interaction between marine porewaters and volcanoclastic sediments (Morad et al., 1996). The source of some of the calcite cement may be from  $\text{Ca}^{2+}$ -rich plagioclase feldspars which have been partially or totally dissolved, but most likely from carbonate fossils which are present in the sandstones, mostly in the Kobbe Formation (Bjørkum and Walderhaug, 1990)

The pyrite mineral ( $\text{FeS}_2$ ) is a common authigenic mineral in sedimentary rocks and it is often found together with organic matter. Pyrite forms due to reaction of detrital iron minerals with  $\text{H}_2\text{S}$  during shallow burial. The sources of  $\text{H}_2\text{S}$  are the bacterial reduction of dissolved sulphate and the decomposition of organic matter. The initial product of this reaction are iron monosulfides, which are unstable and transform to pyrite during early diagenesis (Berner, 1981). Pyrite occurs as framboidal and as blocky crystals in both Snadd and Kobbe Formations (Figure 8.8). The framboidal aggregates indicate early diagenetic minerals forming by reduction of detrital iron in the sulphate reduction zone during early diagenesis and the blocky pyrite crystals are formed after the framboidal aggregates during early diagenesis (Worden and Burley, 2003).

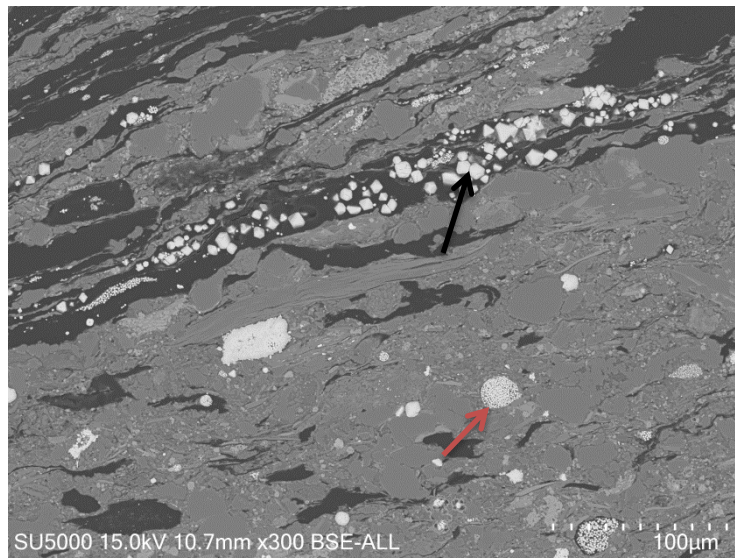


Figure 8.8: Framboidal (red arrow) and blocky pyrite crystals (black arrow) in the Kobbe Formation sandstone at 2230.60 m depth.

### 8.3.2 Mechanical compaction

Mechanical compaction starts immediately after deposition and is function of the vertical effective stress and compressibility of the mineral framework. The mechanical compaction results porosity loss due to grain crushing and rearrangement of the grains (Storvoll et al., 2005, Chuhan et al., 2002). In this study mechanical compaction is the main factor for porosity reduction. The Kobbe Formation is moderately-sorted, very fine-grained sandstone and contains high amount of clay particles. The amount of matrix in the Kobbe Formation is ~7%, while in the Snadd Formation it is 2.6%. Moderate sorting, higher clay and matrix content of the Kobbe Formation reduce the friction between the grains. Therefore, mechanical compaction affects more the Kobbe sandstones than the Snadd Formation.

#### 8.3.2.1 Intergranular volume (IGV)

The intergranular volume decreases with burial depth due to effective stress and overburden. IGV is function of grain size, grain shape, sorting and mechanical compaction. The angular grains will compact more and show lower IGV compared to the rounded grains. The grain-supported samples with high IGV show minimum degree of mechanical compaction, while low IGV shows maximum degree of mechanical compaction. The modal analysis of the Kobbe and Snadd Formations shows different IGV values (Table 6.1). The average IGV for Snadd Formation is 29% and for the Kobbe Formation is 22%, which means less compaction

in the Snadd Formation than in the Kobbe Formation. The carbonate cemented samples represent the highest IGV due to the cement shut down mechanical compaction, thus these samples show minimum degree of compaction.

### **8.3.3 Diagenesis at intermediate depth (2-3.5 km; 65-120°C)**

The precipitation of quartz cement starts from 70-80°C at 2-3 km depth and this temperature interval is called transition zone. Precipitation of quartz cement increases the stiffness of the grain framework, therefore mechanical compaction stops (Storvoll et al., 2005). 2-4 % quartz cement is required to stop further mechanical compaction (Bjørlykke and Jahren, 2015). In the studied sandstones the amount of quartz cement (0,2-1,3%) is not high enough to shut down mechanical compaction.

Albitisation is replacement of K-feldspar or plagioclase feldspar by albite and occurs at around 90°C temperature. The albite is more stable at deeper depth and higher temperature due to sodium is the dominant cation in the porewater. Albitisation of plagioclase will discharge  $\text{Ca}^{2+}$  and it may be the source of calcite cement in the samples (Bjørlykke and Jahren, 2015). In the Kobbe and Snadd Formations albite is abundant mineral to explain the low contents of plagioclase and K-feldspar; however precipitation of authigenic kaolinite may also indicate low content of K-feldspar during early diagenesis.

The recrystallization of kaolinite to dickite starts around 100°C temperature (Vangdal et al., 2014) and it occurs as thicker crystals than kaolinite. Dickite was not observed during the analysis but the maximum calculated temperature (110-125°C) and the lack of illitization may indicate the presence of dickite in Kobbe sandstones.

Authigenic chlorite coating forms due to recrystallization of the precursor clay coating between 80-100°C (Aagaard et al., 2000). In the studied well the maximum temperature has been calculated above the required values for chlorite precipitation. The formation of chlorite requires Fe- and Mg-bearing minerals, such as biotite, iron-rich precursor and rock fragments. The chlorite coating in the Kobbe Formation is non-continuous but quite thick, while it is continuous in the Snadd sandstone. The pore-filling authigenic chlorite builds up fibrous minerals in the pore space and associated with pore-filling kaolinite as filling the micropores in between the kaolinite booklets. The chlorite may be formed when the river water brought

iron-rich material into seawater and the clay particles flocculated in the fluvial-marine mixing zone and infiltrated into sediments to form precursor coating (Ehrenberg, 1993).

#### **8.3.4 Deep burial diagenesis (>3.5-4 km; >120°C)**

Quartz cement may be the latest diagenetic mineral that formed during diagenesis based on quartz generally starts to form at 70-80 °C until all porosity lost at deep burial depths (Ehrenberg, 1990, Worden and Burley, 2003, Bjørlykke and Jahren, 2015). Slightly more quartz overgrowths (Figure 8.6) were observed in the Kobbe Formation due to non-continuous chlorite coating, the finer grain size and the formation has been buried deeper (3.5-3.8 km; 120-125°C) than the Snadd Formation. Quartz cementation is a function of grain size, more surface area is available for quartz overgrowth in finer-grained sediments due to quartz cementation is inversely proportional to grain size (Walderhaug, 1996). The amount of quartz overgrowths in the studied sandstones is not higher than 1.3%, which indicates that the chlorite coating is preventing quartz cementation and preserving porosity at deep burial depth.

Illitization of kaolinite occurs when temperature exceeds 130°C. In the studied formations illite has not been observed. It may be due to kaolinite converted to dickite, which is more stable mineral at deeper depth and higher temperature than kaolinite and it may be due to the maximum calculated temperature has been estimated between 120-125°C.

### **8.4 Reservoir quality**

Reservoir quality is controlled by the depositional environment, diagenesis, mechanical and chemical compaction and the grade of cementation. The reservoir quality is also controlled by depth because at deep burial depth quartz cementation takes place and destroying porosity. If chlorite coating is present at deep burial depth may inhibit quartz cementation and preserve higher porosity than it is expecting at these depths (Ehrenberg, 1993). This chapter represents the reservoir quality of the Snadd and Kobbe sandstones.

#### **8.4.1 Snadd Formation**

The sandstones in the Snadd Formation show good porosity and permeability values (Figure 7.3) due to less effect of mechanical and chemical compaction and the low volume of clay matrix and authigenic minerals. Due to presence of chlorite coating quartz overgrowths are



rare and they are present where chlorite coating is incomplete. The chlorite coating is quite thick and well-developed in the Snadd Formation. Quartz cementation is a function of grain size, more surface area is available for quartz overgrowth in finer-grained sandstone because quartz cementation is inversely proportional to grain size (Walderhaug, 1996). The carbonate cement such as calcite, dolomite and ankerite is abundant in few samples. The source of the calcite cement may be due to dissolution of  $\text{Ca}^{2+}$ -rich plagioclase grains and carbonate fossils. Presence of carbonate fossils may suggest that calcite cement was present where biogenic carbonate was significant. Presence of carbonate cements reducing the porosity and permeability. Dissolution of feldspar and mica grains lead to precipitate authigenic kaolinite in the pore space. Pore-filling kaolinite generally associated with microporosity and pore-filling chlorite and reduces permeability in sandstones because the pore spaces between the kaolinite booklets are too small to be filled with oil due to high capillary entry pressure, thus the oil saturation is reduced in kaolinite-rich sandstones (Bjørlykke and Jahren, 2015). There are few samples at shallower part of the formation which have high porosity and low permeability. Low permeability is due to high contents of clay minerals (pore-filling kaolinite and chlorite). The permeability is function of the grain size, permeability increases with increasing grain sizes in sandstones (Kozeny, 1927). The Snadd Formation consists of mainly fine-grained sandstones hence it represents better permeability and less quartz overgrowths than Kobbe Formation. In conclusion the Snadd Formation sandstones have been interpreted to have good reservoir quality.

#### **8.4.2 Kobbe Formation**

The Kobbe Formation sandstones show very low porosity and permeability (Figure 7.3) due to high clay content and the formation consists of very fine-grained sandstones. The amount of quartz overgrowths is slightly higher than in the Snadd Formation due to non-continuous chlorite coating and the very fine grain size. The chlorite coating is preventing quartz cementation and preserving porosity but the coating is quite thick therefore potentially increasing water saturation and decreasing the porosity in the sandstone (Figure 8.9).



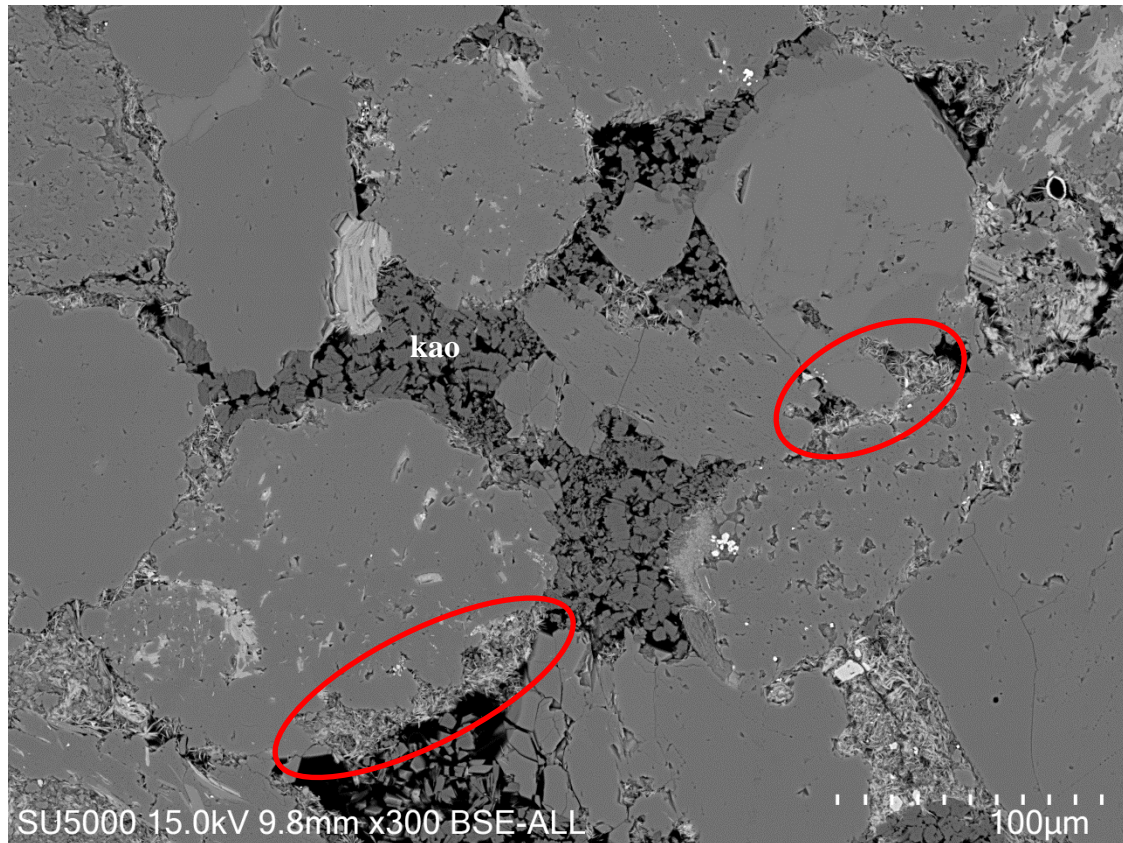


Figure 8.9: Thick chlorite coating (red circles) represents on the grain surfaces in the Kobbe Formation at 2241.65 m depth. Authigenic kaolinite (kao) booklets are present in the pore space.

K-feldspar grains are not present in the Kobbe sandstones and also some of plagioclase and mica grains partially or totally dissolved lead to precipitate authigenic kaolinite in the pore space. The pore-filling kaolinite is associated with microporosity and fibrous chlorite in the pore space reducing porosity and permeability. Due to more clay content and rock fragments the Kobbe sandstone is more likely affected by mechanical compaction than the Snadd Formation, therefore the intergranular volume and porosity is low. The average porosity for Kobbe sandstones is varying from 5 to 7% while in the Snadd Formation from 15 to 17%. The intergranular volume is 22 %, while for Snadd sandstones are 29%. As mentioned above the permeability is function of grain size, due to very fine grain size, the Kobbe sandstones show low permeability values. In conclusion the Kobbe Formation sandstones have been interpreted to have poor reservoir quality.

### 8.4.3 Reservoir quality versus depth

The reservoir quality is decreasing with increasing depth (Byrnes, 1994). Figure 8.10 represents porosity versus permeability according to depth in both Kobbe and Snadd Formations.

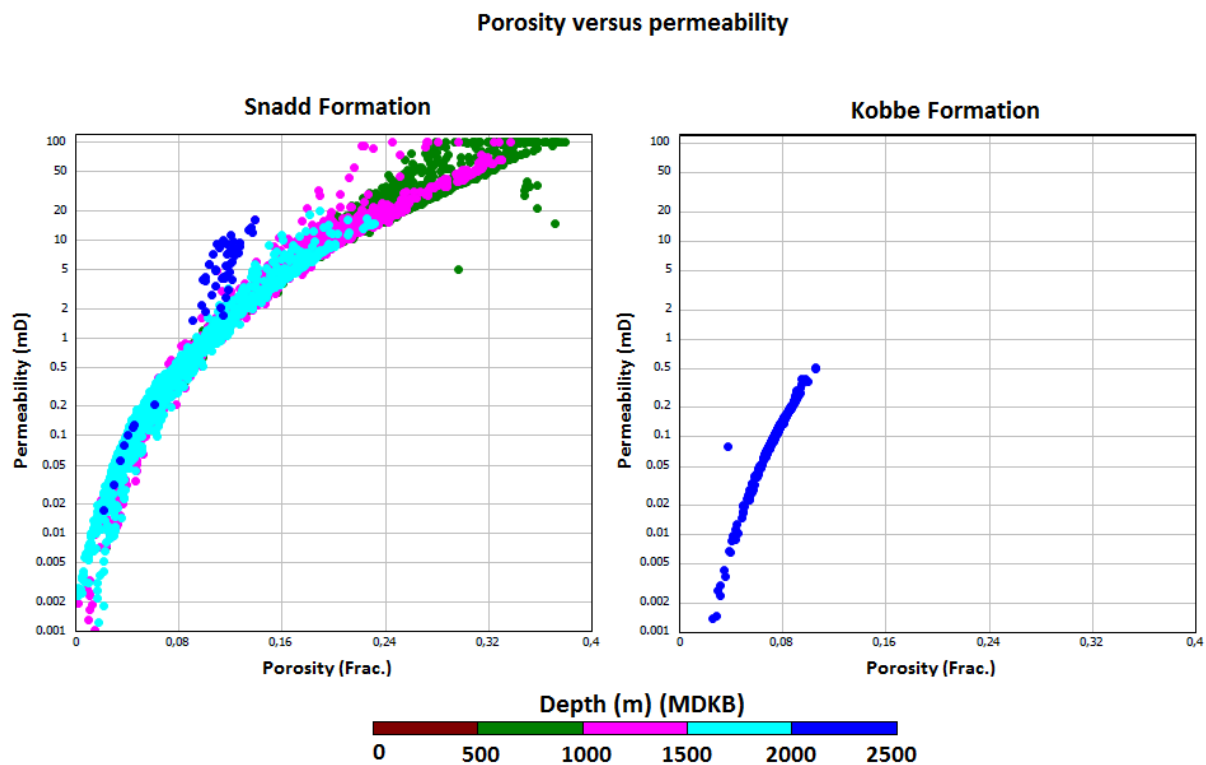


Figure 8.10: Porosity and permeability show decrease with increase of burial depth.

The composition of the Snadd and Kobbe Formations are quite similar but as seen on Figure 8.10 Kobbe sandstones have much lower porosity values than Snadd sandstones. This is due to higher effect of mechanical compaction in the Kobbe Formation compared to the Snadd Formation and the chlorite coating is not so developed, therefore there is more surface area available for quartz overgrowths, which reduces porosity. Presence of chlorite coating at deeper depth preventing quartz cementation and preserving greater porosity than it is expecting at deep burial depths. Due to very fine grain size and the Kobbe Formation has been buried at deeper burial than Snadd Formation, more considerable mechanical and chemical compaction take place in the Kobbe Formation reducing porosity and permeability. Permeability is also represents a decrease with increasing burial depth due to porosity reducing towards deeper depths.

#### **8.4.4 Reservoir quality versus depositional environment**

The depositional environment is one of the main influences of reservoir quality with controlling grain size, sorting, texture, and mineral composition (Bloch, 1994).

As mentioned above the permeability and the volume of the quartz overgrowths are function of grain size therefore grain size has great effect on reservoir quality related to depositional environment.

It is obvious from the modal analysis and petrographic results that the samples with high content of clay and carbonate have much lower porosity and permeability than samples with minor or no clay and carbonate content. The carbonate cement and clay minerals are filling the pore spaces reducing porosity and permeability. Except chlorite coating at deeper depth where it is preventing quartz cementation due to precipitates thin layer of coating on the grains' surfaces, thus preserving porosity. Samples with high clay content may deposited during low energy conditions with minor to moderate bioturbation, such as the palaeosol (Facies 4) from the Snadd Formation, the mudstone (Facies 6) and the siltstone (Facies 2) from the Snadd and the Kobbe Formations. They are representing interdistributary areas on the delta plain and muddy shelf as depositional environment mainly with bays, tidal flat and inter- to supratidal flat subenvironments. The carbonate cemented sandstone representing the Facies 5, may deposited in inter- to supratidal flat on the coastal deltaic plain area in both Kobbe and Snadd Formations. Some of the samples contains of high calcite cement due to high amount of biogenic carbonate in the depositional environments. The source of the calcite is mainly from dissolution of carbonate fossils as precipitate calcite cement in the pore space. The carbonate cement resulted low porosity and permeability in the samples such as in 1 meter thick channel sandstone package at 788.42 m depth and a 7 m thick sandstone package with dolomite, ankerite and calcite at 1292-1299 m depth in Snadd Formation. In the Kobbe Formation the carbonate cemented sandstone occurs at 2214-2215 m depth and at 2221-2222 m depth. The channel sandstone deposits of the Snadd Formation at shallow depth show good reservoir quality but the negative effect on the reservoir quality is the precipitation of diagenetic chlorite and kaolinite in the pore space. Kaolinite is filling the pores and associated with microporosity and fibrous chlorite, which is filling the space in between the kaolinite booklets and reducing porosity and permeability. The chlorite coating that preventing quartz cementation in sandstones, deposited in an environment where river water is mixing with

marine water and the clay particles flocculated and infiltrated into sediments to form a precursor coating (Ehrenberg, 1993).

The Kobbe Formation has poor reservoir quality due to it is mainly deposited during low energy conditions such as prodelta, muddy shelf, inter-to supratidal mud and mixed flats. The Kobbe sandstones have very fine grain size and high clay content that is also represent poor reservoir quality. Due to high amount of clay particles in between the grains, mechanical compaction has larger effect in Kobbe sandstones than in Snadd sandstones. Therefore Kobbe has low IGV (22%), whereas the IGV in the Snadd Formation is higher (30%).

## **8.5 Estimated uplift in the study area**

The presence of quartz overgrowths in both formations indicate 70-80 °C temperature because quartz cementation starts at these temperatures and continue until all the porosity lost (Ehrenberg, 1990, Bjørlykke and Jahren, 2015, Walderhaug, 1994). The main source of quartz cementation is dissolution of silica along stylolites but due to the low amount of quartz cement, stylolite was not observed in the sandstones. The present temperature at the transition zone is around 15 °C (Figure 7.4) and it indicates that the formations have been buried at deeper depth then uplifted. Authigenic kaolinite is present in both formations but illite is not observed during petrographic analysis. Illitization occurs when temperature exceeds 130 °C without uplift (Bjørlykke et al., 1986, Bjørlykke and Jahren, 2015).

The maximum estimated uplift after petrophysical analysis is 1600 m by using Mondol (2009) 50:50 kaolinite:silt compaction curve and 1300 m by using Storvoll et al., (2005) compaction curve on the Bjarmeland Platform. Numerous studies have been done for uplift and erosion estimation of the Barents Sea area (Ohm et al., 2008, Henriksen et al., 2011a, Baig et al., 2016) and they are similar to the results presented in this study (Table 7.3). Baig et al. (2016) has been interpreted approximately 1250-2400 m uplift for the Bjarmeland Platform, while Ohm et al. (2008) estimated 1000-2000 m uplift.

The estimated temperature values (Table 7.4) show that with 1.6 km uplift the temperature (120-125°C) did not exceed the boundary of illitization of kaolinite (130 °C) in the Kobbe Formation, explaining no illite observed in the study area. In the Snadd Formation the estimated uplift values (1.3 km and 1.6 km) represents the beginning of quartz cementation, explaining slightly more quartz overgrowths in the Kobbe Formation.

## 9. Conclusion

The aim of the thesis was to understand the reservoir quality of the Middle to Late Triassic Snadd Formation and the underlying Middle Triassic Kobbe Formation located in the SW Barents Sea area. This chapter is a summary of the observations and interpretations made during the work.

- The provenance has been interpreted as south-eastern source area for both Snadd and Kobbe Formations, due to there is no significant difference between the two sandstones.
- The depositional environments has been interpreted as tide-dominated delta system:
  - Kobbe Formation is deposited during low energy conditions; prodelta, inter- to supratidal flats.
  - Snadd Formation is deposited in tidal channel, distributary channel and mouth bars.
- Mechanical compaction is the main factor in porosity reduction, due to reorientation of grains and grain crushing. Quartz cementation has minor effect on porosity loss.
  - IGV reflects the degree of mechanical compaction and shows significant relationship with grain size, shape and sorting.
  - High IGV values indicate minimum degree of mechanical compaction, while low IGV values indicate opposite.
  - The average IGV of the Kobbe Formation is lower (22%) than of the Snadd Formation (29%), indicates higher effect of mechanical compaction in the Kobbe sandstones than in the Snadd sandstones.
- The amount of matrix and authigenic clays has strong effect on porosity loss in sandstones.
  - Kobbe Formation has higher clay and matrix content than the Snadd Formation, thus mechanical compaction affects more in Kobbe sandstones and preserving less porosity than in the Snadd sandstones.
- Pore-filling authigenic chlorite and chlorite coating are also present in the sandstone samples. The precursor of the authigenic chlorite coating is early diagenetic:
  - The early diagenetic Fe-rich coating may represent a source for recrystallized authigenic chlorite coating between 80-100°C.

- The chlorite may be formed when river water brought iron-rich material into seawater and the clay particles flocculated in the fluvial-marine mixing zone and infiltrated into sediments to form precursor coating.
- The chlorite coating is well-developed in the Snadd Formation, while it is non-continuous in the Kobbe Formation, resulted slightly more quartz overgrowths in the Kobbe sandstones.
- Pore-filling authigenic kaolinite has been sourced from the dissolved mica and feldspar grains during early diagenesis.
  - Kaolinite is generally associated with pore-filling fibrous chlorite and microporosity, reducing porosity and permeability in the sandstones samples.
- Carbonate cement is present in both Kobbe and Snadd Formations:
  - Early diagenetic siderite is present as rhombic shape grains and small spherulitic patches in the sandstones.
  - Calcite cemented samples show the highest IGV, due to calcite cement preventing mechanical compaction. Calcite cement has been precipitated during early diagenesis. The main source of calcite cement may be the carbonate fossils present in the samples.
  - Ankerite and dolomite cement are present only in the Snadd Formation and has been formed after the calcite and siderite cements.
- The presence of quartz overgrowths indicate that the two formations have been buried at deeper depth and higher temperature than at present:
  - The maximum uplift has been estimated between 1.3-1.6 km. The Kobbe Formation was buried between 3.5-3.8 km, while the Snadd Formation has been buried until 2.6-2.9 km.
  - The maximum temperature the sandstone samples have been exposed to is 120-125 °C for the Kobbe Formation and 90-100°C for the Snadd Formation.
  - The temperature did not exceed 130°C, explains illitization of kaolinite was not observed in the sandstone samples.
- The Snadd Formation sandstones have been interpreted to have good reservoir quality, while the Kobbe Formation sandstones have poor reservoir quality.
  - The difference in reservoir quality between the Kobbe and Snadd Formation is mainly due to grain size, clay and matrix content of the sandstones.

## **9.1 Further work**

The depositional environment indicated in this project is based on a limited amount of data. For further studies more wells should be studied and correlated with seismic data to interpret a certain depositional environment and to get an idea about lateral and vertical extension of the reservoirs.

More accurate description of the mineralogical composition and textural features can be done with including more core and thin section samples, paying more attention to precursor chlorite coating and to siderite cement.

The siderite cement was not certain analysed during this study, it could be further studied by microprobe analysis and analysing the  $\delta^{18}\text{O}$  content in the samples, which may give more certain information about the provenance.

The maximum estimated temperatures suggest the presence of dickite, further analyses needed to observe dickite in the sandstone samples.



## **REFERENCES**

- AAGAARD, P., JAHREN, J., HARSTAD, A., NILSEN, O. & RAMM, M. 2000. Formation of grain-coating chlorite in sandstones. Laboratory synthesized vs. natural occurrences. *Clay Minerals*, 35, 261-269.
- ALI, S. A., CLARK, W. J., MOORE, W. R. & DRIBUS, J. R. 2010. Diagenesis and reservoir quality. *Oilfield Review*, 22, 14-27.
- BAIG, I., FALEIDE, J. I., JAHREN, J. & MONDOL, N. H. 2016. Cenozoic exhumation on the southwestern Barents Shelf: Estimates and uncertainties constrained from compaction and thermal maturity analyses. *Marine and Petroleum Geology*, 73, 105-130.
- BERGAN, M. & KNARUD, R. 1993. Apparent changes in clastic mineralogy of the Triassic-Jurassic succession, Norwegian Barents Sea: Possible implications for palaeodrainage and subsidence. *Arctic Geology and Petroleum Potential, Norwegian Petroleum Society (NPF), Special Publication*, 2, 481-493.
- BERNER, R. A. 1980. *Early diagenesis: A theoretical approach*, Princeton University Press.
- BERNER, R. A. 1981. A new geochemical classification of sedimentary environments. *Journal of Sedimentary Research*, 51.
- BJØRØY, M., VIGRAN, J. O. & RØNNINGSLAND, T. 1979. *Source rock evaluation of Mesozoic shales from Svalbard*, Institutt for Kontinentalsokkelundersøkelser.
- BJØRKUM, P. A. & WALDERHAUG, O. 1990. Geometrical arrangement of calcite cementation within shallow marine sandstones. *Earth-Science Reviews*, 29, 145-161.
- BJØRLYKKE, K. 1998. Clay mineral diagenesis in sedimentary basins—a key to the prediction of rock properties. Examples from the North Sea Basin. *Clay minerals*, 33, 15-34.
- BJØRLYKKE, K. 2010a. *Petroleum geoscience: From sedimentary environments to rock physics*, Springer Science & Business Media.
- BJØRLYKKE, K. 2010b. Shales, silica deposits and evaporites. *Petroleum Geoscience*. Springer.
- BJØRLYKKE, K. 2015. Subsurface water and fluid flow in sedimentary basins. *Petroleum Geoscience*. Springer.
- BJØRLYKKE, K., AAGAARD, P., DYPVIK, H., HASTINGS, D. & HARPER, A. 1986. Diagenesis and reservoir properties of Jurassic sandstones from the Haltenbanken area, offshore mid-Norway. *Habitat of hydrocarbons on the Norwegian continental shelf*, 275-286.
- BJØRLYKKE, K., HØEG, K. & MONDOL, N. H. 2015. Introduction to Geomechanics: stress and strain in sedimentary basins. *Petroleum Geoscience*. Springer.
- BJØRLYKKE, K. & JAHREN, J. 2015. Sandstones and sandstone reservoirs. *Petroleum Geoscience*. Springer.
- BLOCH, S. 1994. Influence of depositional environment on reservoir quality prediction.
- BREIVIK, A. J., GUDLAUGSSON, S. T. & FALEIDE, J. I. 1995. Ottar Basin, SW Barents Sea: a major Upper Palaeozoic rift basin containing large volumes of deeply buried salt. *Basin research*, 7, 299-312.
- BUE, E. P. & ANDRESEN, A. 2014. Constraining depositional models in the Barents Sea region using detrital zircon U–Pb data from Mesozoic sediments in Svalbard. *Geological Society, London, Special Publications*, 386, 261-279.
- BYRNES, A. P. 1994. Empirical methods of reservoir quality prediction.

- CHUHAN, F. A., KJELDSTAD, A., BJØRLYKKE, K. & HØEG, K. 2002. Porosity loss in sand by grain crushing—Experimental evidence and relevance to reservoir quality. *Marine and Petroleum Geology*, 19, 39-53.
- COMPTON, R. R. 1962. Manual of field geology. *Soil Science*, 93, 295.
- DALLAND, A., WORSLEY, D. & OFSTAD, K. 1988. *A Lithostratigraphic Scheme for the Mesozoic and Cenozoic and Succession Offshore Mid-and Northern Norway*, Oljedirektoratet.
- DALLMANN, W. K. 1999. *Lithostratigraphic lexicon of Svalbard: review and recommendations for nomenclature use: Upper Palaeozoic to Quaternary bedrock*, Norsk Polarinstitut.
- DEER, W. A., HOWIE, R. A. & ZUSSMAN, J. 1992. *An introduction to the rock-forming minerals*, Longman London.
- DORÉ, A. 1991. The structural foundation and evolution of Mesozoic seaways between Europe and the Arctic. *Palaeogeography, Palaeoclimatology, Palaeoecology*, 87, 441-492.
- DORÉ, A. 1995. Barents Sea geology, petroleum resources and commercial potential. *Arctic*, 207-221.
- DOTT JR, R. H. 1964. Wacke, Graywacke and Matrix--What Approach to Immature Sandstone Classification? *Journal of Sedimentary Research*, 34.
- EHRENBERG, S. 1990. Relationship between diagenesis and reservoir quality in sandstones of the Garn formation, Haltenbanken, mid-Norwegian Continental shelf (1). *AAPG bulletin*, 74, 1538-1558.
- EHRENBERG, S. 1993. Preservation of anomalously high porosity in deeply buried sandstones by grain-coating chlorite: examples from the Norwegian continental shelf. *AAPG Bulletin*, 77, 1260-1286.
- FALEIDE, J., VÅGNES, E. & GUDLAUGSSON, S. Late Mesozoic–Cenozoic evolution of the southwestern Barents Sea. Geological Society, London, Petroleum Geology Conference series, 1993a. Geological Society of London, 933-950.
- FALEIDE, J. I., GUDLAUGSSON, S. T. & JACQUART, G. 1984. Evolution of the western Barents Sea. *Marine and Petroleum Geology*, 1, 123IN1129IN5137-128IN4136IN8150.
- FALEIDE, J. I., SOLHEIM, A., FIEDLER, A., HJELSTUEN, B. O., ANDERSEN, E. S. & VANNESTE, K. 1996. Late Cenozoic evolution of the western Barents Sea-Svalbard continental margin. *Global and Planetary Change*, 12, 53-74.
- FALEIDE, J. I., TSIKALAS, F., BREIVIK, A. J., MJELDE, R., RITZMANN, O., ENGEN, O., WILSON, J. & ELDHOLM, O. 2008. Structure and evolution of the continental margin off Norway and the Barents Sea. *Episodes*, 31, 82-91.
- FALEIDE, J. I., VÅGNES, E. & GUDLAUGSSON, S. T. 1993b. Late Mesozoic-Cenozoic evolution of the south-western Barents Sea in a regional rift-shear tectonic setting. *Marine and Petroleum Geology*, 10, 186-214.
- GABRIELSEN, R. 1984. Long-lived fault zones and their influence on the tectonic development of the southwestern Barents Sea. *Journal of the Geological Society*, 141, 651-662.
- GABRIELSEN, R. H., FAERSETH, R. B. & JENSEN, L. N. 1990. *Structural Elements of the Norwegian Continental Shelf. Pt. 1. The Barents Sea Region*, Norwegian Petroleum Directorate.
- GADING, M. 1993. Triassic evolution in the Barents Sea, Norwegian and Russian sectors: a seismic and sequence stratigraphic approach. *Doctor ingenioravhandling. Trond heim. Norway: Institute for Geologi og Bergteknikk*.

- GLØRSTAD-CLARK, E., BIRKELAND, E., NYSTUEN, J., FALEIDE, J. & MIDTKANDAL, I. 2011. Triassic platform-margin deltas in the western Barents Sea. *Marine and Petroleum Geology*, 28, 1294-1314.
- GLØRSTAD-CLARK, E., FALEIDE, J. I., LUNDSCHIEN, B. A. & NYSTUEN, J. P. 2010. Triassic seismic sequence stratigraphy and paleogeography of the western Barents Sea area. *Marine and Petroleum Geology*, 27, 1448-1475.
- GUDLAUGSSON, S., FALEIDE, J., JOHANSEN, S. & BREIVIK, A. 1998. Late Palaeozoic structural development of the south-western Barents Sea. *Marine and Petroleum Geology*, 15, 73-102.
- HALLAND, E., MUJEZINOVIC, J. & RIIS, F. 2014. CO<sub>2</sub> Storage Atlas: Norwegian Continental Shelf. *Norwegian Petroleum Directorate, PO Box*, 600.
- HENRIKSEN, E., BJØRNSETH, H., HALS, T., HEIDE, T., KIRYUKHINA, T., KLØVJAN, O., LARSEN, G., RYSETH, A., RØNNING, K. & SOLLID, K. 2011a. Uplift and erosion of the greater Barents Sea: impact on prospectivity and petroleum systems. *Geological Society, London, Memoirs*, 35, 271-281.
- HENRIKSEN, E., RYSETH, A., LARSEN, G., HEIDE, T., RØNNING, K., SOLLID, K. & STOUPAKOVA, A. 2011b. Tectonostratigraphy of the greater Barents Sea: implications for petroleum systems. *Geological Society, London, Memoirs*, 35, 163-195.
- JACOBSEN, V. W. & VAN VEEN, P. 1984. The Triassic offshore Norway north of 62°N. *Petroleum geology of the north European margin*. Springer.
- JOHANSEN, S., GUDLAUGSSON, S., SVÅNÅ, T. & FALEIDE, J. 1994. Late Paleozoic evolution of the Loppa High, Barents Sea. *Part of unpublished PhD thesis, University of Oslo, Oslo*, 25.
- JOHANSEN, S., OSTISTY, B., BIRKELAND, Ø., FEDOROVSKY, Y., MARTIROSIAN, V., CHRISTENSEN, O. B., CHEREDEEV, S., IGNATENKO, E. & MARGULIS, L. 1992. Hydrocarbon potential in the Barents Sea region: play distribution and potential. *Arctic Geology and Petroleum Potential, Norwegian Petroleum Society (NPF), Special Publication*, 2, 273-320.
- KOZENY, J. 1927. *Über kapillare Leitung des Wassers im Boden: (Aufstieg, Versickerung und Anwendung auf die Bewässerung)*, Hölder-Pichler-Tempsky.
- LARSEN, R., FJÆRAN, T. & SKARPNES, O. 1993. Hydrocarbon potential of the Norwegian Barents Sea based on recent well results. *Arctic geology and petroleum potential*, 321-331.
- LARSEN, G., ELVEBAKK, G., HENRIKSEN, L. B., KRISTENSEN, S., NILSSON, I., SAMUELSBERG, T., SVÅNÅ, T., STEMMERIK, L. & WORSLEY, D. 2002. Upper Palaeozoic lithostratigraphy of the Southern Norwegian Barents Sea. *Norwegian Petroleum Directorate Bulletin*, 9, 76.
- MAGOON, L. B. & DOW, W. G. 1994. *The petroleum system: From source to trap*, American Association of Petroleum Geologists.
- MARTINSEN, O., SØMME, T., THURMOND, J., HELAND-HANSEN, W. & LUNT, I. Source-to-sink systems on passive margins: theory and practice with an example from the Norwegian continental margin. Geological Society, London, Petroleum Geology Conference series, 2010. Geological Society of London, 913-920.
- MONDOL, N. H. Porosity and permeability development in mechanically compacted silt-kaolinite mixtures. 2009 SEG Annual Meeting, 2009. Society of Exploration Geophysicists.
- MONDOL, N. H. 2015. Well Logging: Principles, Applications and Uncertainties. *Petroleum Geoscience*. Springer.

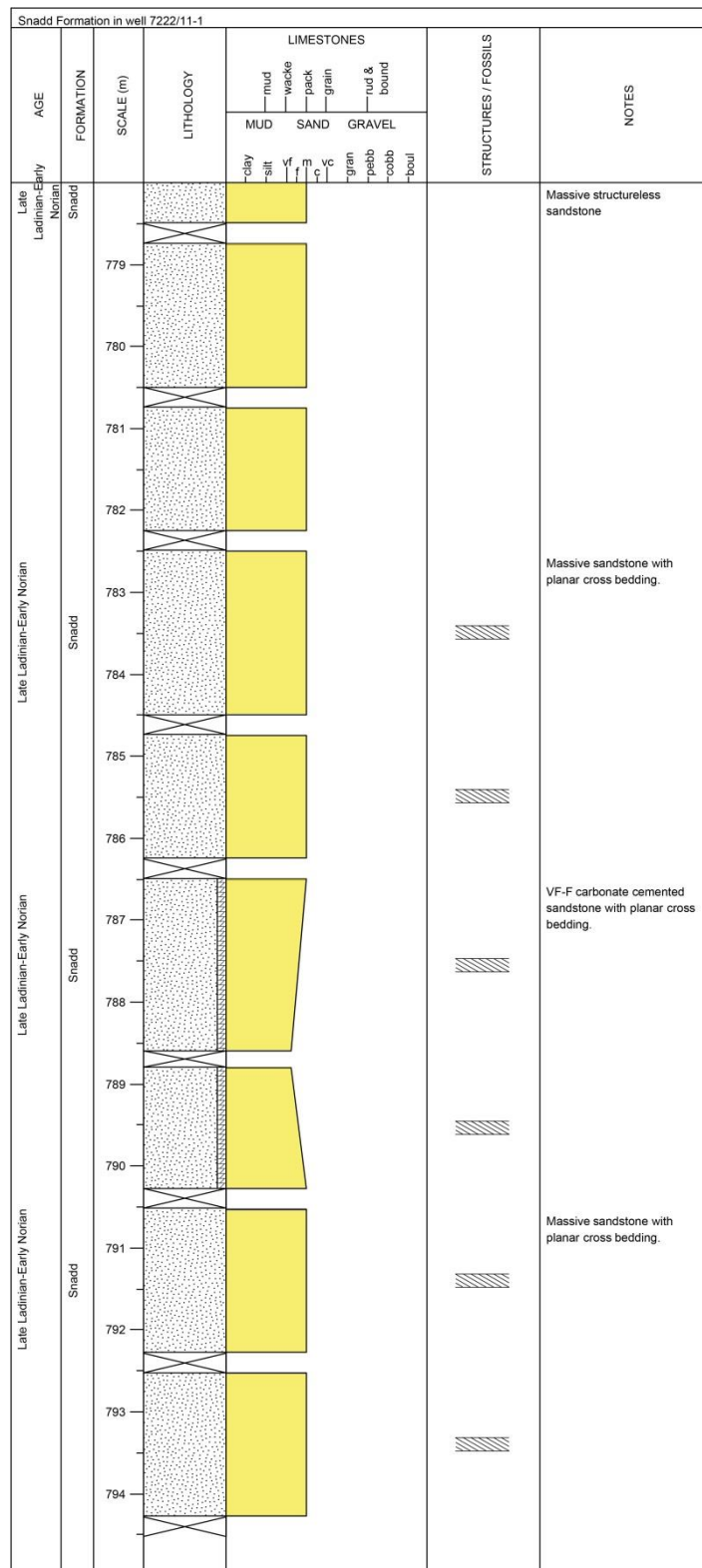
- MOORE, D. M. & REYNOLDS, R. C. 1989. *X-ray Diffraction and the Identification and Analysis of Clay Minerals*, Oxford university press Oxford.
- MORAD, S., DE ROS, L. F. & AL-AASM, I. 1996. Origin of low  $\delta$  18 O, pre-compactional ferroan carbonates in the marine Stø Formation (Middle Jurassic), offshore NW Norway. *Marine and Petroleum Geology*, 13, 263-276.
- MOZLEY, P. S. 1989. Relation between depositional environment and the elemental composition of early diagenetic siderite. *Geology*, 17, 704-706.
- MØRK, A., DALLMANN, W., DYPVIK, H., JOHANNESSEN, E., LARSEN, G., NAGY, J., NØTTVEDT, A., OLAUSSEN, S., PCHELINA, T. & WORSLEY, D. 1999. Mesozoic lithostratigraphy. *Lithostratigraphic lexicon of Svalbard. Upper Palaeozoic to Quaternary bedrock. Review and recommendations for nomenclature use*, 127-214.
- MØRK, A., EMBRY, A. F. & WEITSCHAT, W. 1989. Triassic transgressive-regressive cycles in the Sverdrup Basin, Svalbard and the Barents Shelf. *Correlation in hydrocarbon exploration*. Springer.
- MØRK, A., KNARUD, R. & WORSLEY, D. 1982. Depositional and diagenetic environments of the Triassic and Lower Jurassic succession of Svalbard.
- MØRK, A., VIGRAN, J., KORCHINSKAYA, M., PCHELINA, T., FEFILOVA, L., VAVILOV, M., WEITSCHAT, W., VORREN, T., BERGSAGER, E. & DAHL-STAMMES, Ø. 1992. Triassic rocks in Svalbard, the Arctic Soviet islands and the Barents Shelf: bearing on their correlations. *Arctic Geology and Petroleum Potential, Norwegian Petroleum Society (NPF), Special Publication*, 2, 457-479.
- MØRK, M. B. E. 1999. Compositional variations and provenance of Triassic sandstones from the Barents Shelf. *Journal of Sedimentary Research*, 69, 690-710.
- NICHOLS, G. 2009. *Sedimentology and stratigraphy*, John Wiley & Sons.
- OHM, S. E., KARLSEN, D. A. & AUSTIN, T. 2008. Geochemically driven exploration models in uplifted areas: Examples from the Norwegian Barents Sea. *AAPG bulletin*, 92, 1191-1223.
- POWERS, M. C. 1953. A new roundness scale for sedimentary particles. *Journal of Sedimentary Research*, 23.
- PRYOR, W. & VANWIE, W. A. 1971. The 'Sawdust Sand'; an Eocene sediment of floccule origin. *Journal of Sedimentary Research*, 41, 763-769.
- RIDER, M. & KENNEDY, M. 2011. *The geological interpretation of well logs: Rider-French Consulting, Ltd.*
- RIIS, F., LUNDSCHIEN, B. A., HØY, T., MØRK, A. & MØRK, M. B. E. 2008. Evolution of the Triassic shelf in the northern Barents Sea region. *Polar Research*, 27, 318-338.
- SANTIN, C. E., ABEL, M., GOLDBERG, K. & DE ROS, L. F. 2009. Automatic Detection of the Degree of Compaction in Reservoir Rocks Based on Visual Knowledge.
- SKJOLD, L. J. 1998. Triassic sequence stratigraphy of the southwestern Barents Sea.
- SMELROR, M., PETROV, O., LARSEN, G. B. & WERNER, S. 2009. Geological history of the Barents Sea. *Norges Geol. undersøkelse*, 1-135.
- STEEL, R. J. & WORSLEY, D. 1984. Svalbard's post-Caledonian strata—an atlas of sedimentational patterns and palaeogeographic evolution. *Petroleum geology of the North European margin*. Springer.
- STORVOLL, V., BJØRLYKKE, K. & MONDOL, N. H. 2005. Velocity-depth trends in Mesozoic and Cenozoic sediments from the Norwegian Shelf. *AAPG bulletin*, 89, 359-381.
- TIMUR, A. An investigation of permeability, porosity, and residual water saturation relationships. SPWLA 9th annual logging symposium, 1968. Society of Petrophysicists and Well-Log Analysts.

- TORSKAYA, T. S., JIN, G. & TORRES-VERDIN, C. Pore-level analysis of the relationship between porosity, irreducible water saturation, and permeability of clastic rocks. SPE Annual Technical Conference and Exhibition, 2007. Society of Petroleum Engineers.
- VANGDAL, B., MIDTBØ, R. E. A., LITLABØ, R. & JOHNSEN, A. L. The kaolinite to dickite transformation as a geothermometer [Abstract]: Reservoir Quality of Clastic and Carbonate Rocks: Analysis, Modelling and Prediction. 2014. The Geological Society of London, May 2014.
- WALDERHAUG, O. 1994. Temperatures of quartz cementation in Jurassic sandstones from the Norwegian continental shelf--evidence from fluid inclusions. *Journal of Sedimentary Research*, 64.
- WALDERHAUG, O. 1996. Kinetic modeling of quartz cementation and porosity loss in deeply buried sandstone reservoirs. *AAPG bulletin*, 80, 731-745.
- WELTON, J. E. 1984. *SEM petrology atlas*, American Association of Petroleum Geologists Tulsa^ eOklahoma Oklahoma.
- WILSON, M. D. & PITTMAN, E. D. 1977. Authigenic clays in sandstones: recognition and influence on reservoir properties and paleoenvironmental analysis. *Journal of Sedimentary Research*, 47.
- WORDEN, R. & BURLEY, S. 2003. Sandstone diagenesis: the evolution of sand to stone. *Sandstone Diagenesis: Recent and Ancient*, 4, 3-44.
- WORSLEY, D. 2008. The post-Caledonian development of Svalbard and the western Barents Sea. *Polar Research*, 27, 298-317.
- WYLLIE, M. & ROSE, W. D. 1950. Some theoretical considerations related to the quantitative evaluation of the physical characteristics of reservoir rock from electrical log data. *Journal of Petroleum Technology*, 2, 105-118.
- ZHANG, J., WONG, T.-F., YANAGIDANI, T. & DAVIS, D. M. 1990. Pressure-induced microcracking and grain crushing in Berea and Boise sandstones: acoustic emission and quantitative microscopy measurements. *Mechanics of Materials*, 9, 1-15.
- ZIEGLER, P. 1988a. Laurussia—the old red continent.
- ZIEGLER, P. A. 1988b. EVOLUTION OF THE ARCTIC-NORTH ATLANTIC AND THE WESTERN TETHYS--A VISUAL PRESENTATION OF A SERIES OF PALEOGEOGRAPHIC-PALEOTECTONIC MAPS\*. *AAPG memoir*, 43, 164-196.

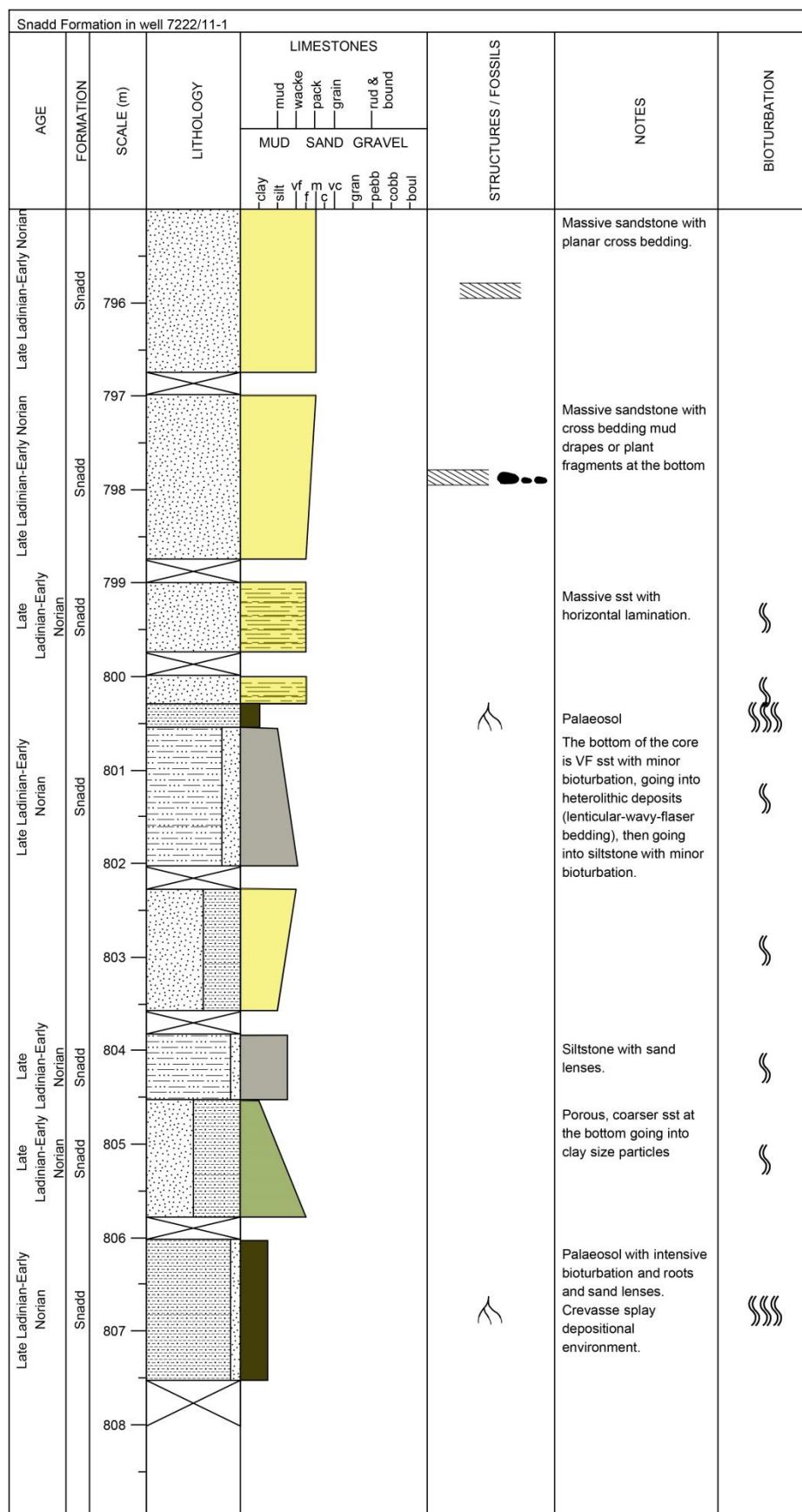
[http://gis.npd.no/factmaps/html\\_21/](http://gis.npd.no/factmaps/html_21/)

# APPENDIX

## Appendix A: Sedimentological data

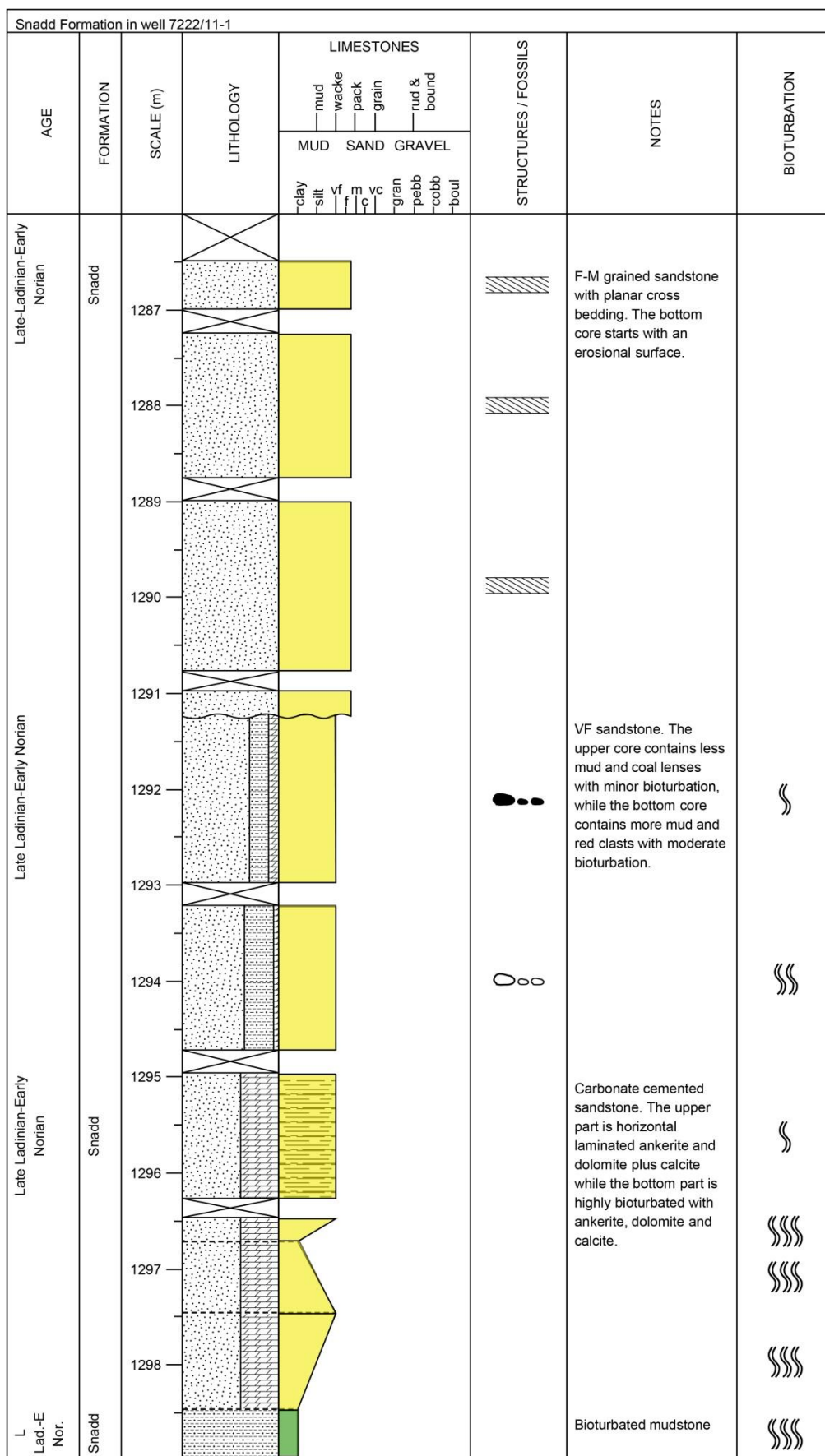


A.1: Sedimentary log of Core 1 of the Snadd Formation in well 7222/11-1.

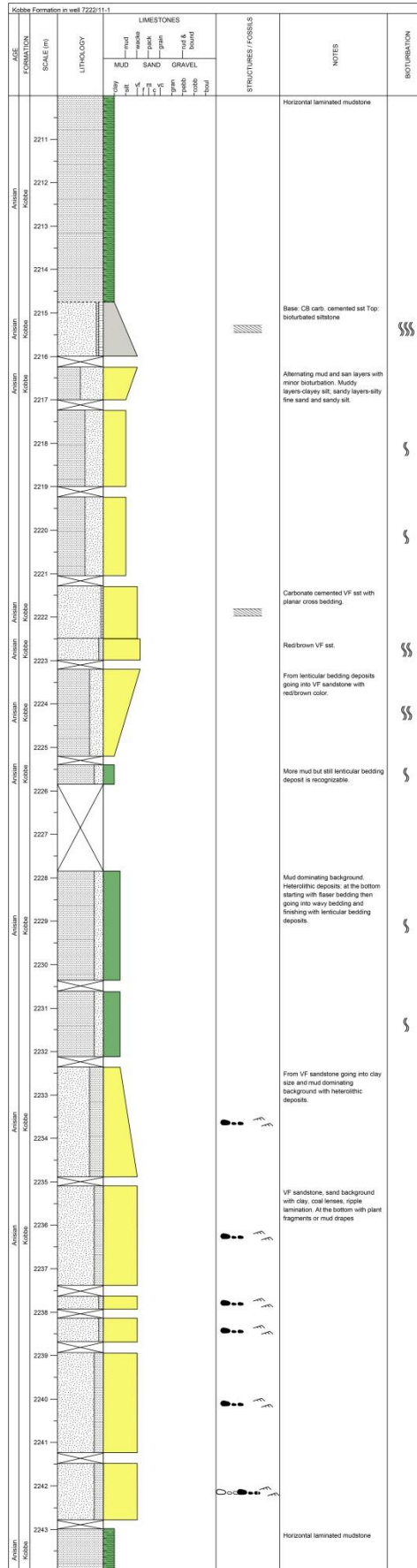


A.2: Sedimentary log of Core 2 and lower Core 1 of the Snadd Formation in well 7222/11-1.





A.3: Sedimentary log of Core 3 of the Snadd Formation in well 7222/11-1.



A.4: Sedimentary log of the Kobbe Formation in well 7222/11-1.

## Appendix B: Petrographic data

B.1: Samples selected for petrographic analysis from Kobbe and Snadd Formations.

Well	Formation	Samples #	Clay fraction #	Depth (m)	Petrographic investigation				
					BX	CFX	PC	S	S - Stubs
7222/11-1	Snadd Formation	S1	15	778.80	*	*	*	*	
		S2		780.50	*		*		*
		S3	14	782.70	*	*	*		
		S4		784.10	*		*		
		S5		787.60	*		*		
		S6	13	788.42	*	*	*	*	
		S7		790.70	*		*		
		S8	12	792.65	*	*	*		
		S9		794.65	*		*		
		S10	11	796.65	*	*	*		
		S11		797.60	*			*	*
		S12	10	799.20	*	*	*		
		S13		802.20	*				
		S14		804.60	*		*		*
		S15	9	806.60	*	*		*	
		S16	8	1287.40	*	*	*		
		S17		1290.70	*		*		
		S18		1292.15	*				
		S19	7	1293.80	*	*	*		
		S20	6	1297.60	*	*		*	
	Kobbe Formation	K1		2214.75	*		*	*	*
		K2	5	2217.60	*	*			
		K3	4	2221.50	*	*	*		
		K4		2230.60	*		*	*	
		K5		2233.60	*		*	*	*
		K6	3	2235.65	*	*	*		
		K7		2237.65	*		*		
		K8	2	2239.65	*	*	*		
		K9		2240.65	*		*		
		K10	1	2241.65	*	*	*	*	*

BX – Bulk XRD

CFX – Clay fraction XRD

PC – Point counting

S – SEM investigation

B.2: Point counting results for Snadd (left) and Kobbe (right) Formations in well 7222/11-1 (amounts are presented in %).

Sample	Depth (m)	Quartz		Feldspar		Rock fr.	Porosity		Qtz overgr.	Chlorite		Kaolinite	Siderite	Carbonate	IGV	Matrix
		Monocrystalline	Polycrystalline	Plg	Kfs		Primary	Secondary		Coating	Pore-filling					
S1	778.80	31,25	5,75	8,2	2,3	17,2	12,25	4,25	1,3	4,3	5,8	5,3	-	-	30,95	2
S2	780.50	24,2	5	4,25	2,75	25,2	10,5	5,2	1,2	5,9	6,9	6,6	-	-	33,2	2
S3	782.70	28,7	2	5,4	1,6	24,2	8,75	6,75	0,3	8,1	6,8	3,5	-	-	31,15	3,7
S4	784.10	30	5,5	5,5	2	21,2	10,72	9,98	0,75	5,75	4,25	2,25	-	-	25,72	2
S5	787.60	26,2	4	4	1,5	25,5	13,7	7	1,25	4,25	5,5	4,5	-	-	31,7	2,5
S6	788.42	24,4	9,6	6,25	4,25	13,7	0,25	3,75	-	-	0,5	-	-	34,7	37,95	2,5
S7	790.70	31,2	6,8	4,7	1	23	9,25	7,25	-	5,5	5,5	3	-	-	25,95	2,7
S8	792.65	30,2	9	5,2	2	14,7	13,7	9	-	4,6	4,4	4,2	0,5	-	29,6	2,2
S9	794.65	25	10	5,7	2,5	22,7	10,14	8,4	-	3,9	4,9	3,4	0,3	-	24,6	2
S10	796.65	42,25	6,25	2,9	0,3	12,5	21,2	7	-	6,5	0,5	-	-	-	28,7	0,5
S12	799.20	32,5	4,5	4	1,5	20,2	11,2	8,5	1	6,75	6	1,25	-	-	28,7	2,5
S14	804.60	28,2	5,5	5	2,5	21,5	6,5	8	0,5	6,25	7,75	3,5	-	-	29,2	4,7
S16	1287.40	45,6	4,6	3,9	1,3	14,5	11,5	6,2	-	5,25	5,25	-	-	-	23,7	1,7
S17	1290.70	37,5	7,2	3,5	1,5	16,7	8,7	9,5	0,75	4,5	8,25	-	-	-	23,9	1,7
S19	1293.80	29,5	4,5	4,25	2,25	23,2	4,9	6,3	-	5	5	-	-	7,7	29,9	7,2

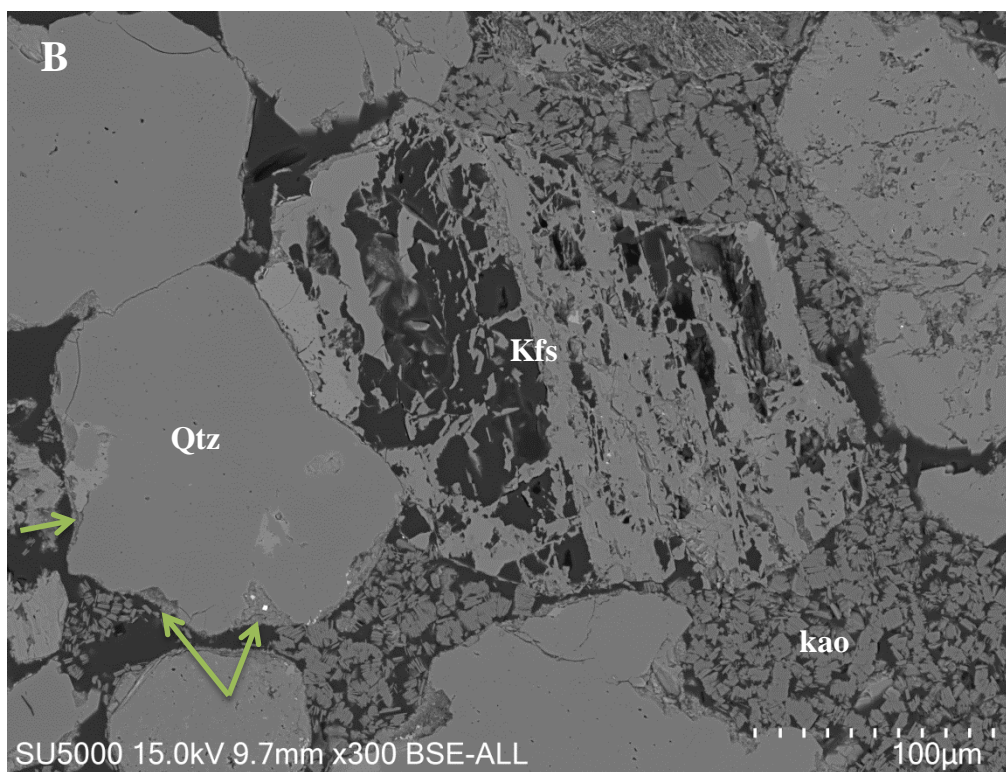
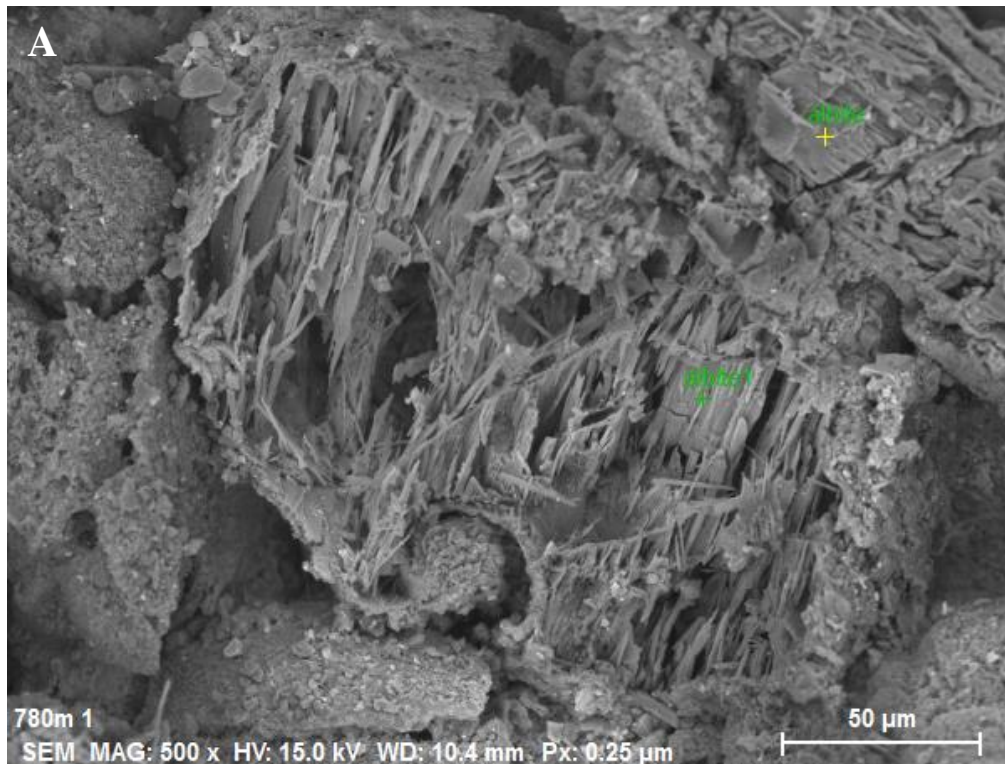
Samples	Depth (m)	Quartz		Feldspar		Rock fr.	Porosity		Qtz overgr.	Chlorite		Kaolinite	Siderite	Carbonate	IGV	Matrix
		Monocrystalline	Polycrystalline	Plg	Kfs		Primary	Secondary		Coating	Pore-filling					
K1	2214.75	21	3,5	6	-	34	1,5	1,7	-	-	1	-	-	21,5	33,7	9,7
K3	2221.50	34,2	2,5	8,5	-	34	3,5	1,2	0,2	1,6	7	-	1,1	-	19,5	6
K4	2230.60	42	9	9,2	-	13,7	0,5	1	-	-	0,5	0,75	-	19,25	25	4
K5	2233.60	46,4	4,8	10,7	-	15,7	1,3	2,4	-	1,5	6,1	1,7	-	-	19,6	9,2
K6	2235.65	49	3,2	10	-	12,7	5,2	3	0,7	1,7	7,1	1	-	-	21,9	6,2
K7	2237.65	48,5	5	9,2	-	11,5	4	4,5	0,25	3	6	3,3	-	-	21,2	4,7
K8	2239.65	46,8	4,7	11,5	-	14,2	2,7	2,5	1	1,75	3,5	3,25	-	-	20,2	8
K9	2240.65	50	6	6,5	-	14,5	4,3	2,2	0,5	1,5	5,5	0,7	-	-	20,65	8,2
K10	2241.65	46,6	6,9	7,7	-	18	1,75	1,75	0,25	2	5,75	2,5	-	1	18,95	5,7

B.3: XRD Bulk results for Snadd and Kobbe Formations in well 7222/11-1.

Snadd Fm	Depth (m)	Quartz (%)	Plagioclase (%)	K-feldspar (%)	Chlorite (%)	Kaolinite (%)	Muscovite (%)	Biotite (%)	Siderite (%)	Pyrite (%)	Calcite (%)	Dolomite (%)	Ankerite (%)	Heavy minerals (%)
S1	778.80	49,48	15,95	17,33	3,19	5,80	trace	4,53	0,76	trace	x	x	x	2,94
S2	780.50	34,25	22,73	12,89	7,32	5,57	14,50	trace	trace	0,71	x	x	x	2,02
S3	782.70	68,26	3,86	7,61	4,71	2,29	11,01	trace	0,73	trace	x	x	x	1,53
S4	784.10	72,07	13,03	7,38	1,80	1,42	trace	2,21	0,68	trace	0,26	x	x	1,16
S5	787.60	58,29	19,06	8,22	2,47	5,50	1,67	2,95	0,13	0,09	0,62	x	x	1,01
S6	788.42	54,59	5,30	5,28	1,45	1,99	trace	4,47	0,67	0,32	24,12	x	x	1,81
S7	790.70	72,04	11,27	6,97	2,40	4,55	1,67	trace	0,41	0,11	x	x	x	0,58
S8	792.65	67,24	14,42	4,92	2,15	4,87	3,16	trace	0,35	0,25	0,71	x	x	1,93
S9	794.65	70,98	12,48	7,90	3,00	1,95	1,84	trace	0,77	trace	x	x	x	1,09
S10	796.65	73,89	8,14	4,84	2,00	1,90	trace	trace	trace	0,26	0,41	x	x	1,11
S11	797.60	26,52	16,09	6,40	3,44	6,19	3,25	trace	7,26	25,14	1,16	x	x	4,56
S12	799.20	71,35	9,37	8,35	2,30	5,00	1,76	trace	0,70	trace	x	x	x	1,18
S13	802.20	42,14	21,40	9,33	8,40	5,15	9,88	trace	trace	trace	x	x	x	3,70
S14	804.60	67,69	11,56	8,67	4,32	3,14	2,49	trace	trace	trace	0,47	x	x	1,65
S15	806.60	21,86	31,27	12,45	5,25	14,33	trace	8,79	trace	0,68	1,32	x	x	4,05
S16	1287.40	67,49	15,28	4,64	2,67	1,38	4,61	trace	trace	0,29	x	x	x	3,65
S17	1290.70	74,39	13,68	4,23	3,42	x	1,39	trace	0,19	0,17	0,53	x	x	2,02
S18	1292.15	50,83	11,38	5,86	2,44	x	trace	trace	trace	trace	1,12	5,21	28,37	trace
S19	1293.80	61,07	14,73	3,75	4,43	x	3,43	trace	3,47	2,09	trace	x	x	4,23
S20	1297.60	3,02	7,72	6,74	5,10	x	trace	x	trace	trace	3,33	13,88	53,61	6,61

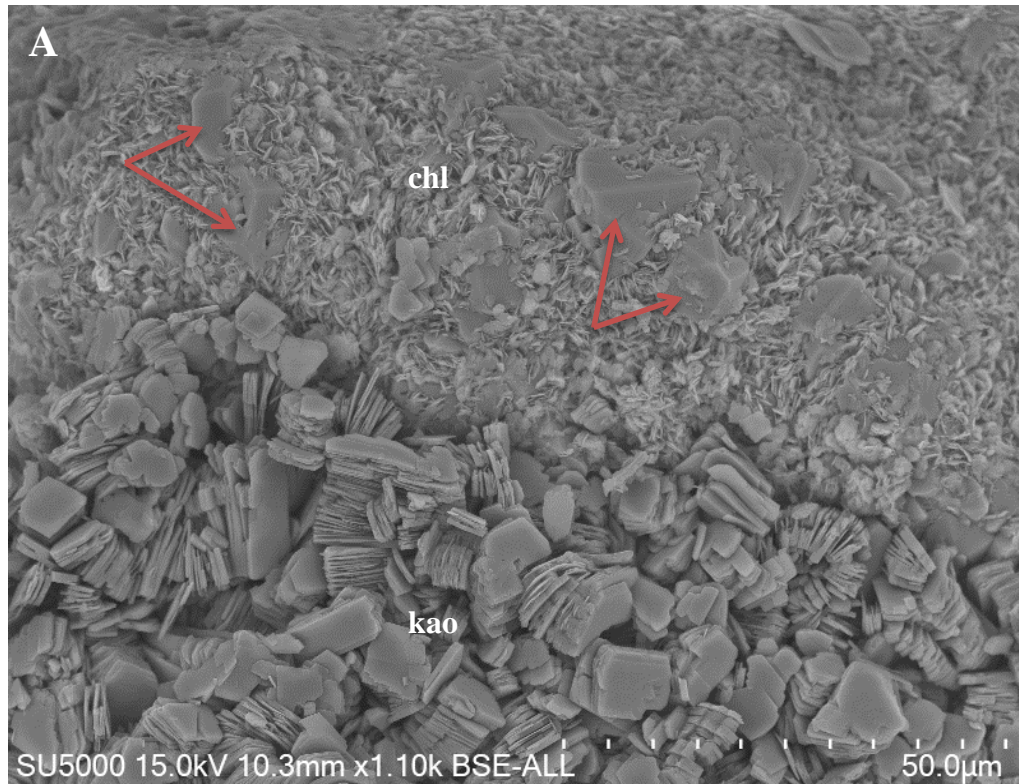
Kobbe Fm	Depth (m)	Quartz (%)	Plagioclase (%)	K-feldspar (%)	Chlorite (%)	Kaolinite (%)	Muscovite (%)	Biotite (%)	Siderite (%)	Pyrite (%)	Calcite (%)	Heavy minerals (%)
K1	2214.75	48,31	16,38	x	4,00	1,72	1,25	trace	5,38	1,11	10,81	8,80
K2	2217.60	29,16	27,84	x	13,59	3,02	4,15	trace	1,30	trace	trace	1,59
K3	2221.60	78,83	4,95	x	4,66	1,41	4,52	trace	1,69	trace	trace	3,94
K4	2230.60	30,68	27,30	x	11,36	9,00	7,72	trace	2,81	3,41	7,36	0,35
K5	2233.60	49,05	15,50	x	12,43	8,14	9,57	trace	2,43	1,32	trace	1,56
K6	2235.65	56,10	34,75	x	4,34	1,62	2,05	trace	0,66	0,48	trace	trace
K7	2237.65	71,92	17,71	x	2,71	2,10	2,16	trace	0,71	0,22	1,18	1,29
K8	2239.65	59,61	25,02	x	5,72	2,52	4,60	trace	trace	1,13	trace	1,41
K9	2240.65	41,60	32,01	x	14,01	3,27	6,96	trace	0,94	0,62	0,59	trace
K10	2241.65	56,69	18,95	x	6,33	7,26	8,88	trace	trace	0,94	0,94	0,21

## Appendix C: SEM pictures



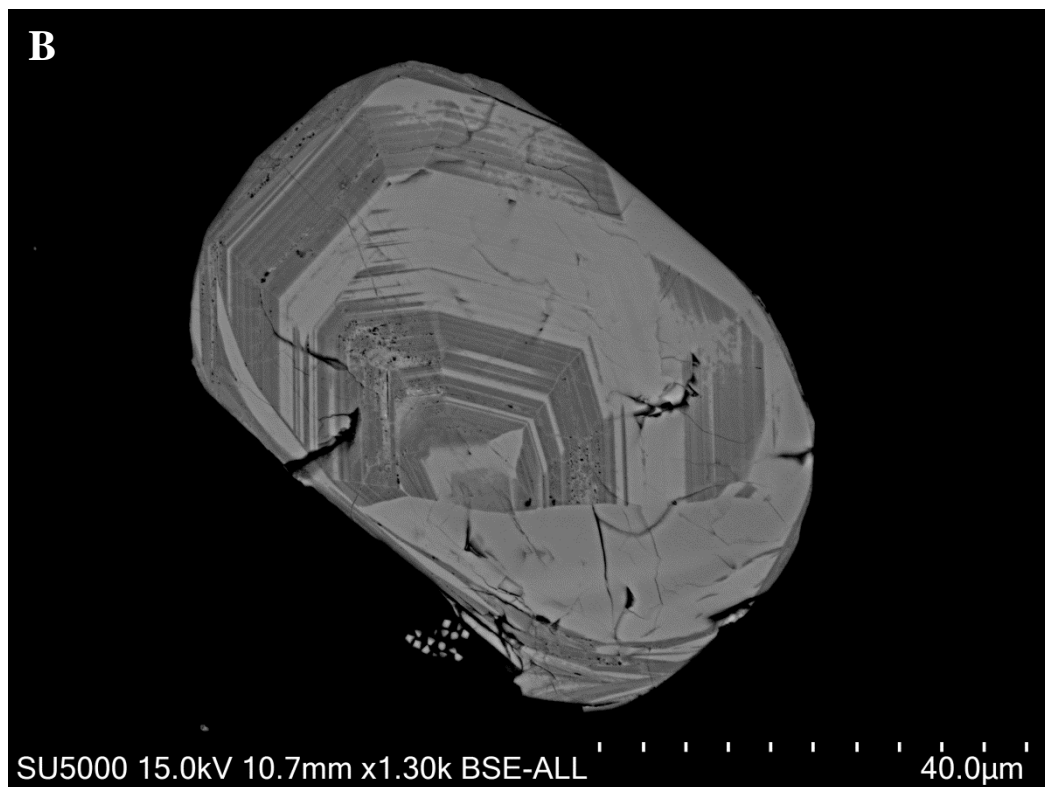
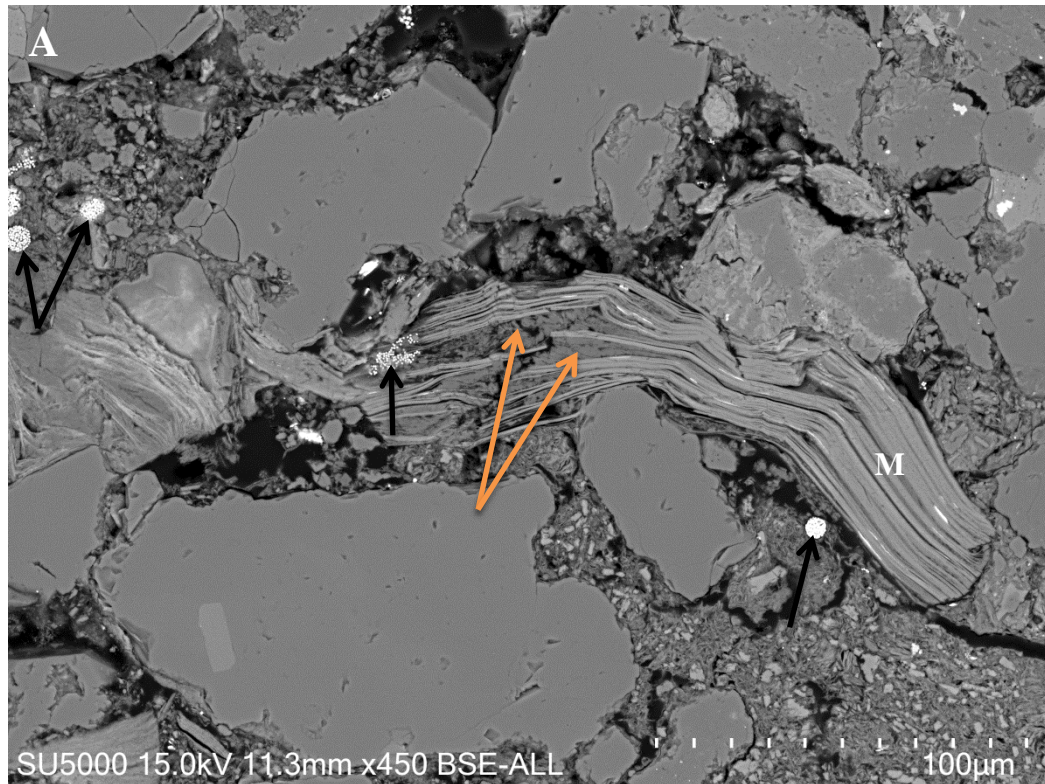
C.1: A: Partially dissolved albite at 780.50 m depth in the Snadd Formation; B: Albitisation of microcline (Kfs) is present in the Snadd Formation at 778.80 m depth. Qtz - quartz; kao - kaolinite; red arrows show chlorite coating.



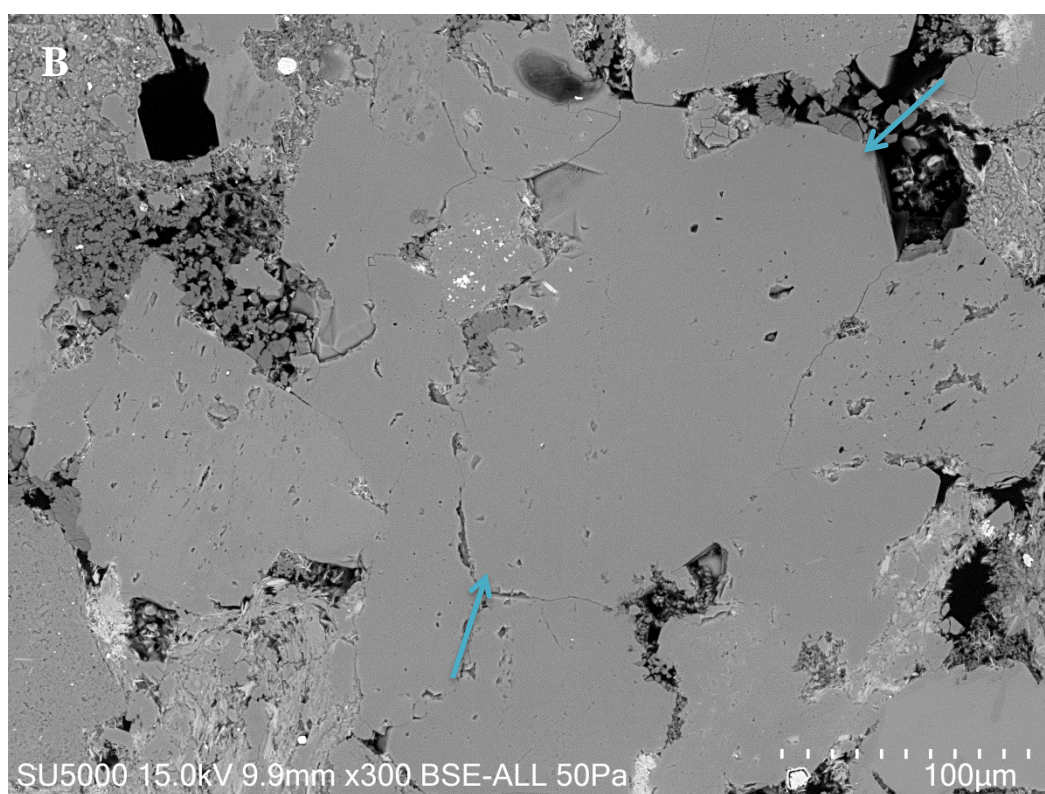
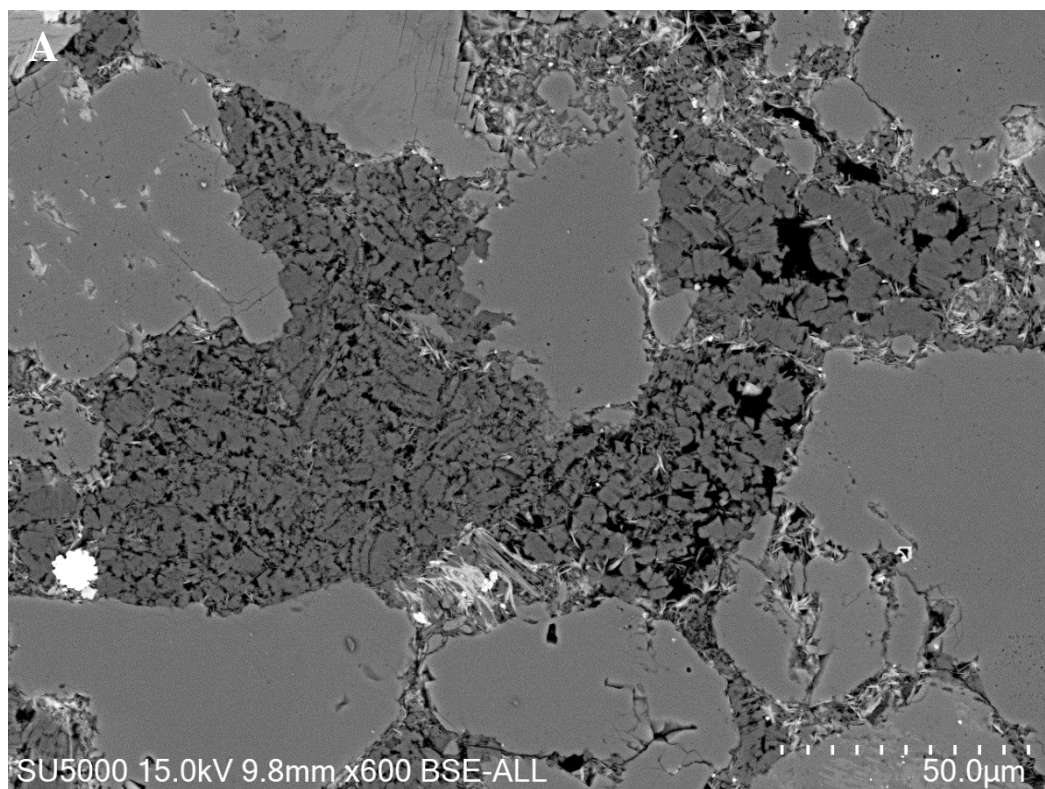


C.2: A: The sample represent authigenic kaolinite (kao), chlorite coating (chl) and quartz overgrowths (red arrows) at 780.50 m depth in the Snadd Formation; B: Well-developed chlorite coating (chl) with K-feldspar (Kfs) at 780.50 m depth in the Snadd Formation.



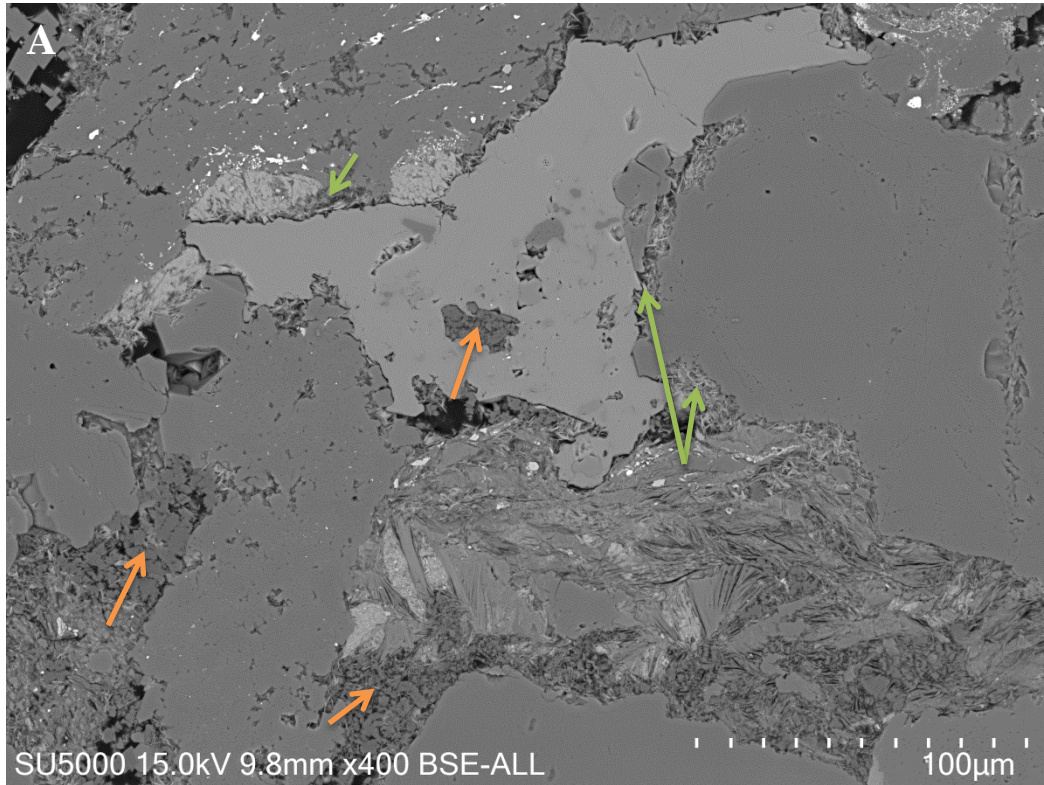


C.3: A: Folded muscovite (M) grain due to mechanical compaction, being replaced by kaolinite (orange arrows). Black arrows show framboidal pyrite aggregates at 806.60 m depth in the Snadd Formation; B: Zircon mineral shows zonation at 2230.60 m depth in the Kobbe Formation.



C.4: A: Authigenic pore-filling kaolinite at 2233.60 m depth in the Kobbe Formation;  
B: The light blue arrows show quartz overgrowths at 2233.60 m depth in the Kobbe Formation.





C.5: A: The sample shows thick chlorite coating (green arrows) around the detrital grains. The pore space filled with kaolinite (orange arrows), calcite and chlorite at 2241.65 m depth in the Kobbe Formation. B: Non-continuous chlorite coating and quartz overgrowths at 2233.60 m depth in the Kobbe Formation.